

The Subdetonative Ram Accelerator Starting Process

by

Eric Schultz

A thesis submitted in partial fulfillment
of the requirements for the degree of

Master of Science in Aeronautics and Astronautics

University of Washington

1997

Approved by _____
(Chairperson of Supervisory Committee)

Program Authorized
to Offer Degree _____ Aeronautics and Astronautics _____

Date _____ March 21, 1997 _____

In presenting this thesis in partial fulfillment of the requirements for a Master's degree at the University of Washington, I agree that the Library shall make its copies freely available for inspection. I further agree that extensive copying of this thesis is allowable only for scholarly purposes, consistent with "fair use" as prescribed in the U.S. Copyright Law. Any other reproduction for any purposes or by any means shall not be allowed without my written permission.

Signature_____

Date_____

University of Washington

Abstract

The Subdetonative Ram Accelerator Starting Process

by Eric Schultz

Chairperson of the Supervisory Committee
Professor Adam P. Bruckner
Department of Aeronautics and Astronautics

The ram accelerator is a hypervelocity launcher in which a subcaliber projectile, similar in shape to the centerbody of a ramjet, travels supersonically through a tube filled with premixed gaseous fuel and oxidizer. A conventional gun initially boosts the projectile to supersonic entrance velocity. An experimental investigation has been undertaken to improve understanding of transition from the conventional gun to the ram accelerator, referred to as the “starting process”. Developing a robust starting process is instrumental for utilizing the ram accelerator in a variety of applications. Four possible outcomes of a start attempt have been identified. A successful start is achieved when supersonic flow is maintained throughout the diffuser, and the shock system is stabilized on the projectile body through propellant energy release. A sonic diffuser unstart is caused by conditions upstream of the throat resulting in subsonic flow in the diffuser. A wave fall-off occurs when insufficient energy is released from the propellant to keep the shock system on the body from receding behind the base. A wave unstart is caused by conditions downstream of the throat resulting in disorgment of the shock system on the body into the diffuser. Piston experiments were conducted to define detonation limits for several propellants, study the association of detonations with the wave unstart process, gain knowledge of the obturator dynamics as it transitions from the launch tube into the ram accelerator tube, and investigate the effects of mass, geometry, and launch tube air pressure variations on propellant ignition. Projectile experiments were used to explore the limits to successful starting, study the association of detonations with the wave unstart

process, improve understanding of the flowfield in the launch tube and ram accelerator tube, and investigate the effects of Mach number, propellant chemistry, obturator geometry and mass, and throat area variations on the starting process. Along with experimental results, a review of past research as well as the current understanding of the starting process is presented.

Table of Contents

	Page
List of Figures	iii
List of Tables.....	v
1. Introduction.....	1
2. Starting Process Overview	4
2.1. Non-idealities of the Starting Process	5
2.2. Possible Outcomes of a Start Attempt.....	8
2.3. Maximum Performance Starting Conditions.....	13
2.4. Historical Perspective	14
2.5. Literature Review	17
3. Experimental Procedure.....	30
3.1. Piston Experiments.....	31
3.2. Projectile Experiments	33
4. Results.....	36
4.1. Mach Number and Energy Release	36
4.2. Throat Area	41
4.3. Piston/Obturator Configuration	44
4.4. Launch Tube Residual Air Pressure	47
4.5. Unique Experiments	48
5. Analysis.....	52
5.1. Flowfield.....	52
5.2. Obturator Dynamics	56

	Page
5.3. Detonation Wave Unstart	61
5.4. Quasi-One-Dimensional Model	64
5.5. Starting Envelope	66
5.6 Time Scales	68
6. Recommendations.....	73
7. Conclusions.....	75
8. References.....	77
Appendix A: Projectile Experiment Data	81
Appendix B: Piston Experiment Data.....	113

List of Figures

	Page
1.1 Ram accelerator propulsive mechanism at subdetonative velocities.....	1
1.2 Ram accelerator facility diagram	2
1.3 Standard ram accelerator projectile.....	2
1.4 Two 16 gm obturator configurations	2
2.1 Idealized starting process	4
2.2 Gas compression between obturator and entrance diaphragm	5
2.3 Launch tube venting	6
2.4 Possible outcomes of an attempted start	8
2.5 Experiment resulting in a successful start	9
2.6 Experiment resulting in a sonic diffuser unstart.....	10
2.7 Non-reactive experiment resulting in a wave fall-off.....	11
2.8 Reactive experiment resulting in a wave fall-off.....	11
2.9 Experiment resulting in a wave unstart originating on projectile body.....	12
2.10 Experiment resulting in a wave unstart originating in projectile wake	12
2.11 Unique projectile configurations	16
2.12 Current ram accelerator facility locations	18
2.13 Ram accelerator tube cross sections.....	25
3.1 Instrument station configuration near entrance diaphragm	30
3.2 Propellant properties	32
3.3 Representative shock velocity versus distance data for piston experiments	33
3.4 Projectile configurations used in experiments.....	35
3.5 Projectile area profiles.....	35
4.1 Start attempt results with standard projectile in nominal propellant class	38
4.2 Start attempt results in carbon dioxide diluted propellants	39
4.3 Start attempt results with short projectile.....	39
4.4 Start attempt results in argon diluted propellants	40
4.5 Throat area variations in nominal propellant class.....	42

	Page
4.6 Throat area variations with variable propellant class	43
4.7 Experimental versus theoretical results of sonic diffuser unstart Mach number.....	43
4.8 Piston/obturator mass variations	45
4.9 Geometry variations in piston experiments	46
4.10 Obturator geometry variations in projectile start experiments	47
4.11 Residual launch tube pressure effects on detonation initiation	47
4.12 Data from piston experiments in which marginal detonations occurred.....	49
4.13 Experiment in which a wave fall-off occurred, followed by a wave unstart	50
5.1 Tube wall pressure and luminosity data from the launch tube	53
5.2 Tube wall pressure and luminosity data from the ram accelerator tube	54
5.3 Data from obturator geometry variation wave fall-off experiments.....	55
5.4 Experimental and predicted piston and shock $t-x$ data	57
5.5 Ignition effects on piston and shock $t-x$ data at 25 atm fill pressure	58
5.6 Ignition effects on piston and shock $t-x$ data at 50 atm fill pressure	58
5.7 Piston and shock $t-x$ data for mass variation	60
5.8 Piston and shock $t-x$ data for geometry variation	60
5.9 Quasi-one-dimensional flowfield model	64
5.10 Limits of operation predicted by quasi-one-dimensional model.....	65
5.11 Generalized ram accelerator starting envelope.....	67
5.12 Induction time versus Mach number for $Q_{CJ} = 4.78$ propellants	72

List of Tables

	Page
2.1 Factors influencing the starting process	8
2.2 Statistical results of start attempts for HS647 through HS1320.....	15
2.3 Ram accelerator facility characteristics.....	17
3.1 Projectile configurations.....	34
4.1 Summary of piston detonation conditions.....	37
4.2 Piston experiments in 25 atm $1.5\text{CH}_4+2\text{O}_2+5.5\text{CO}_2$	49
5.1 Detonation frequency in conjunction with wave unstarts	61

Acknowledgments

The starting process comes as close to being the proverbial “can of worms” as anything I have ever worked on. Nothing this difficult to study and bewildering to comprehend would have been possible without the support of the ram accelerator research group at the University of Washington. Adam Bruckner not only served as my advisor, but also provided an amazing amount of freedom to explore my own ideas and present the fruits of my labor on many occasions. Carl Knowlen and Andrew Higgins were never-ending sources of discussion and opinion, to whom I owe a great deal of my intellectual growth over the past year and a half. Jesse Stewart, Josh Elvander, and Dave Buckwalter supplied numerous helpful questions and comments during our weekly marathon research meetings, through heavy e-mail traffic, and office banter. Their assistance with lab tasks, creation of the figures contained herein, and helping with computational efforts is also greatly appreciated. Finally, frequent assistance from Dennis Peterson with machine shop work and last minute figure creation by Ryan Schwab has not gone unnoticed.

1. Introduction

The ram accelerator is a hypervelocity launcher in which a projectile, similar in shape to the centerbody of a ramjet, travels supersonically through a tube filled with premixed gaseous fuel and oxidizer.¹ A schematic of the idealized flowfield of the thermally choked ram accelerator propulsive mode is presented in Fig. 1.1. The propellant flowing over the projectile nose is ram compressed by a series of reflected shocks and expands supersonically relative to the projectile behind the throat. The propellant then encounters a normal shock system followed by a subsonic combustion zone which releases the chemical energy and chokes the flow. The combustion supported normal shock system generates a high base pressure which accelerates the projectile down the tube. This mode of ram accelerator operation is observed at projectile velocities below the Chapman-Jouguet detonation velocity (V_{CJ}) of the combustible gas mixture.^{2,3} The research described here lies completely within the subdetonative velocity regime.

A schematic of the 38.1 mm bore University of Washington (UW) ram accelerator facility is presented in Fig. 1.2.⁴ It consists of a light gas gun initial launcher with a 6 m launch tube, a launch tube dump tank, 16 m of ram acceleration tube, a final dump tank, and a catcher tube. The standard projectile shown in Fig. 1.3 is typically fabricated of 7075-T6 aluminum alloy and consists of two pieces, the nose and body, which screw together at the throat. Primary characteristics of the standard projectile include a 10° half-angle nose, 5 fins to stabilize the subcaliber projectile in the tube, a mass of approximately 75 gm, and a flow throat-to-tube area ratio (A_{throat}/A_{tube}) of 0.42. A polycarbonate obturator, two types of which are shown in Fig. 1.4, is glued to the projectile base to prevent blow-by of the gas from the initial launcher, and to assist in propellant ignition in the ram accelerator section.

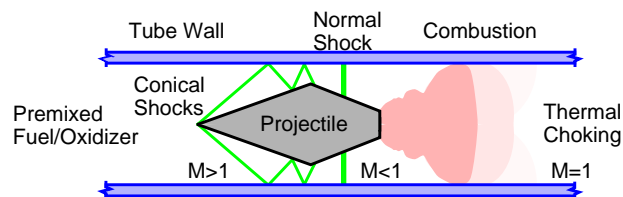


Fig. 1.1 Ram accelerator propulsive mechanism at subdetonative velocities.

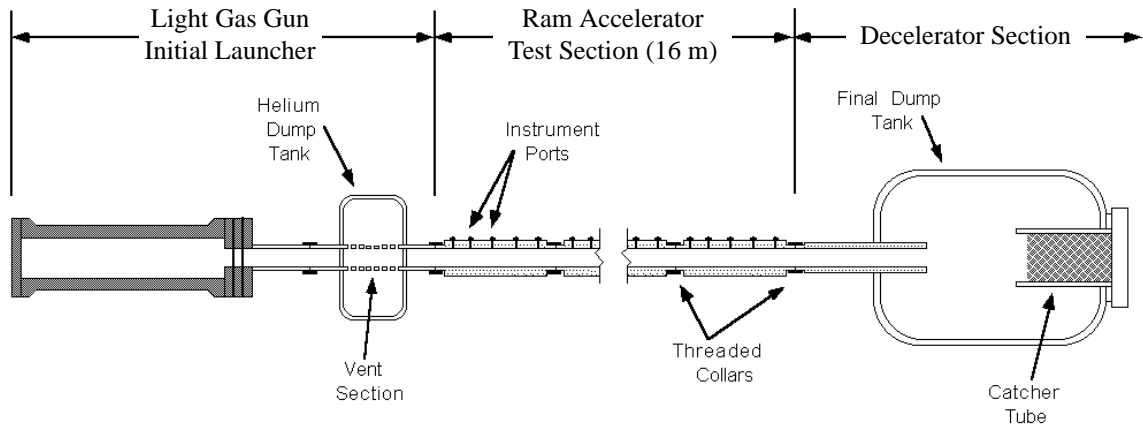


Fig. 1.2 Ram accelerator facility diagram.

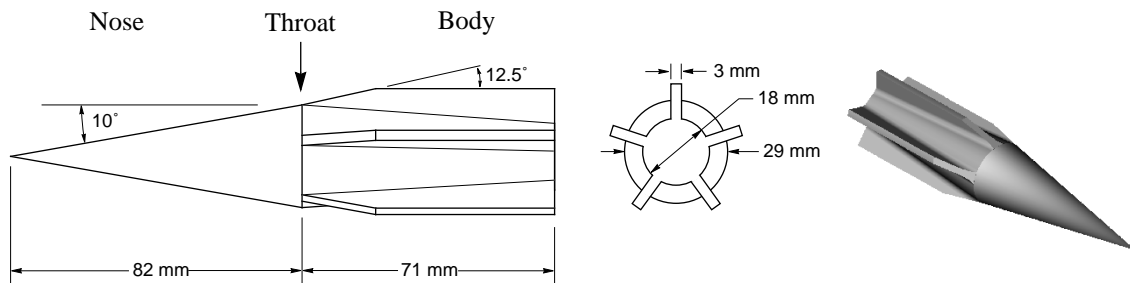
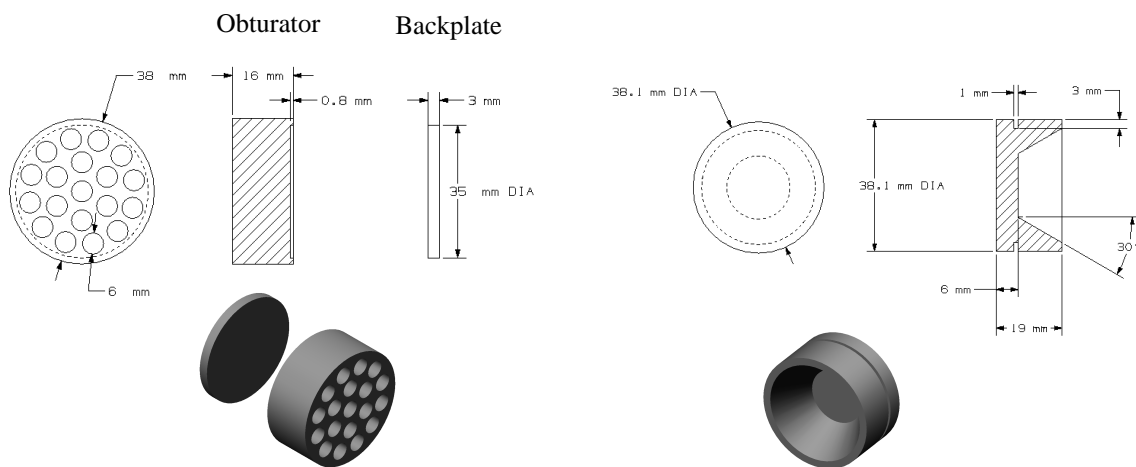


Fig. 1.3 Standard ram accelerator projectile.



a) Perforated obturator with backplate.

b) Solid obturator with Bridgman seal.

Fig. 1.4 Two 16 gm obturator configurations.

The propellant characteristics are tailored by the type and concentration of fuel, oxidizer, and diluent used in the mixture. Typical fuels used are methane (CH_4) and hydrogen (H_2), while diluents include nitrogen (N_2), argon (Ar), carbon dioxide (CO_2), helium (He), or additional fuel. The oxidizer is oxygen (O_2) in all cases. Fill pressures in the UW facility are generally 5-50 atm. Propellant properties of interest include the acoustic speed and the heat release parameter $Q = \Delta q/c_p T$, where the equilibrium heat release (Δq) is normalized by the constant pressure specific heat capacity (c_p) and the temperature of the quiescent gas mixture (T). Chemical reactions rates, induction lengths, and activation energies, collectively referred to as “reactivity parameters”, are also of interest but are more difficult to quantify under typical ram accelerator operating conditions.

Experimental data are collected through instrument stations spaced every 40 cm along the length of the ram accelerator tubes. Every 2 m tube section has five instrument stations along its length, each station with either three or four instrument ports located about the circumference of the tube. Electromagnetic transducers provide a time-distance history of the projectile by detecting the passage of a magnet in the projectile throat. Piezoelectric pressure transducers allow measurement of the flowfield pressure at the tube wall, and fiber optic luminosity sensors detect visible light emission in the tube.

Ram accelerator operation at projectile velocities of 1 to 2.7 km/s and Mach numbers from 2.5 to 8 has been observed to date. Sustained accelerations are commonly on the order of 25,000 g, with peak accelerations up to 50,000 g. The gasdynamics of the ram accelerator are such that the device can theoretically be scaled up or down in size.⁵ Potential applications include hypersonic vehicle flight testing, supersonic and hypersonic propulsion research, validation of reacting flow computational fluid dynamic codes, tactical and strategic defense, and direct launch to orbit of acceleration-insensitive payloads. A number of other ram accelerator facilities are now operating in the United States and abroad due to the wide range of basic and applied research opportunities that the technology offers.⁶⁻¹⁰

2. Starting Process Overview

The idealized UW starting process, illustrated in Fig. 2.1, begins with the helium filled light gas gun accelerating a perforated obturator with backplate and projectile from rest down 6 m of evacuated launch tube. A Mylar “entrance diaphragm” separates the evacuated launch tube from the high pressure, propellant-filled ram accelerator tube. The projectile pierces the entrance diaphragm and enters the propellant with the obturator at supersonic “entrance velocity”. The propellant is ram compressed up to the projectile throat and expands over the body where it encounters the obturator. A normal shock is driven onto the projectile body as the obturator and backplate separate from the projectile and rapidly decelerate. The propellant energy is released in a combustion zone behind the normal shock which thermally chokes the flow. The choked flow stabilizes the normal shock on the projectile body, creating a high pressure zone at the base of the projectile that results in sustained acceleration as the projectile travels down the tube. The starting process is loosely defined as the period between projectile acceleration from rest to the point where the flowfield illustrated in Fig. 1.1 is stabilized.

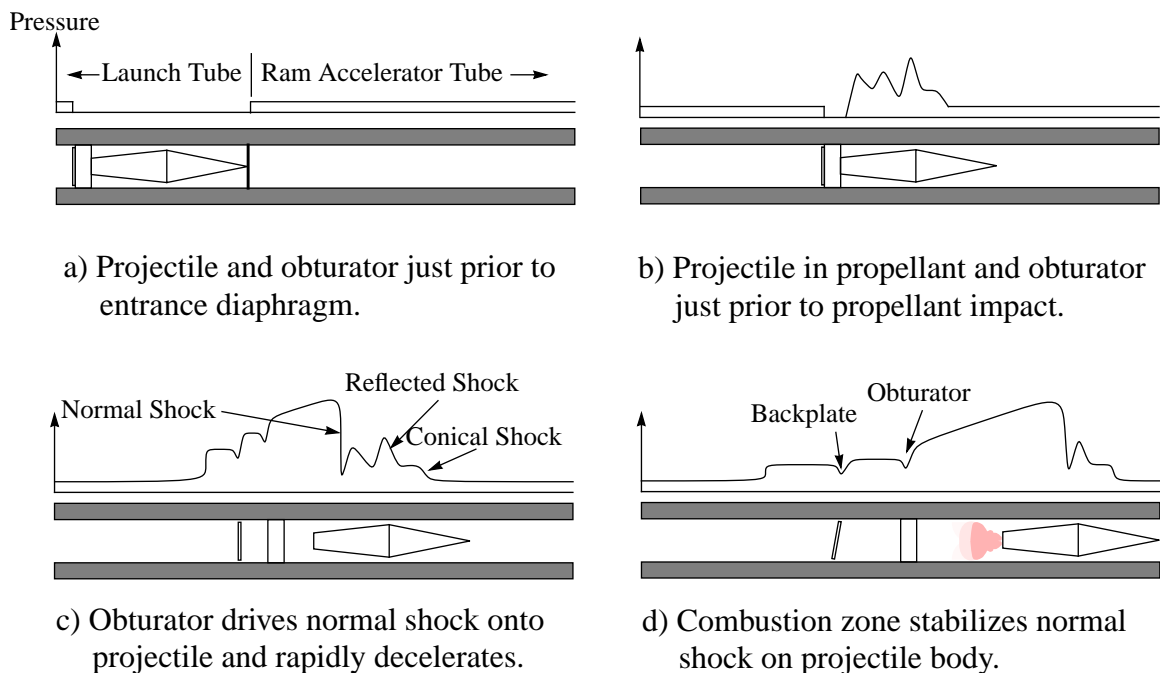


Fig. 2.1 Idealized starting process.

2.1 Non-idealities of the Starting Process

A more detailed inspection of the starting process reveals many non-idealities with the potential to affect a start attempt. A brief description of each is provided in the following paragraphs. Most of this research effort has involved experiments aimed at improving the understanding of the role these non-idealities play.

The gas released from the initial launcher can cause structural failure of the obturator depending on the gas pressure, obturator geometry and material, and the projectile base area. Maximum initial launcher gas pressure is 340 atm, accelerating the standard obturator and projectile from rest to approximately 1150 m/s. The average acceleration experienced in the launch tube is 11,000 g, with peak acceleration up to 45,000 g given by an $F = ma$ expression for the maximum pressure acting over the obturator at full tube area.

The launch tube is not perfectly evacuated, and some gas from the initial launcher does blow-by the obturator. The residual launch tube air and blow-by gas are compressed between the obturator and entrance diaphragm, illustrated in Fig. 2.2, as the projectile accelerates down the launch tube. A series of 36 holes, 6.4 mm in diameter, is distributed

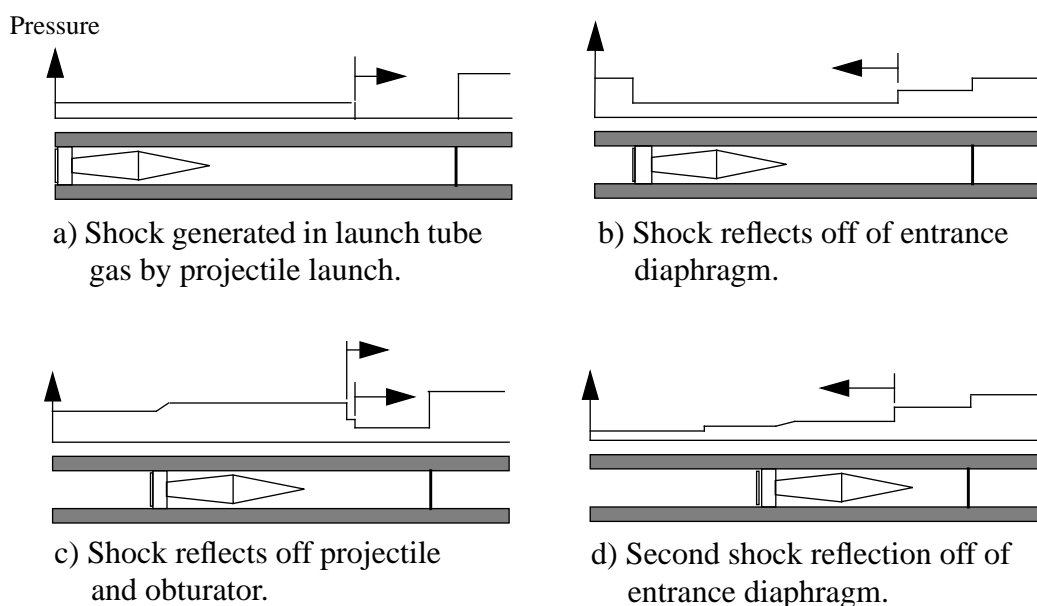


Fig. 2.2 Gas compression between obturator and entrance diaphragm.

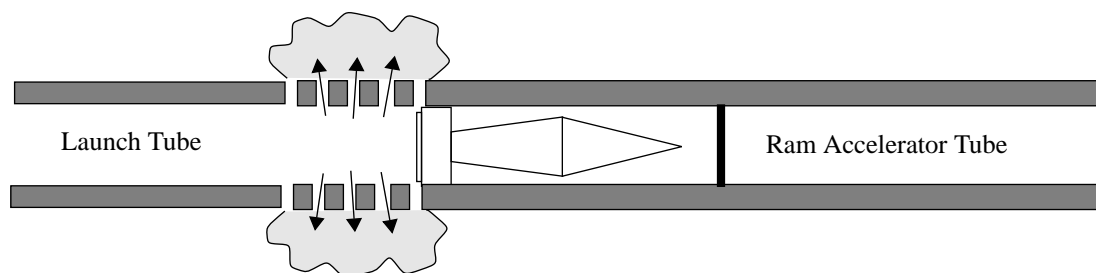


Fig. 2.3 Launch tube venting.

over a 305 mm section of tube, beginning 600 mm from the entrance diaphragm. The perforated area is 3.2% of the tube section area containing the holes, and allows venting of gases in the launch tube to an evacuated dump tank as shown in Fig. 2.3.

Perforated and solid obturator geometries are used, as illustrated in Fig. 1.4. The perforated obturator requires a backplate to seal it against the initial launcher gas. The backplate is glued with cyanoacrylate to the perforated obturator, and will separate when a sufficiently high pressure differential exists across it. Similarly, the solid or perforated obturator is glued to the base of the projectile, and will separate from the projectile when a sufficiently high pressure differential exists. The entrance diaphragm will rupture if the pressure differential across it exceeds a certain level, depending primarily on the Mylar thickness.

If the compressed launch tube gas does not break the entrance diaphragm, then the projectile nose will. The dynamics of the diaphragm rupture will vary, depending on what time scale this event occurs relative to the motion of the projectile and launch tube shocks. Other potential effects from the entrance diaphragm impact are that the projectile may be damaged, and the geometry and dynamics of the obturator could be changed. Projectile condition upon entrance is of concern because a damaged or eroded geometry can significantly affect the propellant flowfield, especially in the case of severe projectile canting.¹¹ Short obturator lengths may allow the obturator to tumble in the tube if struck by diaphragm fragments, influencing the area profile encountered by the flow.

The propellant is compressed as it passes through a conical shock generated by the projectile nose, and then through reflections of this shock between the projectile and the

tube wall. The propellant expands as it encounters an increasing area behind the throat, but the fin leading edges in the throat area create high pressure stagnation regions and complex oblique shock patterns. The geometry-dependent, three-dimensional, turbulent flowfield on the projectile body contains mixed regions of subsonic and supersonic flow, shock reflections between the body and tube wall, shock-shock intersections,¹² and shock interactions with the boundary layers on the projectile surface and at the tube wall. The shock system supported by the obturator is typically idealized as a single normal shock, but is more likely a complicated system of reflected oblique shocks and/or lambda shocks forming a shock train which renders the flow subsonic relative to the projectile.^{13,14}

The obturator dynamics can continue to affect the flowfield about the projectile as long as there exists a subsonic region between the obturator and projectile. Obturator dynamics will be affected by its mass, geometry, and the pressure differential across it. Once the backplate has dislodged from a perforated obturator, the flow can expand through the exposed obturator perforations. A significant pressure differential across the obturator will cause the perforations to act as choked orifices. Flow occlusion will be altered by a short length obturator if it tumbles in the tube when subjected to a non-uniform pressure distribution.

Propellant variables dictated by the chemical composition and ambient environment include the reactivity parameters (acoustic speed, finite reaction rates, activation energy, induction time, and energy release), temperature, pressure, and velocity. The propellant is initially quiescent at room temperature with a fill pressure up to 50 atm. Variation of the type and relative amounts of fuel, oxidizer, and diluent allows tailoring of the propellant chemical properties. The reactivity parameters are typically coupled in such a manner that it is difficult to control one without affecting the others.

The exact mechanism by which the propellant is ignited and combustion stabilized behind the throat is unclear. There are numerous contributing factors, summarized in Table 2.1, present in the starting process. Ignition and stabilization of the combustion process is probably dependent in some way on all of these factors.

Table 2.1 Factors Influencing the Starting Process

<u>Projectile</u>	<u>Obturator</u>	<u>Initial Launcher</u>	<u>Ram Accelerator</u>
• Geometry	• Geometry	• Residual air	• Entrance diaphragm
• Mach number	• Mach number	• Blow-by gas	• Propellant
• Mass	• Mass	• Venting	
• Material	• Material	• Driver pressure	

2.2 Possible Outcomes of a Start Attempt

There are four possible results of a ram accelerator start attempt at supersonic entrance velocity: a successful start, sonic diffuser unstart, wave fall-off, or wave unstart. Each of these phenomena, illustrated in Fig. 2.4, is described in the following paragraphs.

A successful start (Fig. 2.4a) is accomplished by satisfying two criteria: obtaining supersonic flow past the projectile throat and stabilizing a high pressure shock system on the body by igniting the propellant in a combustion zone behind the shock system. A successful start is defined in the context of this work as a projectile which has accelerated for more than 2 m beyond the entrance diaphragm. At this point the obturator is thought to be decoupled from the acceleration process and a change in mixture via staging can be

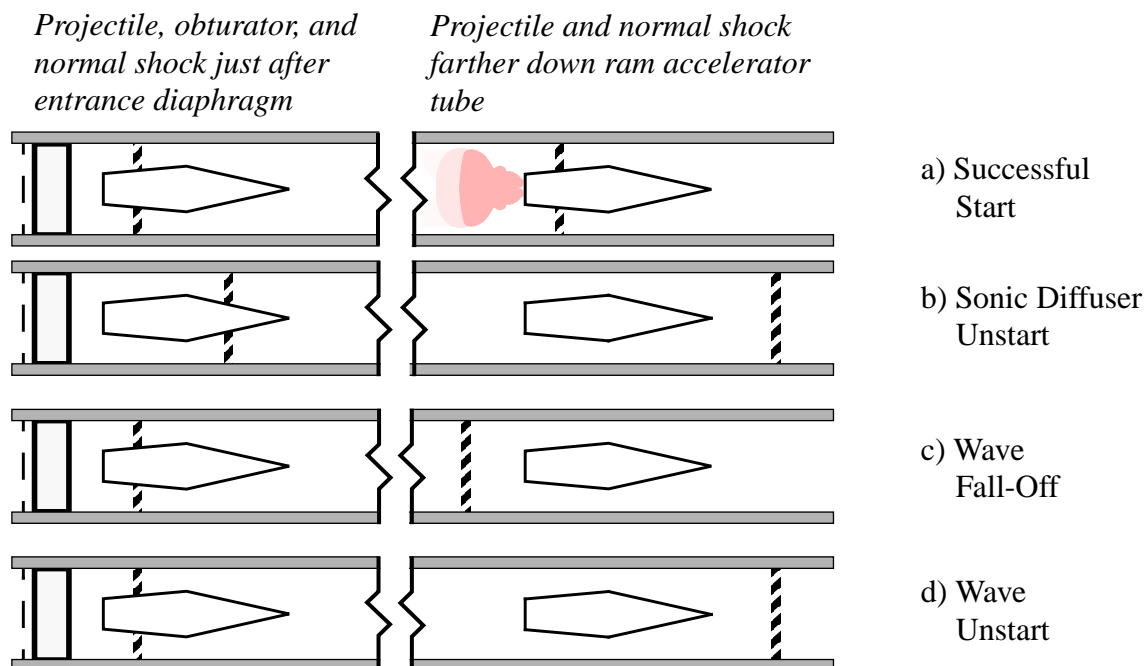
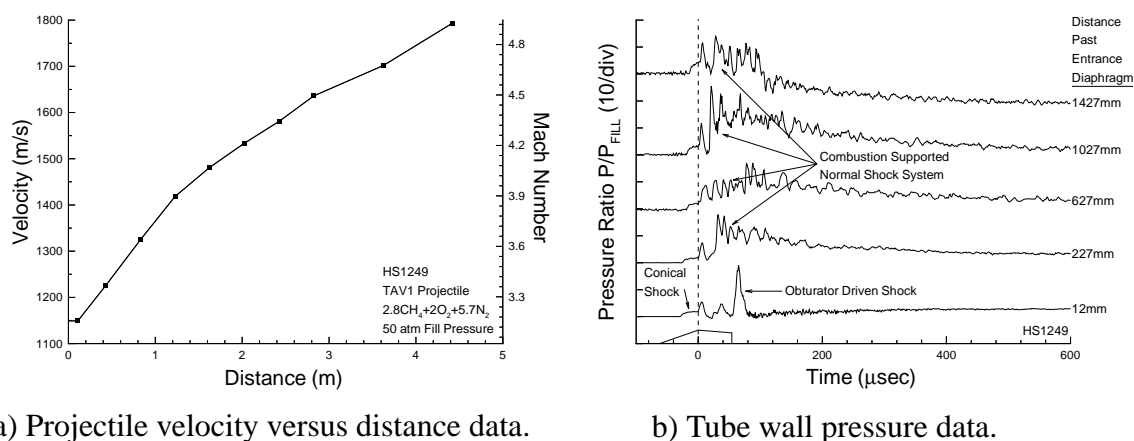


Fig. 2.4 Possible outcomes of an attempted start.



a) Projectile velocity versus distance data.

b) Tube wall pressure data.

Fig. 2.5 Experiment resulting in a successful start.

made at the 2 m tube joint.^{2,15} Plots of projectile velocity versus distance and tube wall pressure data for a successful ram accelerator start are presented in Fig. 2.5. A distance of 0 m is assigned to the location of the entrance diaphragm. The tube wall pressure data, presented as measured pressure normalized by tube fill pressure, are shown as a series of traces which originate from different instrumentation stations along the tube. A projectile outline is shown scaled relative to the average velocity. The lowest pressure trace, 12 mm after the entrance diaphragm, clearly shows the obturator-driven shock. The conical shock from the projectile nose tip is evident as the first pressure rise. Reflected oblique shocks, appearing as periodic pressure fluctuations, extend into the full tube area behind the projectile.¹² The projectile velocity is steadily increasing for over 2 m of travel and the stabilized combustion-supported shock system is evident in the pressure traces. The pressure trace from 1427 mm shows the tail of the signal decaying below the actual pressure at the tube wall due to thermal drifting of the piezoelectric transducer.

A sonic diffuser unstart (Fig. 2.4b) occurs when the flow is rendered sonic ahead of the throat due to upstream conditions. The flow chokes ahead of the throat when a projectile enters the propellant at a sufficiently low Mach number. A sonic diffuser unstart will also occur if the flow reaches sonic conditions ahead of the throat due to upstream combustion or projectile drag deceleration to a sufficiently low Mach number. Compression waves emanating from the sonic region coalesce into a shock and propagate

ahead of the projectile, causing rapid deceleration in the resulting high pressure zone on the projectile nose. The projectile Mach number necessary for supersonic flow through the diffuser to the throat (M_{sdu}) is given for steady, isentropic, quasi-one-dimensional flow by the area-Mach number relation,

$$\left(\frac{A_{tube}}{A_{throat}}\right)^2 = \frac{1}{M_{sdu}^2} \left[\frac{2}{\gamma+1} \left(1 + \frac{\gamma-1}{2} M_{sdu}^2 \right) \right]^{\frac{\gamma+1}{\gamma-1}} \quad \text{Eqn. 2.1}$$

where $\gamma = c_p / c_v$ is the ratio of specific heats of the gas mixture. A supersonic diffuser is a necessary, but not sufficient, condition for a successful ram accelerator start, and thus M_{sdu} forms an approximate low Mach number limit for attempting to start the ram accelerator. Figure 2.6 contains projectile velocity versus distance and tube wall pressure data from a shot which resulted in a sonic diffuser unstart caused by a low entrance Mach number. The projectile velocity steadily decreases upon entrance, and the pressure trace 227 mm past the entrance diaphragm shows the shock which arises after a sonic diffuser unstart.

A wave fall-off (Fig. 2.4c) occurs when the combustion-supported shock system recedes from the projectile body because of insufficient heat release. The projectile outruns the shock system and decelerates due to drag as it travels down the tube. Figures 2.7 and 2.8 contain projectile velocity versus distance and tube wall pressure data from shots which resulted in wave fall-offs in non-reactive and reactive mixtures, respectively.

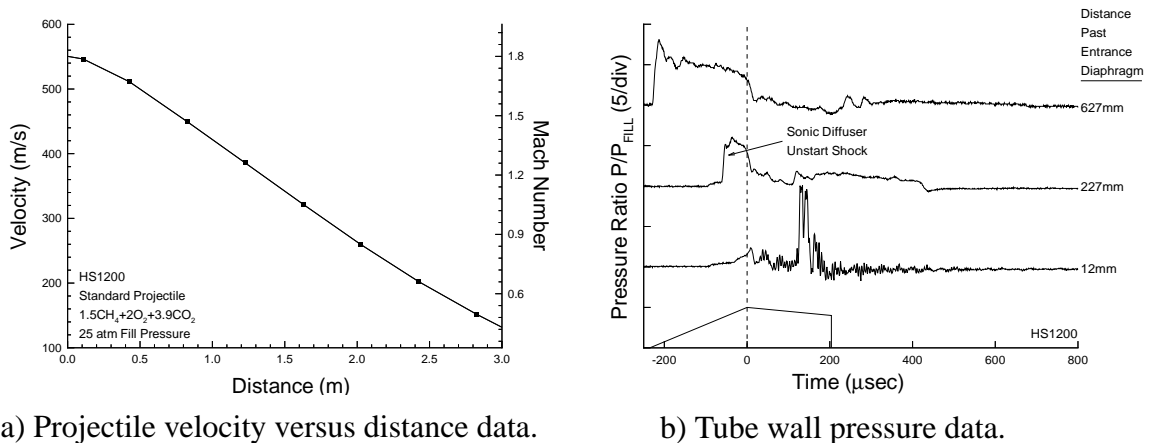


Fig. 2.6 Experiment resulting in a sonic diffuser unstart.

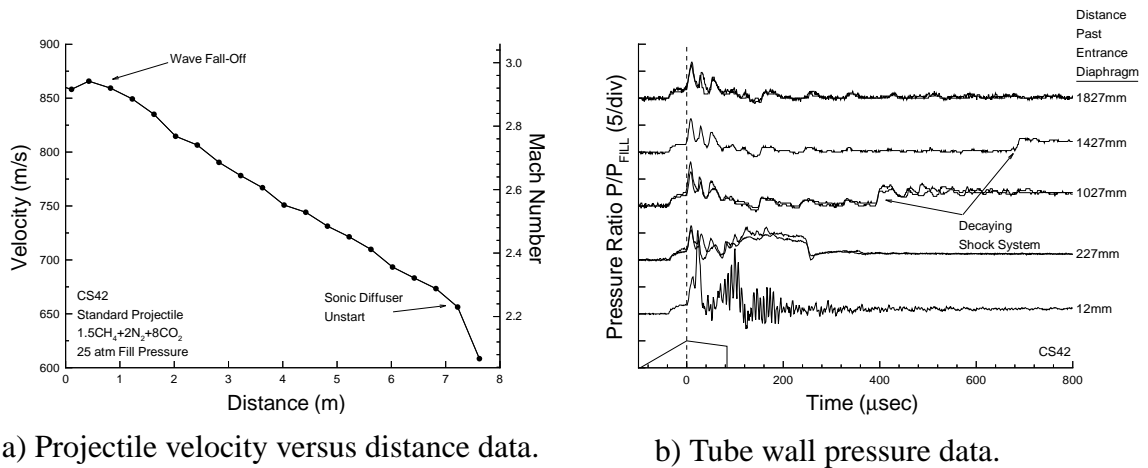


Fig. 2.7 Non-reactive experiment resulting in a wave fall-off.

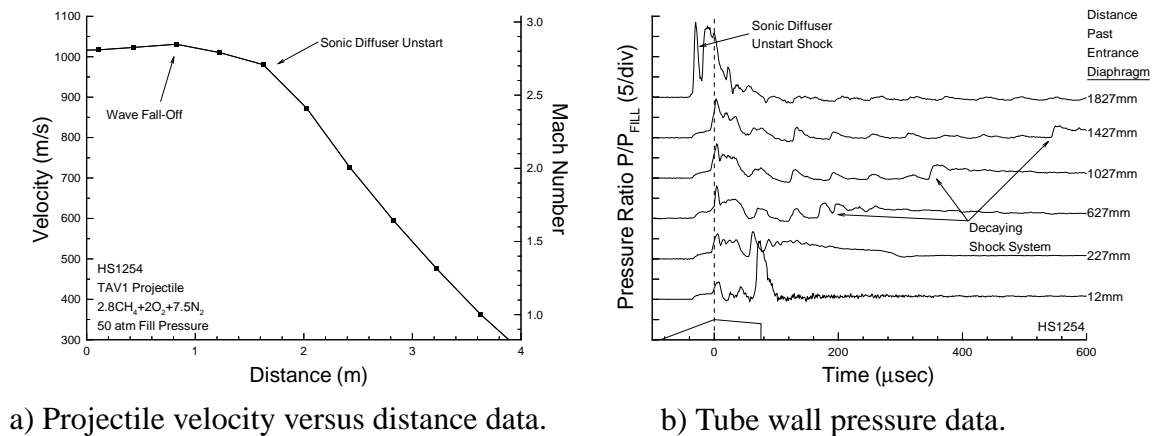


Fig. 2.8 Reactive experiment resulting in a wave fall-off.

Note the similarity of the shock system recession from the projectile base in the pressure plots, regardless of the presence of oxygen in the mixture. Both experiments shown eventually resulted in a sonic diffuser unstart after decelerating due to drag for some distance.

A wave unstart (Fig. 2.4d) is caused by conditions downstream of the throat resulting in disorgment of the shock system on the body into the diffuser. The projectile then rapidly decelerates in the high pressure region behind the shock. Figure 2.9 contains projectile and shock velocity versus distance and tube wall pressure data from a shot which resulted in a wave unstart. The wave velocity and pressure amplitude indicate that

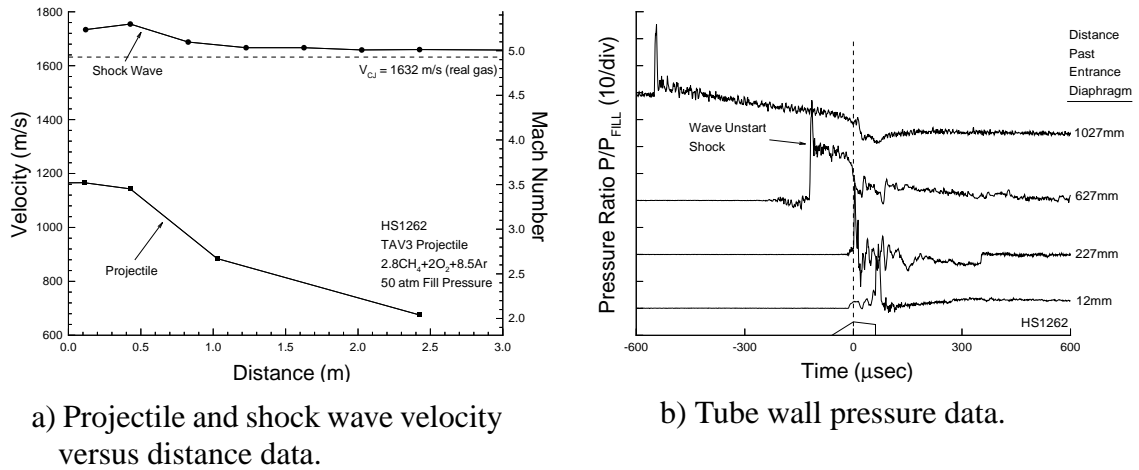


Fig. 2.9 Experiment resulting in a wave unstart originating on projectile body.

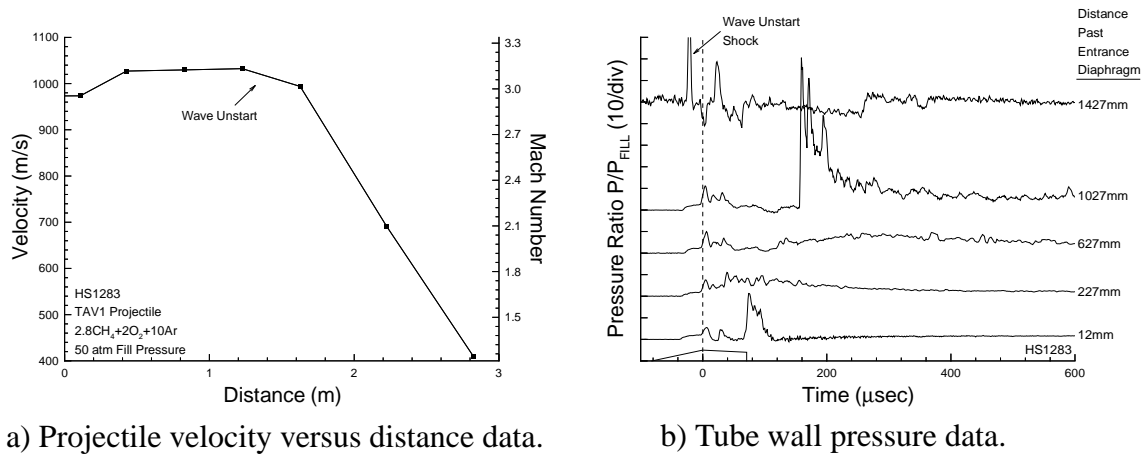


Fig. 2.10 Experiment resulting in a wave unstart originating in projectile wake.

the unstart wave is a detonation. Due to limited instrumentation density (approximately three projectile lengths between every instrument station) the location of detonation initiation relative to the projectile cannot be accurately discerned. Significant variation in pressure history data observed during different wave unstarts suggests that there exists more than one wave unstart mechanism. For example, projectile velocity versus distance and tube wall pressure data from a shot in which the unstart wave developed in the projectile wake are presented in Fig. 2.10. A high amplitude shock in the projectile wake

is first observed 1027 mm past the entrance diaphragm, which has surged beyond the projectile throat by 1427 mm.

The exact mechanism(s) by which a wave unstart occurs is unknown, although several hypotheses have been suggested. The following synopsis will be limited to the gasdynamic wave unstart hypotheses, as structural behavior leading to a wave unstart has already been well documented.^{11,16} The obturator and/or compressed launch tube gases may drive a shock system onto the body with such a forward velocity relative to the projectile that it overruns the throat. Alternatively, the wave unstart could be due to the combustion region releasing too much energy for the projectile Mach number.¹⁷ Conditions may be such that the mixture detonates behind the throat, resulting in a detonation wave propagating ahead of the throat. Theories of shock-boundary layer interactions causing separation that leads to a wave unstart in high energy propellants have also been suggested.^{18,19} Another concept is that as the projectile Mach number increases, the strength of the reflected shocks may grow to the point where propellant ignition takes place between the body and tube wall. Combustion between the body and tube wall, possibly propagating forward through the boundary layer, may contribute to the wave unstart mechanism. Excessive energy release occurring on the projectile nose was once thought to play a major role in the wave unstart process, but has been ruled out to an extent as a result of combustion stripping and re-ignition experiments.²⁰ Note that under the definitions set forth here, combustion in the diffuser would result in a sonic diffuser unstart and not a wave unstart.

2.3 Maximum Performance Starting Conditions

Ram accelerator performance is maximized at subdetonative velocities by operating at relatively low Mach numbers and in the highest energy release (Q) propellants possible.¹⁵ Greater thrust has been demonstrated analytically and experimentally in high Q propellants versus low Q propellants.²¹ The impetus for starting at a decreased Mach numbers is that relatively low Mach numbers have also been analytically and experimentally shown to increase the ram accelerator thrust. Furthermore, low Mach number starting is important to utilize the improved propulsive efficiency provided by the

ram accelerator over conventional guns by transitioning from gun to ram accelerator at lower velocity,⁵ and to minimize aerodynamic heating. Facilities with launch tube length constraints or low pressure initial launchers which can supply limited entrance velocity will be constrained to start at low Mach number.

2.4 Historical Perspective

The UW ram accelerator was conceived in 1983, and the facility became operational in 1985. Projectile firings into combustible mixtures are referred to as “hot shots” and given the designator HS, while projectile experiments in non-combustible mixtures are referred to as “cold shots” and given the designator CS. Piston experiments are frequently conducted in which a cylindrical object (typically an obturator) is fired into the ram accelerator to check instruments, track shocks, or investigate propellant reactive characteristics without the complication and expense of a projectile. Pistons shot into non-combustible mixtures are referred to as “slug shots” with the designator SS, while piston (sometimes attached to a subcaliber sphere) experiments in combustible mixtures are referred to as “detonation shots” with the designator DS. There have been 1320 hot shots, 63 cold shots, 116 slug shots, and 285 detonation shots conducted at the UW ram accelerator between September 27, 1985 and March 10, 1997.

The two facilities used prior to January 1990 (corresponding to HS1 - HS156 and HS157 - HS646) were similar to the one currently in operation, but the ram accelerator sections were 4.9 and 12.2 m long, respectively. The launch tube was 7.3 m long with twice the venting dump tank volume in communication with a 1.5 m long vent section (7% area perforation). The light gas gun, vacuum system, and diaphragm techniques were the same as currently used. A major difference from the typical starting process employed today was the use of a gunpowder ignitor system for some of the experiments.¹ A pellet mounted at the center of the entrance diaphragm was swallowed by a pitot tube in the projectile nose tip and struck a primer, igniting a black powder charge whose hot exhaust ejected from the projectile base. This relatively complicated starting mechanism was discarded after HS274 when it was discovered that starting was possible by gasdynamic means only. Inconsistent ram accelerator performance in multi-stage experiments prior to

October 1990 led to the discovery that propellant composition was inaccurate from one shot to another. The gas handling system received a major upgrade at this point (corresponding to HS754), after which the control of mixture composition and shot reproducibility was significantly improved.

From April 1990 to the present, the facility has been configured in the manner described previously. Appendix A contains a database of hot shot experimental data pertaining to the starting process from HS647 through HS1320. A statistical summary of the outcome for the 618 attempted starts with nominal projectile geometries in this hot shot range is presented in Table 2.2. Most start failures are attributed to specific investigations of the starting process; the nominal starting process has an 89% success rate. The “Other Unstart” designation indicates that the evidence is inconclusive as to whether a sonic diffuser unstart or wave unstart occurred, and “Unknown” refers to shots for which data are not available. Several experiments with unique projectile configurations are not included in this database of hot shots, including the quasi-two-dimensional and hollow projectiles shown in Fig. 2.11.

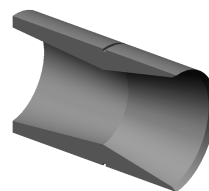
Table 2.2 Statistical results of start attempts for HS647 through HS1320.

Successful Start	67%
Wave Fall-Off	6%
Sonic Diffuser Unstart	<1%
Wave Unstart	11%
Other Unstart	2%
Human Error	1%
Unknown	12%

The “standard” projectile geometry has not changed radically from that shown in Fig. 1.3 during the operational lifetime of the UW ram accelerator. Projectiles with variations in nose cone angle, nose length, throat diameter, body length, body taper angle, base diameter, number of fins, fin thickness, fin rake angle, and fin location have been used



a) Quasi-2D projectile.



b) Hollow projectile (cut-away view).

Fig. 2.11 Unique projectile configurations.

in experiments. Projectile materials used include polycarbonate, magnesium, aluminum, and titanium, sometimes used in conjunction with brass or copper bearing surfaces and Teflon or nickel coatings. The masses of projectiles fired range from 50 gm to 110 gm, and are commonly on the order of 75 gm for an aluminum projectile.

The typical obturator geometry is the perforated configuration shown in Fig. 1.4a. The obturator is usually made of polycarbonate, although sometimes a magnesium or aluminum faceplate is attached for increased strength. Obturator mass (including backplate for perforated geometries) is typically around 16 gm, but masses from 10 to 36 gm have been used.

The nominal propellant mixture for the starting process is $2.8\text{CH}_4+2\text{O}_2+5.7\text{N}_2$, with small perturbations in the methane and nitrogen content. Methane- and oxygen-based propellants with carbon dioxide, argon, or helium as diluents have also produced successful starts. Propellant fill pressures from 10 to 50 atm have been used, with projectile entrance velocities typically around 1150 m/s (Mach 3.1). Successful starts have been achieved at a minimum entrance velocity of 715 m/s and a maximum entrance velocity of 1361 m/s. Helium up to 340 atm pressure is the primary light gas gun constituent, although on occasion the pressure has been increased to 375 atm and/or hydrogen added to attain higher entrance velocities or to handle more massive projectiles. Stationary blocks within the breech can also be removed for better initial launcher performance by allowing a larger volume of driver gas.

2.5 Literature Review

The following sections summarize information from the ram accelerator literature which pertain to the starting process. Research conducted at the UW is discussed in detail because it is most pertinent to this investigation, and that from other organizations is briefly summarized. The information is organized according to facility, because no two facilities are the same. Unless otherwise noted, projectile geometries used by the different facilities are similar with conical forebody, constant diameter or tapered midsection, and either a blunt base or conical afterbody. The exact projectile configurations used are available in the cited references. The locations of ram accelerator facilities currently in use are presented in Fig. 2.12, and Table 2.3 (arranged in historical order) contains general characteristics of each. All facilities are operational with the exception of the one at Saitama, Japan which is currently under construction. Two other facilities, the Impact Research Laboratory in Albuquerque, NM and Elgin Air Force Base, FL, were operational in the past but have since ceased ram accelerator activity.

Table 2.3 Ram accelerator facility characteristics.

#	Location	Bore	Initial Launcher	Launch Tube	Ram Tube
1	Seattle, WA	38 mm Smooth	Light Gas Gun	6 m	16 m
2	Aberdeen, MD	120 mm Smooth	Powder Gun	4.7 m	9.2 m
3	St. Louis, France	30 mm Railed 30 mm Smooth 90 mm Smooth	Powder Gun Powder Gun Powder Gun	1.8 m 3.3 m 9.4 m	7.2 m 6 m 16 m
4	Sendai, Japan	25 mm Smooth	Powder Gun	4 m	6 m
5	Hiroshima, Japan	15 x 20 mm Railed	Light Gas Gun	3 m	2 m
6	Mianyang, China	37 mm Smooth	Powder Gun	4.9 m	4.8 m
7	Seoul, South Korea	22 mm	Powder Gun	N/A	15 m
8	Saitama, Japan	20 mm Smooth	N/A	N/A	N/A

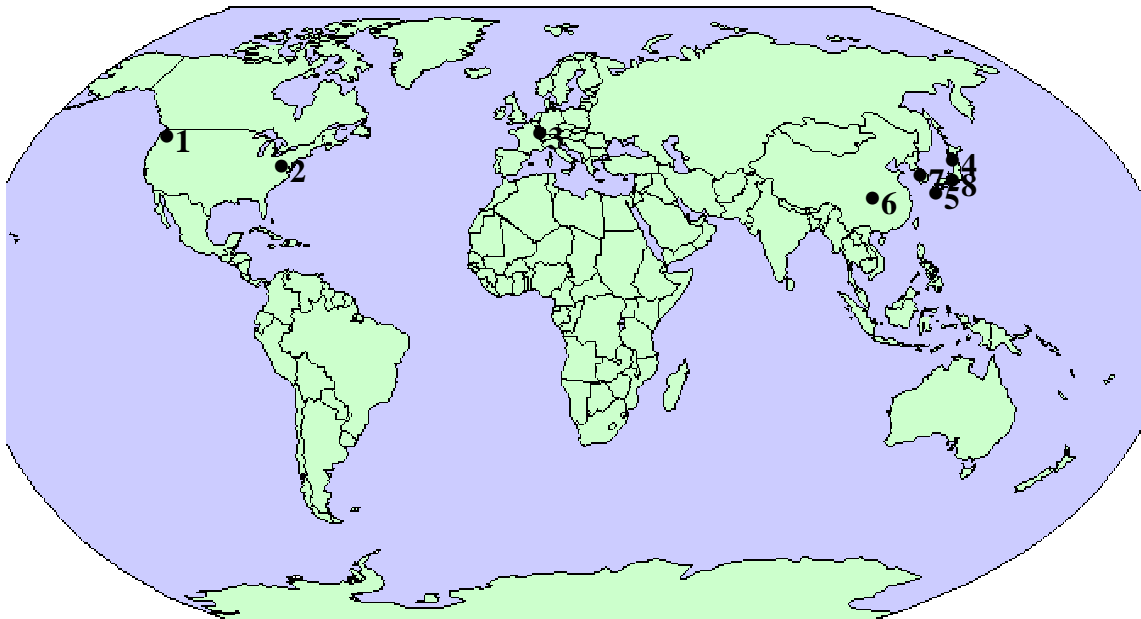


Fig. 2.12 Current ram accelerator facility locations.

2.5.1 University of Washington

The understanding of the starting process at the University of Washington (UW) facility in Seattle, WA, USA has been furthered by several efforts. An experimental investigation by Burnham et al.^{22,23} utilized a Highly Instrumented Tube Section (HITS) to provide high spatial resolution pressure and luminosity measurements of the flowfield around the projectile during the starting process. The HITS is 180 mm long with four circumferential instrument stations every 20 mm, and was placed immediately before and after the entrance diaphragm. A discussion of diagnostic deficiencies of the piezoelectric pressure transducers and fiber optic luminosity probes was provided. The pressure transducers may lag in time response by a few microseconds, and dynamic response combined with recess distance from the tube wall can cause amplitude overshoot of 35%. The luminosity sensors were found to be unreliable (30 to 40% failure rate), and therefore a “no luminosity” signal was disregarded. These sensors also have the tendency to detect light occurring away from their instrument stations because of reflections in the tube.

The sonic diffuser unstart Mach number (M_{sdu}) for the standard projectile and propellant was found through a series of cold shots (25 atm $2.7\text{CH}_4+7.8\text{N}_2$) to occur

between Mach 2.51 and 2.63. It was noted that in the case of a sonic diffuser unstart, pressure transducer measurements immediately after the entrance diaphragm appeared nominal. The unstart shock wave ahead of the throat was only observed after 70 mm of travel past the entrance diaphragm.

Hot shots (25 atm $2.7\text{CH}_4+2\text{O}_2+5.8\text{N}_2$ with standard projectile at nominal entrance velocity) were conducted to investigate the use of solid obturators, variation in launch tube residual air pressure, and obturator blow-by. In all cases (both cold and hot shots) the compression of the launch tube gases between the obturator and entrance diaphragm was observed by the pressure transducers and luminosity sensors. Shock reflections were tracked and a radiating luminosity region was detected just prior to the entrance diaphragm.

Successful starts were obtained with solid 11 gm obturators, although the discussion points out that the solid obturator is less forgiving than the perforated geometry because the solid obturator generated shock was closer to the projectile throat. This statement is regarded as speculative in light of the measured shock location difference of a few microseconds, and the instrumentation time resolution being of the same order.

The residual air pressure in the launch tube was raised above nominal (5 torr) to 50 torr. A successful start occurred with an entrance diaphragm thickness of 1.8 mm, but an immediate unstart upon entrance resulted for a diaphragm thickness of 0.7 mm. The conclusion made was that the compressed launch tube gas caused the thinner diaphragm to rupture prematurely. A shock propagated into the propellant ahead of the projectile, initiating combustion and thus reducing the effective projectile Mach number below M_{sdu} .

An undersized solid obturator (37.1 mm diameter) with 5% blow-by area resulted in an immediate unstart upon entrance with a diaphragm thickness of 1.8 mm. The blow-by gas contributed to the compressed launch tube gas, prematurely rupturing the diaphragm. The same conclusion as for the elevated residual air pressure start failure was made: the shock propagating into the propellant ahead of the projectile ignited the gas and decreased the effective projectile Mach number below M_{sdu} . Ideas were presented for using multiple diaphragms and/or adding launch tube vents just prior to the entrance diaphragm to

alleviate the diaphragm pre-break problem occurring in situations with relatively high levels of blow-by or residual air pressure.

A wave fall-off occurred when a 40 mm long buffer section filled with 25 atm $2.7\text{CH}_4+7.8\text{N}_2$ was placed between the launch tube and the propellant-filled tube. Reducing the residual air pressure to 0.5 torr and limiting blow-by to a minimum through the use of a solid obturator with a Bridgman seal also resulted in a wave fall-off. These experiments identified the compressed launch tube gas as a primary ignition source in the starting process. The ram accelerator was unable to start under otherwise nominal conditions in the absence of the compressed launch tube gas contacting the propellant.

The computational investigation by Burnham et al.^{22,23} utilized a one-dimensional unsteady code to examine launch tube gas compression, and both two-dimensional and axisymmetric, unsteady, reacting (global induction/reaction time model) Euler codes to study entrance into the propellant. Through modeling of blow-by and residual air pressure, the one-dimensional code was able to accurately reproduce the experimental launch tube data. Very high pressure and temperature regions were verified in the immediate vicinity of the entrance diaphragm. The addition of a quasi-one-dimensional projectile area profile to the obturator did not significantly affect the computational results in the launch tube.

The axisymmetric unsteady Euler reacting code was unable to capture the combustion stabilization process near the projectile base because of its inviscid nature. The code was able to determine limits for obtaining supersonic flow through the diffuser. Results from transition simulations with the projectile, obturator, and compressed launch tube gas entering the ram accelerator section qualitatively displayed the observed experimental phenomena. Relatively low compressed launch tube gas pressure and temperature (obtained by minimizing residual air and/or blow-by in the simulation) resulted in little propellant energy release and therefore a wave fall-off. Relatively high compressed launch tube gas pressure and temperature (obtained by increasing residual air and/or blow-by in the simulation) resulted in a shock propagating into the propellant ahead of the projectile causing choking of the diffuser. Some cases were found in which the compressed launch tube gas would cause a shock to initially propagate ahead of the

projectile, but for which the projectile diffuser was able to swallow the shock a short time after entrance into the propellant.

An experimental investigation is currently being carried out by Stewart et al.^{24,25} to look at the effects of plugging the launch tube vent holes and increasing the launch tube residual air pressure. Significantly higher levels of launch tube gas compression are reached in the ventless versus vented configuration. Hot shots conducted into $2.8\text{CH}_4+2\text{O}_2+5.7\text{N}_2$ at 1150 m/s entrance velocity with a 0.7 mm thick Mylar entrance diaphragm have identified a limit to successfully start in ventless configuration with 5 torr residual air in the launch tube. A successful start occurs for propellant fill pressures at or above 30 atm, while an immediate unstart upon entrance results if the fill pressure is 25 atm. A diaphragm thickness of 1.4 mm permitted a successful start at 25 atm fill pressure, indicating that the dynamics of the diaphragm play a role in the starting process.

Experiments were conducted in the vented configuration with the same propellant and entrance velocity, but at 50 atm fill pressure and with a 3.6 mm thick Mylar diaphragm, for residual air pressures from 5 to 212 torr. Increasing compression of the launch tube gas was consistently observed as the residual air pressure was increased. A successful start occurred at or below 160 torr residual air pressure, and an immediate unstart upon entrance at 176 torr and above. A cold shot resulted in an immediate unstart upon entrance for a residual air pressure of 207 torr, indicating that the cause of the unstart is not combustion related. The compressed launch tube gas drives a shock into the propellant, either through premature rupture of the entrance diaphragm or when pierced by the projectile nose. This shock raises the propellant temperature and induces mass motion away from the projectile. This combination decreases the effective projectile Mach number, resulting in a sonic diffuser unstart.

No data have been formally presented regarding the effect of the diaphragm on the projectile, but several experiments have been conducted which assure that minimal projectile damage is incurred by passing through the diaphragm. Some of the experiments by Stewart et al. utilized a 3.6 mm thick Mylar entrance diaphragm and resulted in successful starts. Other experiments demonstrated that the projectile performance is not

affected by passing through 0.7 mm of Mylar diaphragm every 4 m of travel down the entire 16 m ram accelerator tube.

Due to the limited diagnostics available for use in the extreme environment of the UW ram accelerator, there is no direct evidence of whether or not thermal choking actually occurs between the projectile and the obturator. However, the excellent agreement between experimental velocity versus distance data and that predicted by an end-state Hugoniot analysis performance code provides strong support for the case that a thermally choked region does exist at full tube area behind the projectile travelling at subdetonative velocities.²⁶ Luminosity measurements for projectiles at subdetonative velocities indicate that the primary combustion zone is at or behind the base of the projectile.

A few experiments were conducted by Higgins et al.^{17,18} in which a driving standard projectile (already successfully started) was run through 4 m of inert gas to strip the combustion wave, and then transitioned back into a combustible mixture. In the case of a Mach 4.2 projectile entering $2.8\text{CH}_4+2\text{O}_2+3.8\text{N}_2$ at 25 atm pressure, a new combustion wave formed in the projectile wake, propagated towards the projectile, attached itself to the base, and accelerated the projectile. The combustion stripping and re-ignition experiment demonstrated that successful starting can occur under certain conditions without the presence of an obturator and residual launch tube gas. Other similar experiments transitioning from inert gas into different propellants at different Mach numbers resulted in either no propellant ignition (similar to a wave fall-off in start attempts with an obturator) or in wave unstarts.

McFall et al.²⁷ performed a numerical analysis of a zero velocity starting process which may allow ram accelerator operation without an initial launcher. The projectile and obturator begin at rest in a launch tube filled with low pressure gas. A diaphragm ahead of the projectile separates the low pressure launch tube from the high pressure, propellant filled tubes. The diaphragm is ruptured, causing the high pressure propellant to expand into the launch tube and over the projectile. The effective Mach number and ignition characteristics are tailored such that thrust is provided to the projectile in a manner analogous to normal operation, where the projectile is travelling through a quiescent

propellant. This shock/expansion tube type of starting process would accelerate the projectile up to Mach numbers suitable for entrance into quiescent propellant. The numerical analysis examined the basic gasdynamic and kinetic issues associated with the zero velocity start technique. Variables explored included the Mach number, sound speed, projectile and obturator location relative to the burst diaphragm, launch tube gas pressure, and propellant gas pressure. The numerical results indicate that the technique is feasible, although as yet no experimental efforts have been conducted to support these findings.

2.5.2 Army Research Laboratory

Kruczynski et al.^{6,28,29} reports experimental results and Nusca et al.³⁰ discusses computational investigations on the starting process of the Army Research Laboratory (ARL) facility in Aberdeen, MD, USA. The entrance diaphragm is made of polyvinyl chloride (PVC), and a vent section exists in the launch tube. The 4.3 kg aluminum projectile is similar to the standard UW design scaled to 120 mm bore, and a 0.5 kg solid nylon obturator with an aluminum faceplate is used. Successful starts have been achieved in $3\text{CH}_4+2\text{O}_2+10\text{N}_2$ from 50 to 85 atm fill pressure, with an entrance velocity of 1200 m/s. A wave unstart occurred at 100 atm fill pressure with this propellant. An experiment with a relatively short 3 kg projectile fired into 68 atm of $2.6\text{CH}_4+2\text{O}_2+6.9\text{N}_2$ at 1420 m/s entrance velocity also resulted in a successful start.

The numerical simulations of the starting process are based on axisymmetric, unsteady, Reynolds averaged Navier-Stokes equations with a Baldwin-Lomax turbulence model and a global methane/oxygen reaction (1 or 3 step) model for the 50 atm $3\text{CH}_4+2\text{O}_2+10\text{N}_2$ propellant. The simulation is initialized with the obturator (backpressure of 272 atm) attached to the projectile base travelling at Mach 3.5 in the propellant. The projectile and obturator dynamics are updated every 0.2 ms, corresponding to 250 mm of travel at the 1250 m/s entrance velocity. The obturator backpressure is set to atmospheric after 0.4 ms, and the obturator influence is neglected after it separates by five projectile lengths (approximately 1 ms from the start of the simulation).

Flow stagnation on the obturator generates a normal shock on the projectile body and a combustion front on the nose. As the obturator separates, the normal shock is observed to fall off of the projectile body. Combustion continues to occur in the throat region due to shock heating, in the boundary layers of the projectile and tube wall due to viscous heating, and downstream of the normal shock.

The initial normal shock location is consistent with experimental pressure measurements, but the location of the combustion front is inconsistent with experimental luminosity measurements (especially considering the relatively high dilution level of this propellant). Continued combustion ahead of the throat is contradicted by experimental measurements, as is the normal shock falling off the body for a projectile accelerating at subdetonative velocities. The disagreements between the computational results and the experimental data could be a result of inadequate modeling of the obturator dynamics (back pressure, update time step, and blow-by), the kinetics model, the axisymmetric modeling of an inherently three-dimensional flowfield, the turbulence model, and the lack of modeling the complete starting process (i.e., projectile and obturator transition from a partially evacuated launch tube).

2.5.3 Advanced Projects Research Inc.

A 38 mm smooth bore superdetonative facility was once operated by Advanced Projects Research Inc. (APRI) at the Impact Research Laboratory in Albuquerque, NM. Humphrey et al.^{31,32} provides information on the facility and discusses starting issues which arose in this technology demonstration project. A total of 18 shots was attempted. A two-stage light gas gun was used to launch a 120 gm aluminum projectile into a propellant of hydrogen and air (mixture ratio unspecified) at entrance velocities from 2800 to 3200 m/s (approximately Mach 8.2, or 195% V_{CD}). The projectile was supported by a 76 gm assembly consisting of a nylon sabot, a polypropolux obturator, and an aluminum pusher plate. Starting problems addressed included venting of the sabot base pressure, sabot separation, venting of the sabot stripper gas, and obtaining supersonic flow through the diffuser. Various launch tube configurations (all several meters long) were used, including a sabot stripper section filled with 1 atm air and vent sections with several torr

residual air pressure on both sides of the stripper section. A numerical analysis highlighted two modes of achieving supersonic flow through the diffuser prior to entrance into the propellant. One mode involved the projectile overtaking the forward travelling shock weakened by the final vent section, and the other mode required swallowing of the shock after it reflected off the entrance diaphragm. Three successful starts were achieved with a projectile flow throat-to-tube area ratio of 0.43, but no successful starts were achieved with an area ratio of 0.24. Instrumentation difficulties prohibited identification of the combustion mechanism, which may have been shock induced combustion, an oblique detonation wave, or a combusting projectile.³³

2.5.4 Institut of Saint-Louis

The Institut of Saint-Louis (ISL) is a French-German research institute in Saint-Louis, France with three ram accelerators. The starting process of the subdetonative 90 mm smooth bore facility is described by Giraud et al.⁸ Superdetonative studies in two 30 mm bore ram accelerators, one with a railed bore and the other a smooth bore, are described by Seiler et al.^{7,34,35} Smooth and rail bore tube cross sections are illustrated in Fig. 2.13.

The 90 mm facility operates at fill pressures from 30 to 45 atm with projectile entrance velocities of 1330 m/s. The 1.34 kg projectile is similar to the standard UW projectile, while the 0.34 kg obturator is composed of four separate pieces designed to minimize blow-by and separate from the projectile upon propellant impact. The final 4 m

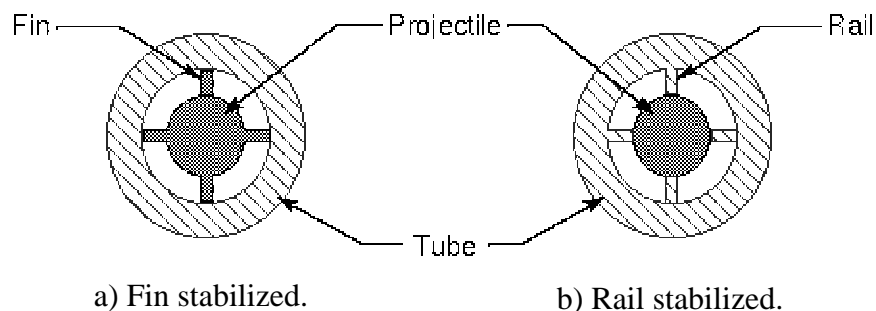


Fig. 2.13 Ram accelerator tube cross sections.

of launch tube before the PVC entrance diaphragm is perforated for powder gun gas venting. Propellants used for the starting process include $3\text{CH}_4+2\text{O}_2+10\text{N}_2$ and $3.6\text{CH}_4+2\text{O}_2+7.5\text{N}_2$. Wave unstarts have been observed upon entrance to a $2.7\text{CH}_4+2\text{O}_2+5.6\text{N}_2$ propellant at 15 and 30 atm. Obturator separation from the projectile has been studied, with the obturator still attached when the projectile nose pierced the entrance diaphragm. A distance of 90 mm between the obturator and projectile and a differential velocity of 190 m/s were observed when the projectile base reached the diaphragm location. Some experiments have been performed to examine the relative importance of the powder gun gas, projectile, and obturator in the propellant ignition process. Interaction of the obturator with the propellant was identified as the primary source of ignition. However, successful starting experiments were conducted in which the obturator was mechanically stripped from the projectile while in the launch tube vent section. Luminosity measurements indicate that the primary combustion region is in the recirculating region behind the bluff projectile base.

The 30 mm railed-bore facility operates with 130 gm axisymmetric projectiles, while a fin-guided projectile (80 to 110 gm depending on the material) is used in the 30 mm smooth bore facility. The launch tube contains vent holes just prior to the entrance diaphragm. No obturator is employed for the rail tube launch process, while the smooth bore uses a 32 gm obturator that is stripped by a 1.5 m long section of launch tube filled with 20 atm carbon dioxide. Successful rail facility superdetonative starts were obtained at an entrance velocity of 1800 m/s in 20 to 27 atm carbon dioxide diluted propellants with methane, ethylene, or hydrogen as fuels. Relatively low diluent concentrations resulted in projectile unstarts shortly after entrance. Start attempts at 1800 m/s in the smooth bore facility have been made in $2\text{H}_2+\text{O}_2+(5.7 - 6.3)\text{CO}_2$ propellants, although they seem to have been unsuccessful. X-ray photography in both facilities reveals significant projectile erosion after leaving the propellant filled tubes. Many material types and coatings have been used in an attempt to alleviate this problem. It is not clear whether any severe projectile erosion or burning occurs during the starting process.

2.5.5 Tohoku University

Sasoh et al.^{9,36,37} report experimental results and flow visualization of the starting process at the Tohoku University facility in Sendai, Japan. Holes are located just prior to the entrance diaphragm for venting of launch tube gases. The launch tube residual air pressure is typically 0.75 to 15 torr, and 0.03 to 0.5 mm thick Mylar serves as the entrance diaphragm. The projectile is scaled to 25 mm bore from the UW standard projectile, and the typical entrance velocity is 1120 m/s. Perforated polycarbonate obturators were found to fail structurally during the powder gun launch process, thus solid polycarbonate or perforated magnesium obturators are currently used. At this time cold shots have shown supersonic flow through the diffuser, but limited success has been achieved with hot shots. One successful start has been achieved, although not reproduced, in 25 atm $2.8\text{CH}_4+2\text{O}_2+4.6\text{N}_2$ at 1211 m/s entrance velocity.

Visualization of projectile travel through the entrance diaphragm into a non-combustible mixture has been performed with a system of aspherical lenses. Holographic interferometry shows a well defined conical shock from the projectile nose just after it pierces the entrance diaphragm. High speed camera pictures reveal shocks reflecting between the obturator and the entrance diaphragm as the launch tube gas is compressed. For experiments with 1 to 2 torr residual air pressure there is no noticeable light emission until the projectile nose pierces the diaphragm; the light produced after this impact may be due to combusting Mylar. An experiment with 10 torr residual air pressure indicates the high temperature nature of the compressed launch tube gas by a luminous region adjacent to the entrance diaphragm prior to projectile arrival.

Hollow projectiles have been shot in a collaborative program between Tohoku University and the UW (Fig. 2.11b). Average projectile mass is 100 gm, and the 10° diffuser angle was increased to 30° at the tip to minimize projectile damage upon impact with the entrance diaphragm. A successful start was achieved in 25 atm $2.8\text{CH}_4+2\text{O}_2+3\text{CO}_2$ at 1100 m/s entrance velocity. Carbon dioxide concentration of 4 moles resulted in a wave fall-off, while 2.5 moles caused a wave unstart. The minimum Mach number for maintaining supersonic flow through the diffuser in this mixture class was 3.5. Numerical simulations of shots into inert gas were conducted to gain an

understanding of the flow through the projectile, as this region could not be monitored during experiments.

2.5.6 Hiroshima University

Chang et al.^{10,38} report experimental results and flow visualization of the starting process at the Hiroshima University rectangular bore facility in Hiroshima, Japan. The launch tube is perforated over the last meter to vent the initial launcher gas behind the 5 gm polypropylene obturator. The 5 gm polypropylene projectile is a two dimensional wedge, guided by the two tube rails running through grooves in the projectile sides. Typical launch tube residual air pressure is 0.9 torr, ram accelerator fill pressure is 1 to 5 atm, and entrance velocities are around 1000 m/s. Cold shots into nitrogen, carbon dioxide, and argon have successfully demonstrated supersonic flow through the diffuser, and the sonic diffuser unstart Mach number in these gases has been identified. The ram acceleration tube contains several windows through which Schlieren visualization of the shock system about the projectile is conducted. Images from experiments compare well with the flowfield characteristics predicted numerically. Successful starts during hot shot experiments have not been reported yet.

Quasi-two-dimensional projectiles were shot in the UW facility at 25 atm fill pressure to support hot shot experiments at Hiroshima University (Fig. 2.11a). The projectile base geometry required the addition of an aluminum faceplate to the standard UW perforated obturator to maintain its structural integrity during the initial launch. Cold shots into pure nitrogen were conducted to identify the sonic diffuser unstart Mach number. An entrance velocity of 1180 m/s into $2.8\text{CH}_4+2\text{O}_2+6.7\text{N}_2$ resulted in a successful start, while lower concentrations of nitrogen led to wave unstarts.

2.5.7 Seoul University

The Seoul National University in Seoul, Korea has conducted a numerical study of the ram accelerator starting process at superdetonative velocities.¹⁹ Axisymmetric, unsteady, Reynolds averaged Navier-Stokes governing equations with a Baldwin-Lomax

turbulence model were used in conjunction with finite rate chemistry to understand projectile transition in a 40 mm bore tube at 2500 m/s from 1 atm air into 25 atm $2\text{H}_2+\text{O}_2+(3.76 - 9)\text{N}_2$. The 150 gm axisymmetric projectile model did not include the rails required to center such a projectile in the tube. Successful starts were observed in propellants with nitrogen concentration from 5 to 9 moles, and for the 9 mole case a thrust equal to drag (constant velocity) condition occurred. Shock-induced or oblique detonation wave combustion occurred over the constant area section or the aft cone in the successful start cases. Oblique detonations were supported by separated regions caused by shock impingement on the projectile boundary layer. Start failures resulted for propellants diluted with 3.76 and 4.5 moles nitrogen; in these cases an oblique detonation wave attached itself to the tip of the projectile nose cone.

2.5.8 China Aerodynamics Research & Development Center

No formal literature exists on the China Aerodynamics Research and Development Center (CARDC) facility in Mianyang, China. However, personal communication with Dr. Lieu Sen of CARDC has indicated that the launch tube has a 2.4 m long vent section, and that Mylar entrance diaphragms are used to separate 20 atm propellant fill pressure from 60 torr residual air pressure in the launch tube. The projectile is scaled to 37 mm bore from the UW standard projectile, and typical entrance velocities are approximately 1150 m/s. Problems have been encountered with the powder gun initial launcher causing failure of perforated polycarbonate obturators. Successful cold shot experiments into pure nitrogen have been conducted, and the sonic diffuser unstart Mach number has been identified. No successful starts in hot shot experiments are known to have been achieved at this time.

3. Experimental Procedure

Projectile experiments form a significant recurring expense for a ram accelerator facility, thus a cost-effective means for characterizing the starting process without projectiles is desirable. Part of this investigation involves piston detonation experiments as an efficient way to study how propellant chemistry, entrance Mach number, launch tube air pressure, and obturator configuration influence the starting process. The remainder of this investigation involves projectile experiments shot under various conditions to study the effect of propellant chemistry, entrance Mach number, throat area, and obturator configuration on the starting process. Much of the pertinent data from the projectile experiments are summarized in tabular form in Appendix A. Data from the piston detonation experiments are summarized in Appendix B.

All projectile and piston experiments were conducted in the UW ram accelerator facility shown in Fig. 1.2.³⁹ A schematic of the instrument station configuration near the entrance diaphragm is presented in Fig. 3.1. There are two instrument stations in the launch tube, 12 and 139 mm before the entrance diaphragm. The first instrument station in the ram accelerator tube is located 12 mm after the entrance diaphragm, followed by a station 227 mm down the tube. There is a 400 mm interval between subsequent stations down the remainder of the ram accelerator tube. All stations were instrumented with electromagnetic sensors and piezoelectric pressure transducers (PCB model 119) at the tube wall. The launch tube stations and first three ram accelerator tube stations also contained fiber optic luminosity sensors for some of the experiments. The gas handling

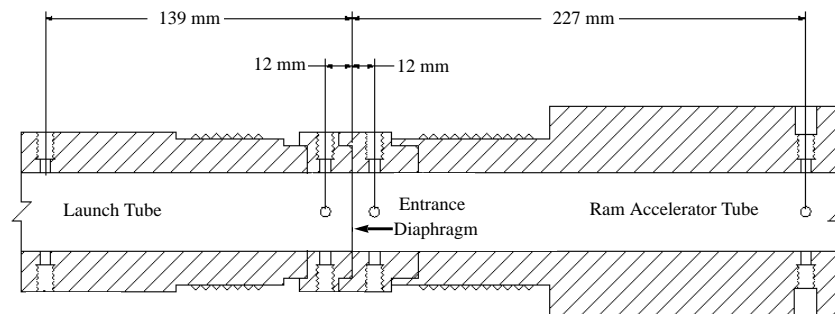


Fig. 3.1 Instrument station configuration near entrance diaphragm.

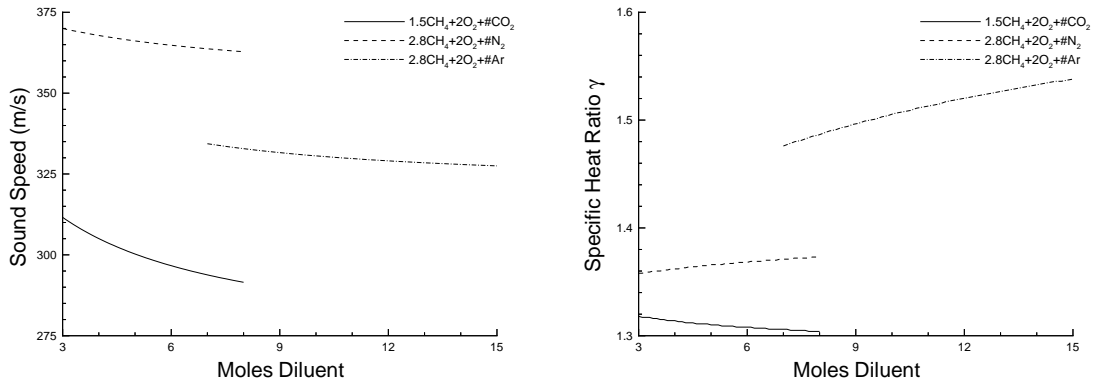
system of the UW facility, supported by gas chromatography, provides absolute mixture accuracy to within 5%, with relative precision of approximately 1% when varying mixtures.

The nominal launch tube residual air pressure was 3 to 5 torr, monitored by a Kistler 4043A1, 0 to 1 atm piezoresistive transducer. Pressure in the launch tube was reduced below 3 torr by adding additional vacuum pumps to the system, while increased pressure was effected by bleeding air into the evacuated launch tube. The entrance diaphragms used were 0.36 and 0.72 mm thick Mylar for 25 and 50 atm fill pressures, respectively. The entrance Mach number was varied by adjusting the gas pressure in the initial launcher to change the projectile or piston velocity history in the launch tube, and through propellant chemistry changes to adjust the sound speed.

The propellant composition was varied by introducing various amounts of carbon dioxide, nitrogen, argon, helium, or hydrogen to fixed amounts of methane and oxygen. A “class” of propellant is characterized by its fuel-oxygen stoichiometry with a variable concentration of a specific diluent. The fill pressure of the carbon dioxide diluted propellants was 25 atm, limited by a combination of the facility’s gas handling system and carbon dioxide’s low liquefaction pressure at 300 K. A fill pressure of 50 atm was used for most experiments in the other propellants. Properties of frequently used propellants are presented in Fig. 3.2. The non-dimensional equilibrium energy release of combustion (Q_{CJ}) and the detonation wave Mach number (M_{CJ}) are both taken at the Chapman-Jouguet state (thermally choked). A chemical equilibrium code utilizing a real gas equation of state was used to compute M_{CJ} and Q_{CJ} because of the significant departure from ideal gas values at fill pressures above 15 atm.⁴⁰ The induction times (τ_{indCJ}) and lengths (L_{indCJ}), referenced to the peak OH radical concentration, were computed for an incident shock of M_{CJ} with the ideal gas CHEMKIN thermochemical routines⁴¹ and the GRI-1.2 reaction mechanism for methane oxidation.⁴²

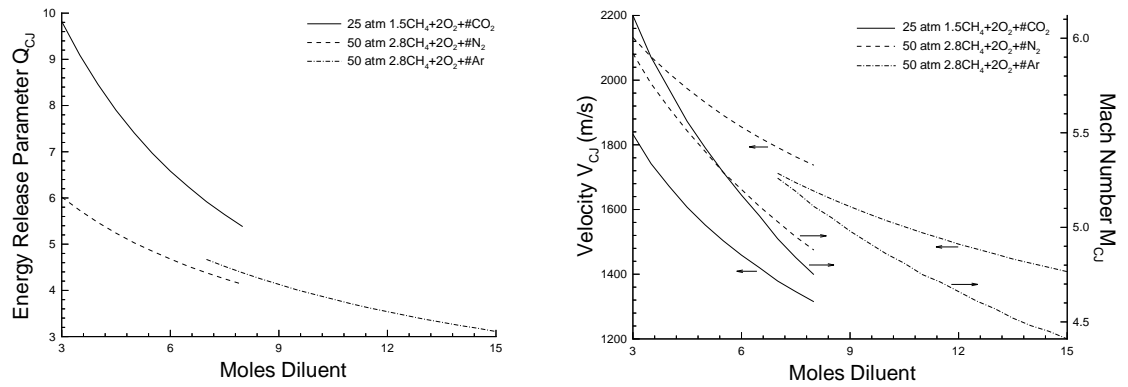
3.1 Piston Experiments

Piston initiated detonation experiments were conducted with various propellants, entrance Mach numbers, piston configurations, and launch tube pressures as a means of



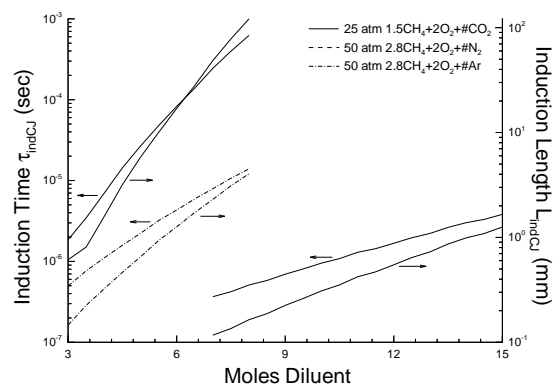
a) Sound speed

b) Specific heat ratio



c) Non-dimensional energy release

d) Detonation velocity and Mach number



e) Detonation induction time and length

Fig. 3.2 Propellant properties.

cost-effectively investigating variables in the starting process. Solid and perforated polycarbonate pistons of 38.1 mm (± 0.5 mm) diameter were used (Fig. 1.4). A magnet epoxied into a circumferential groove allowed tracking of the piston with the electromagnetic sensors. All perforated pistons (13 gm) with backplates (3 gm) were identical to the standard UW ram accelerator obturator. The 16 and 26 gm solid pistons were configured with a Bridgman seal to limit blow-by from the initial launcher. The 36 gm solid pistons did not have a Bridgman seal.

The velocity of the shock created by the piston impacting the mixture was determined by tracking the wave movement down the tube with the piezoelectric pressure transducers. A detonation was determined to have been initiated when the shock velocity was approximately V_{CJ} throughout the 12 m test section. Unsuccessful detonation initiation was indicated by the shock steadily decelerating down the length of the test section. The non-ambiguity of this technique to distinguish between a detonation and a decaying shock is demonstrated by the shock velocity versus distance plot in Fig. 3.3.

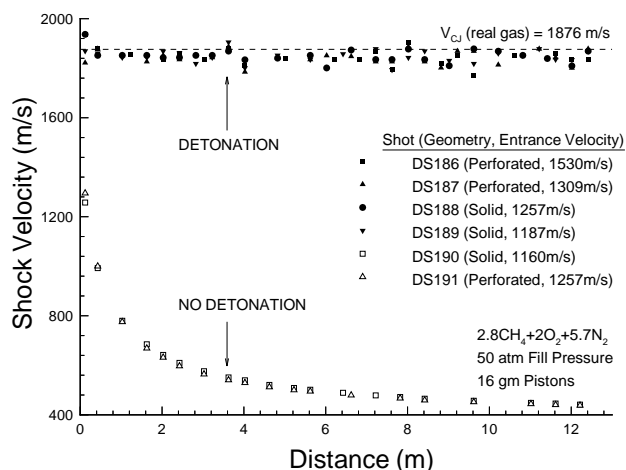


Fig. 3.3 Representative shock velocity versus distance data for piston experiments.

3.2 Projectile Experiments

Projectiles were shot under various conditions to study the effect of changing propellant chemistry, entrance Mach number, projectile geometry, and obturator configuration on the starting process. A magnet in the throat allowed tracking of the

projectile with the electromagnetic sensors. In some cases a magnet was epoxied into a circumferential groove in the obturator to facilitate its tracking as well.

Several different geometry configurations, all made of 7075-T6 aluminum alloy, were used, incorporating changes in throat area (TAV), fin number, body length, and nose angle. Geometric characteristics of five projectile configurations are presented in Table 3.1, along with three-dimensional views in Fig. 3.4. All projectile fins had a constant 12.5° rake angle, and fin thickness varied from 3 mm (for 5 fin projectiles) to 3.8 mm (for 3 and 4 fin projectiles). Note that corresponding changes in base diameter were made to the TAV projectiles in order to maintain the same taper angle. Area profiles of the five projectile configurations are presented in Fig. 3.5. The peak area ratio corresponds to the throat, and the cusp in area ratio between the throat and the base of the body locates the end of the fin rake (where the fin meets the tube wall).

Two polycarbonate obturator geometries of variable mass were used: a perforated obturator (13 gm) with backplate (3 gm) as shown in Fig. 1.4a, and solid obturators (16, 26, and 36 gm) with a Bridgman seal as shown in Fig. 1.4b. The Bridgman seal on the solid obturator is used to limit blow-by from the initial launcher (the obturator base expands under the gas pressure to provide a better full tube area seal). All obturators were 38.1 mm (± 0.5 mm) in diameter.

Table 3.1 Projectile configurations.

Type	Fins	A_{throat}/A_{tube} (Flow)	Nose Angle (°)	Body Length (mm)	Body Taper (°)	Mass (gm)
Standard	5	0.42	10	71.1	4.5	76
Short	4	0.42	15	46.0	6.9	50
TAV 1	3	0.42	10	71.1	4.5	69
TAV 2	3	0.50	10	71.1	4.5	72
TAV 3	3	0.59	10	71.1	4.5	62

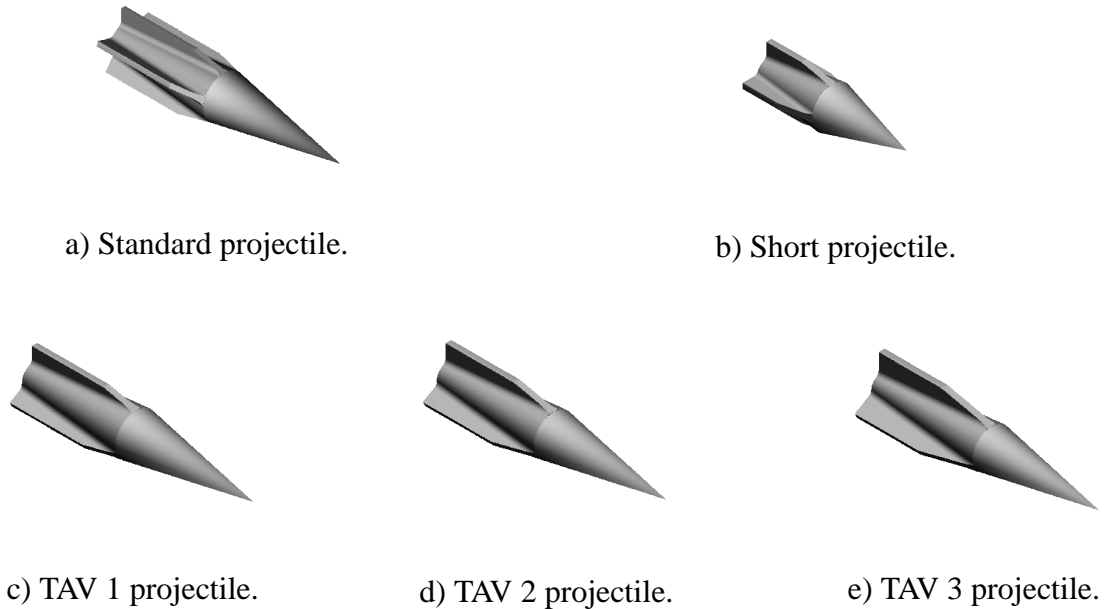


Fig. 3.4 Images of projectiles.

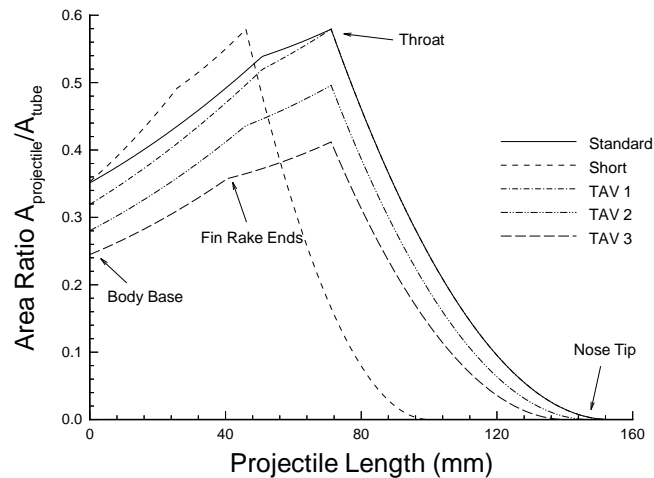


Fig. 3.5 Projectile area profiles.

The result of a start attempt was discerned from the projectile velocity versus distance and tube wall pressure data. Any experiment in which the projectile accelerated for over 2 m was deemed a successful start. Experiments in which the projectile did not accelerate for over 2 m were considered start failures and identified as a sonic diffuser unstart, wave unstart, or wave fall-off, based on analysis of the tube wall pressure data similar to that presented in Chapter 2.

4. Results

Results from projectile and piston experiments are summarized and discussed in the following sections, organized according to the starting process variables investigated. This effort examined only some of the factors in the starting process and represents a cursory investigation, at best, of a very complex environment. Projectile start attempt data are taken from the database of shots in the 16 m system configuration (HS647 through HS1320), and by no means account for all experiments in the history of the UW ram accelerator. The tremendous amount of data presented eliminates the possibility of discussion of each individual data point. Instead, trends and other remarkable features are brought to attention.

4.1 Mach Number and Energy Release

Pistons were fired at various entrance Mach numbers (M_p) into propellants with different amounts of energy release (Q). The piston configuration, propellant characteristics, and limiting M_p observed for detonation and no detonation are presented in Table 4.1. The very fuel-rich $5\text{CH}_4+2\text{O}_2+2\text{He}$ and $5.5\text{CH}_4+2\text{O}_2+1\text{H}_2$ propellants were not detonable at the maximum M_p attainable. In all other propellants, M_p higher than the detonation limit resulted in detonation while lower M_p resulted in no detonation. Increasing diluent concentration (decreasing Q) within a given propellant class always resulted in a higher M_p required for detonation.

Note that Q is a valid means of comparing ignition characteristics across propellants in the same class; propellants in one class with greater Q have lower detonation limits than other propellants in the same class. However, Table 4.1 clearly shows that Q is not a valid means of comparison across different classes. The argon diluted propellant class has lower Q values while having the lowest detonation limits than any of the other classes. Ram accelerator data are often plotted on the energy release versus Mach number (Q - M) plane, and caution must be exercised because propellants from different classes can have very different ignition characteristics.

Table 4.1 Summary of piston detonation conditions.

Propellant	Pressure (atm)	M_{CJ}	Q_{CJ}	Piston Type	No Det M_p	Det M_p	Avg M_p
1.5CH ₄ +2O ₂ +3.5CO ₂	25	5.66	9.1	26gm Solid	3.40	3.67	3.54
				36gm Solid	3.43	3.61	3.52
1.5CH ₄ +2O ₂ +4.5CO ₂	25	5.31	7.9	26gm Solid	3.91	4.00	3.96
				36gm Solid	3.74	3.98	3.86
2.3CH ₄ +2O ₂ +5.7N ₂	50	5.53	6.0	16gm Perforated	3.44	3.61	3.53
				16gm Solid	2.99	3.19	3.09
2.8CH ₄ +2O ₂ +5.7N ₂	50	5.14	4.8	16gm Perforated	3.44	3.58	3.51
				16gm Solid	3.18	3.25	3.22
2.8CH ₄ +2O ₂ +4.5N ₂	50	5.38	5.2	16gm Perforated	3.25	3.36	3.31
				16gm Solid	3.12	3.27	3.20
5CH ₄ +2O ₂ +2He	50	4.89	4.8	16gm Perforated	4.10	No Det	No Det
5.5CH ₄ +2O ₂ +1H ₂	50	4.94	5.1	16gm Perforated	4.30	No Det	No Det
2.8CH ₄ +2O ₂ +8.5Ar	50	4.93	4.2	16gm Perforated	2.67	2.77	2.72
2.8CH ₄ +2O ₂ +11Ar	50	4.65	3.7	16gm Perforated	2.68	2.86	2.77

Results of standard projectile and obturator start attempts in the nominal propellant class are presented in Fig. 4.1. The data are plotted on the Q - M plane and indicate whether a sonic diffuser unstart, wave fall-off, wave unstart, or successful start occurred. Each plot contains data from a 10 atm range of propellant fill pressure. The nominal UW successful starting conditions are evident, with M from 3.0 to 3.3 and Q between 4.6 and 4.9. The 10 to 20 atm fill pressure range (Fig. 4.1a) is marked by a significant number of wave fall-off and wave unstart shots between regions where successful starts occurred, and a few similar data points are noticeable in the 20 to 30 atm range (Fig. 4.1b). This is inconsistent with expectations of a bounded range of conditions under which a successful start can occur, and may be indicative of erratic behavior at relatively low fill pressures.

Several data points exist in these plots which support trends discussed in Section 5.5. The 10 to 20 atm data contain a wave unstart at relatively high Q . The 40 to 50 atm fill pressure range (Fig. 4.1d) illustrates a tendency for wave unstarts to occur as M is

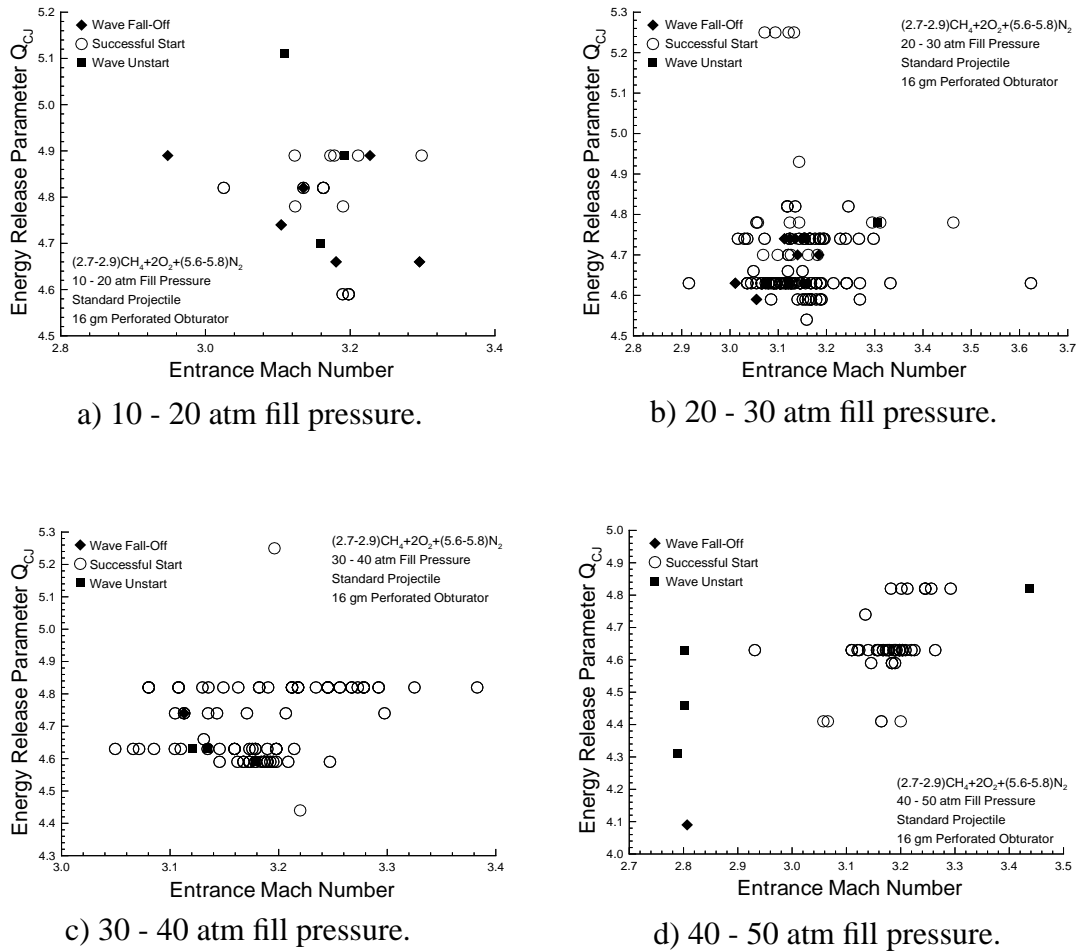


Fig. 4.1 Start attempt results with standard projectile in nominal propellant class.

decreased from successful start conditions. Also, note the wave fall-off at relatively low Q and M , and the wave unstart at high M .

Results of attempts to start a standard projectile and obturator in 25 atm carbon dioxide diluted propellants between Mach 2.5 and 2.9 are presented in Fig. 4.2. Wave fall-offs are observed under conditions of relatively low Q and M , while wave unstarts occurred at relatively high Q and M . There were no successful starts for this particular propellant class at these M , even though Q was varied in such small increments that carbon dioxide concentrations were changed by 0.1 mole.

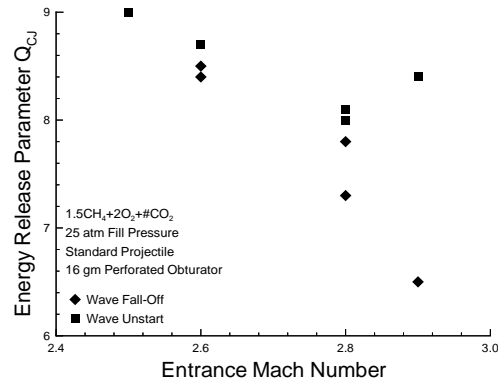
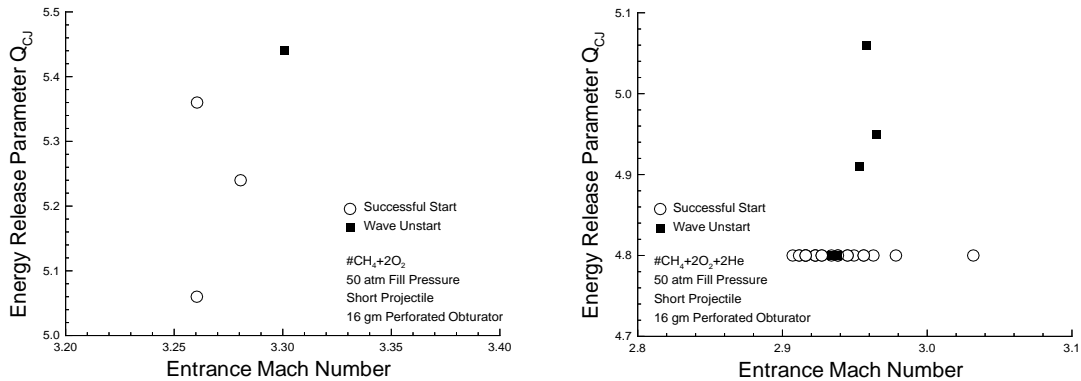


Fig. 4.2 Start attempt results in carbon dioxide diluted propellants.



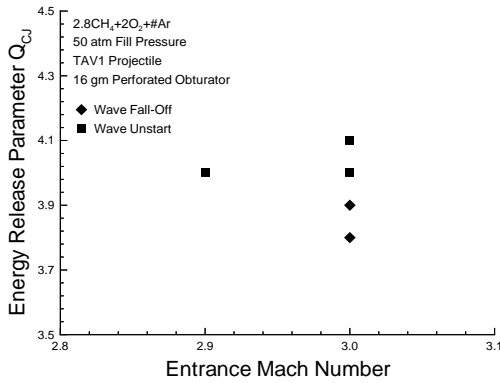
a) No helium dilution in propellant.

b) Two moles helium dilution in propellant.

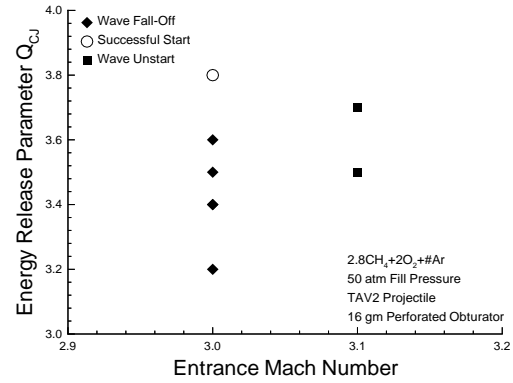
Fig. 4.3 Start attempt results with short projectile.

Successful starting conditions for the short projectile are presented for two 50 atm propellant classes in Fig. 4.3. In the case of a methane/oxygen propellant class (Fig. 4.3a), increasing Q and M above a successful starting condition resulted in a wave unstart. Wave unstarts occurred in a methane/oxygen propellant class diluted with two moles of helium (Fig. 4.3b) when Q was increased at constant M above the successful start regime.

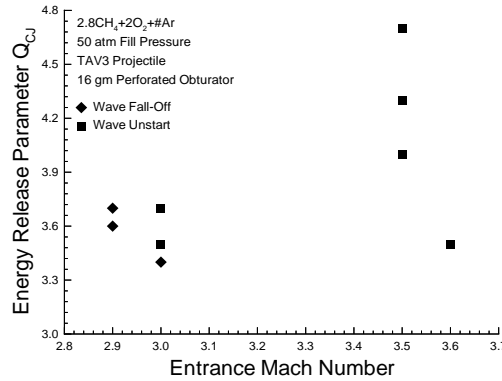
Results of start attempts with throat area variation (TAV) projectiles in 50 atm argon-diluted propellants are presented in Fig. 4.4. The only successful start in an argon-diluted propellant occurred for a TAV2 projectile (Fig. 4.4b). All three projectile geometries exhibited the same trend stated previously. Relatively high Q and M led to a



a) TAV1 projectiles.



b) TAV2 projectiles.



c) TAV3 projectiles.

Fig. 4.4 Start attempt results in argon diluted propellants.

wave unstart, while low Q and M were conducive to a wave fall-off. The wave unstarts most frequently encountered in the experiments presented above occurred 1 to 2 m after entrance, with the exception of the TAV3 wave unstarts around Mach 3.5. These wave unstarts took place less than 0.5 m after entrance, even though the projectile velocity was significantly higher. The change observed in wave unstart character suggests a different wave unstart mechanism.

Relatively low Q and M have been shown to be conducive to a wave fall-off result. In the limit of a non-reactive propellant ($Q = 0$) at Mach numbers above M_{sdu} a wave fall-off will occur, and therefore relatively low propellant energy release is expected to

have the same result. It is also plausible that under conditions of decreasing M there will be a lower limit at which the propellant cannot be ignited, irrespective of Q .

Relatively high Q was observed to lead to wave unstarts. Too little energy release will cause the shock system to recede from the projectile body, and therefore it stands to reason that excessive energy release will push the shock system ahead of the throat (see Section 5.4). Wave unstarts also occurred at higher and lower M than those which permitted a successful start. These phenomena, observed on either side of the successful start regime, suggests multiple mechanisms for producing a wave unstart. A projectile at low M may be ill-suited for containing the combustion wave, while high Mach number projectiles might be conducive to initiating a detonation or other rapid energy release source in the immediate vicinity of the throat.

As previously noted, Q is a parameter which can not be used for comparisons among different mixture classes. In other words, a methane, oxygen, and nitrogen propellant of a particular Q value should not be expected to exhibit the same characteristics as a methane, oxygen, and argon mixture that has the same value. Energy release is quantified by Q , but does not take the other reactive characteristics of a propellant into account. A supporting example is provided by two TAV3 start attempts at Mach 3.5 in $Q_{CJ} = 4.0$ propellants at 50 atm fill pressure, one in $2.8\text{CH}_4 + 2\text{O}_2 + 8\text{N}_2$ and the other in $2.8\text{CH}_4 + 2\text{O}_2 + 10.1\text{Ar}$. With all other conditions held the same, the nitrogen diluted experiment resulted in a successful start while the argon diluted experiment resulted in a wave unstart within 0.5 m of entrance.

4.2 Throat Area

Start results for various flow throat area ratio projectiles in the nominal propellant class are presented in Fig. 4.5. The nominal flow throat area ratio ($A_{throat} / A_{tube} = 0.42$) was able to successfully start from Mach 2.9 to 3.6 in the 20 to 30 atm fill pressure range (Fig. 4.5a) and from Mach 2.9 to 3.3 in the 40 to 50 atm fill pressure range (Fig. 4.5b).

Successful starts in the 20 to 30 atm fill pressure range occurred for several flow throat area ratios below 0.42, illustrating that a reduced flow throat can contain the shock system under standard Q and M conditions as long as the diffuser flow is supersonic. The

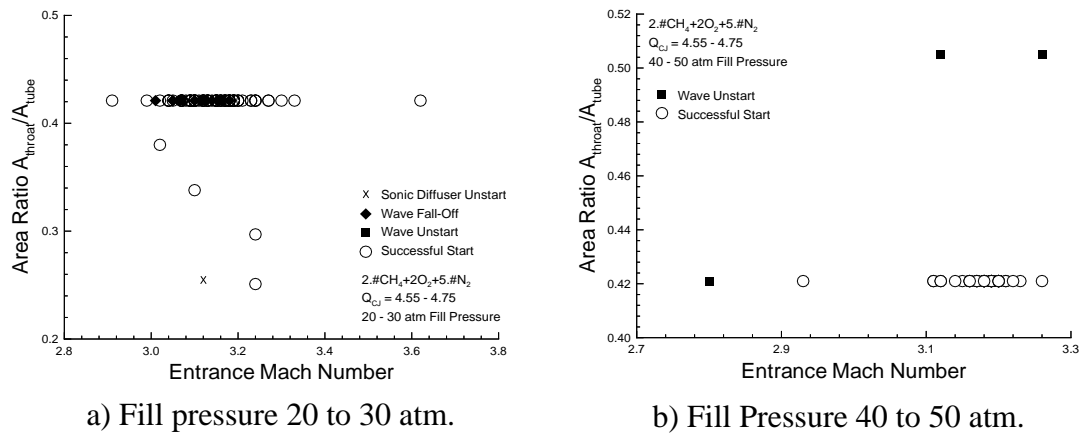


Fig. 4.5 Throat area variations in nominal propellant class.

problem that arises with very small flow throat areas is the increased M for sonic diffuser unstart. An experiment with a 0.25 flow throat area ratio projectile resulted in a sonic diffuser unstart at Mach 3.1, whereas increased flow throat areas permitted a successful start at this M .

A wave unstart occurred in the 40 - 50 atm pressure range when M was decreased to 2.8, consistent with the previous observation of a wave unstart regime at Mach numbers below successful starting conditions. Wave unstarts also resulted in this pressure range when the flow throat area ratio was increased to 0.50 at M where successful starts were observed for the nominal area ratio. Greater flow throat area is conducive to disorgment of the shock system under Q and M conditions in which a smaller flow throat area can contain the shock system.

Start results for TAV projectiles in nitrogen- and argon-diluted propellant classes are presented in Fig. 4.6. Data from both plots indicate that projectiles with increased flow throat area have a tendency to disgorge the shock system that can be contained by reduced flow throat area projectiles at a given Q and M . All three throat area configurations were successfully started in nitrogen-diluted propellants (Fig 4.6a), although under different conditions. Successful starts were achieved by increasing M and decreasing Q as the flow throat area increased. In one case conditions which resulted in a successful TAV2 start caused a TAV3 wave unstart.

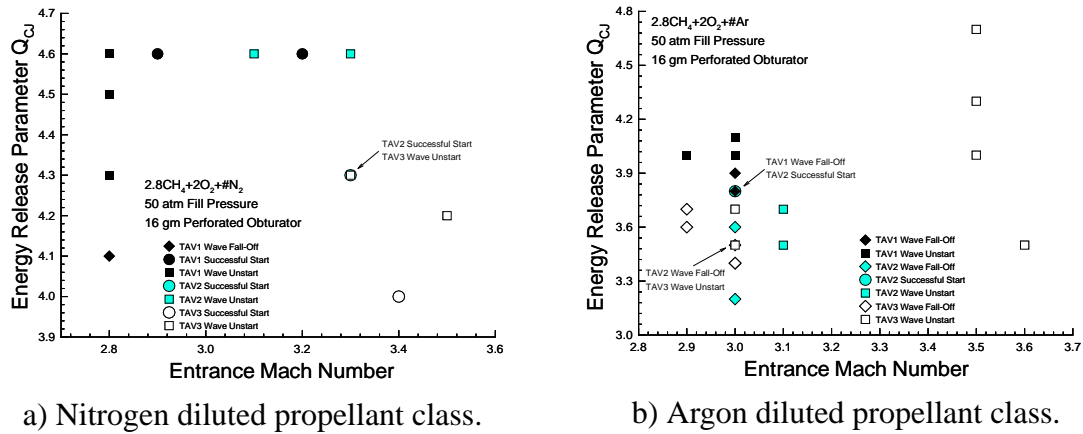


Fig. 4.6 Throat area variations with variable propellant class.

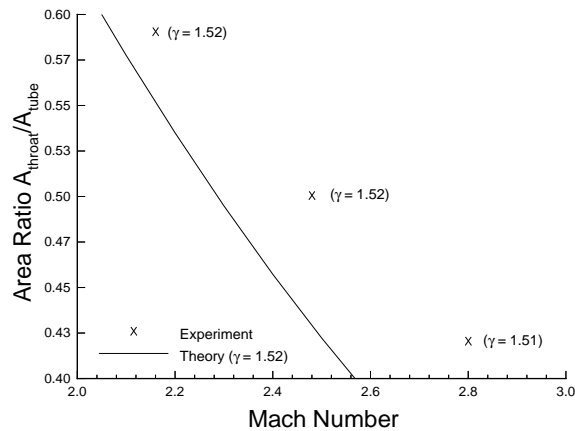


Fig. 4.7 Experimental versus theoretical results of sonic diffuser unstart Mach number.

Wave fall-offs were observed at higher Q for decreased flow throat areas in the argon-diluted propellants (Fig. 4.6b); conditions which resulted in a successful TAV2 start caused a TAV1 wave fall-off. The conclusion that increased flow throat areas require reduced Q and/or increased M to contain the shock system is supported by the data points where a TAV3 wave unstart occurred under the same conditions which resulted in a TAV2 wave fall-off.

Experimental results of increasing the flow throat area to lower M_{sdu} are compared with the theoretical prediction of Eqn. 2.1 in Fig. 4.7. The theory qualitatively demonstrates that M_{sdu} decreases as the flow throat area increases. Quantitatively the

comparison is not exact, in part because of the ideal nature of the theory considered. Also, the experimental data are taken from wave fall-off shots in which the projectile decelerated due to drag until the diffuser could no longer remain supersonic. Initially obtaining supersonic flow through the diffuser is a different gasdynamic process than unchoking an already supersonic diffuser,⁴³ and therefore M_{sdu} required for successful ram accelerator entrance is expected to be different from the Mach number limit measured in this manner.

Note that in all TAV experiments, the throat area was not the only projectile geometry variable changed. In most cases, the base diameter was reduced as the throat diameter was reduced in order to maintain a constant body taper angle. A few TAV projectiles incorporated changes in body length, rather than base diameter, to provide a constant taper angle as the throat diameter varied. Therefore, the results presented in this section can not be attributed to a variation in only the throat area without a more detailed parametric investigation.

4.3 Piston/Obturator Configuration

Results from projectile start attempts and piston experiments in which the piston/obturator mass and geometry were varied are presented in the following sections.

4.3.1 Mass

Results of piston detonation experiments and projectile start attempts in which piston/obturator mass was varied are presented on the Q - M plane in Fig. 4.8. Solid piston mass variation from 26 to 36 gm did not have a noticeable effect on the detonation limits (Fig. 4.8a). A larger mass decelerates less quickly, and so is able to support the shock for a longer period of time. Therefore, one might expect that a piston of greater mass would be able to detonate a propellant at a lower M than a reduced mass piston. This was not observed under the conditions tested, but may play a role if the change in piston mass was more substantial, in the case of marginal detonations (see Section 4.5.1), or where a prolonged DDT type of initiation process is involved. It should also be noted that variation of the initial launcher gas pressure behind the piston should cause much the same

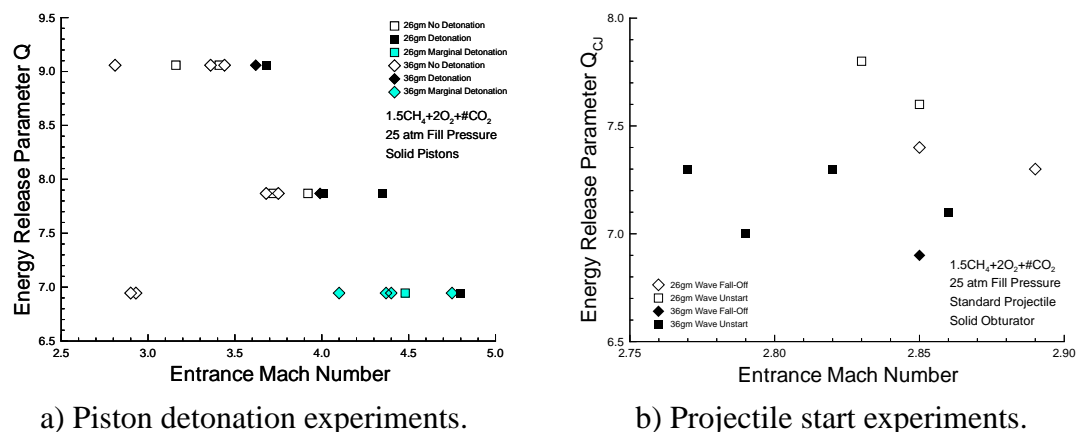


Fig. 4.8 Piston/obturator mass variations.

effect as varying the piston mass, dictating the residence time during which the piston can influence the ignition process. Marginal detonations indicated in Fig. 4.8a will be discussed in Section 4.5.1.

Increasing solid obturator mass seems to promote ignition of the propellant in projectile start attempts (Fig. 4.8b). Wave fall-offs with 25 gm obturators were observed for M above those which result in wave unstarts for 36 gm obturators. Likewise for a given M , the more massive obturator caused a wave unstart at a lower Q than that which resulted in a wave fall-off with the less massive obturator. Greater initial projectile velocity increases were noticed for wave fall-offs with more massive obturators. These results can be explained by the fact that a heavier obturator decelerates less rapidly after entrance and therefore supports the shock system on the projectile body for a longer period of time.

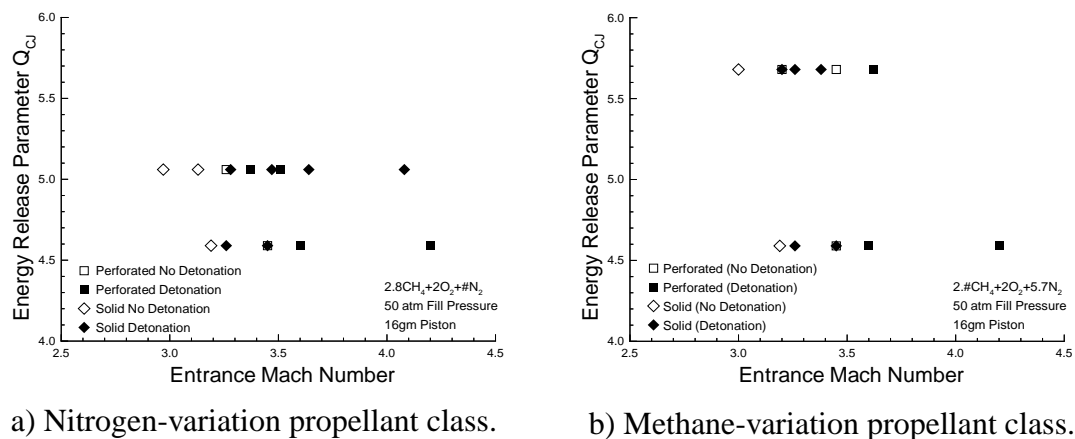
When combustion was indicated by luminosity in carbon dioxide diluted propellant experiments at instrument stations located 639 and/or 1039 mm down the tube, the wave unstarts always resulted in a detonation wave. When combustion was not indicated by luminosity at these stations, the unstart wave velocity steadily decayed. The lack of observation of luminosity for shots that wave unstarted without resulting in detonation may indicate that these unstarts had little to do with combustion, but rather were caused by the obturator overdriving the normal shock system past the throat. This hypothesis

correlates well with the fact that wave unstarts without indications of luminosity and no detonation were only observed for shots with the more massive 26 and 36 gm obturators. An infinitely massive obturator would not separate from the projectile base, resulting in a wave unstart. Therefore, at some increased obturator mass it is expected that start failures will occur independent of any combustion process. Experiments in non-reactive mixtures would confirm whether or not combustion played a role in the more massive obturator wave unstarts presented here.

4.3.2 Geometry

Results of piston experiments for which the 16 gm piston geometry was varied from perforated to solid in nitrogen-variation and methane-variation propellant classes are presented in Figs. 4.9a and 4.9b, respectively. In both propellant classes, the solid geometry caused a detonation at reduced M for a given Q . Perforations allow pressure relief to the back side of the piston, therefore weakening the transmitted shock and mitigating detonation initiation.

Projectile start attempt results with 16 gm obturator geometry variations are presented in Fig. 4.10, and are in agreement with the piston detonation experiments. The solid geometry caused wave unstarts to occur under conditions which resulted in successful starts with a perforated geometry. These observations are due to the stronger



a) Nitrogen-variation propellant class.

b) Methane-variation propellant class.

Fig. 4.9 Geometry variations in piston experiments.

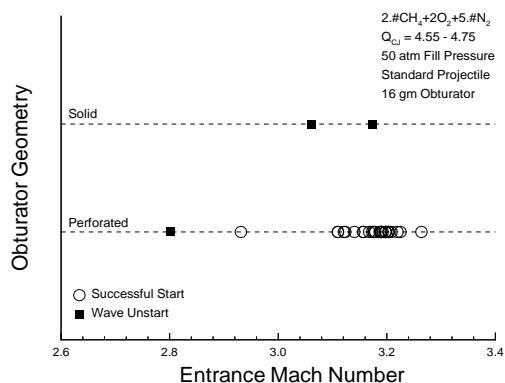


Fig. 4.10 Obturator geometry variations in projectile start experiments.

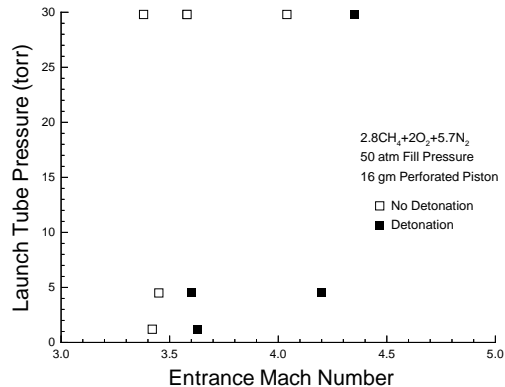


Fig. 4.11 Residual launch tube pressure effects on detonation initiation.

shock system generated by the solid geometry. Successful starts have occurred with 10 gm solid obturators in the Q and M range plotted in Fig. 4.10 at 25 atm fill pressure, and therefore the solid geometry itself does not always result in start failure.

4.4 Launch Tube Residual Air Pressure

Piston experiments in which the launch tube pressure was varied are presented in Fig. 4.11. The launch tube air pressure is plotted versus M and indicate whether or not a detonation occurred. The 1 and 5 torr launch tube pressures have similar detonation limits, and increased M is necessary to detonate the propellant at 30 torr launch tube pressure. This result indicates that ignition may be insensitive to small changes in launch tube pressure, but relatively large pressure changes affect the ignition process. Increased

launch tube pressure will cause greater cushioning of the unsteady piston impact and may separate the backplate from the perforated piston, resulting in lower transmitted shock strength and thereby mitigating detonation initiation.

4.5 Unique Experiments

During the course of this investigation, a few experiments were conducted which exhibited unique phenomena. Piston experiments which resulted in marginal detonations and a projectile start experiment in which a wave fall-off was observed followed by a wave unstart are presented in the following sections.

4.5.1 Marginal Detonations

A marginal detonation is defined in the context of this work as a piston-generated shock which travels at V_{CJ} for some distance, but decays before reaching the end of the 12 m long test section. All marginal detonations occurred in $1.5\text{CH}_4+2\text{O}_2+5.5\text{CO}_2$ at 25 atm fill pressure, and propagated for several meters before quenching. Table 4.2 summarizes the data from the piston detonation experiments in this propellant. Propagation distances of the marginal detonations are noted in the “Result” column. Marginal detonations were observed for 26 and 35 gm solid piston masses, and no correlation between piston Mach number and distance of marginal detonation propagation is evident.

The shock velocity versus distance data for these experiments are plotted in Fig. 4.12, illustrating the shock decay after several meters of travel. Different plots symbols indicate data from separate experiments, and the solid symbol denotes the experiment which resulted in a detonation (Table 4.2). Sufficient data do not exist to declare the exact cause of the detonation quenching, although it is clear that something occurred behind the lead shock which caused the decay. Factors involved may include the piston dynamics, initial launcher gas, pressure relief via communication with the evacuated launch tube vent system, or imperfections in the surface of the tube.

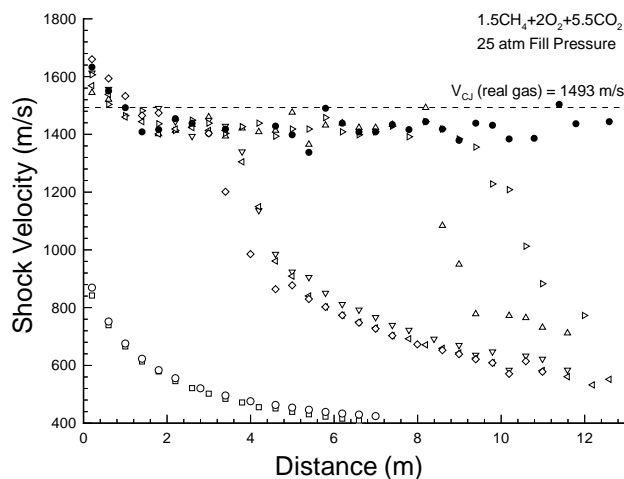


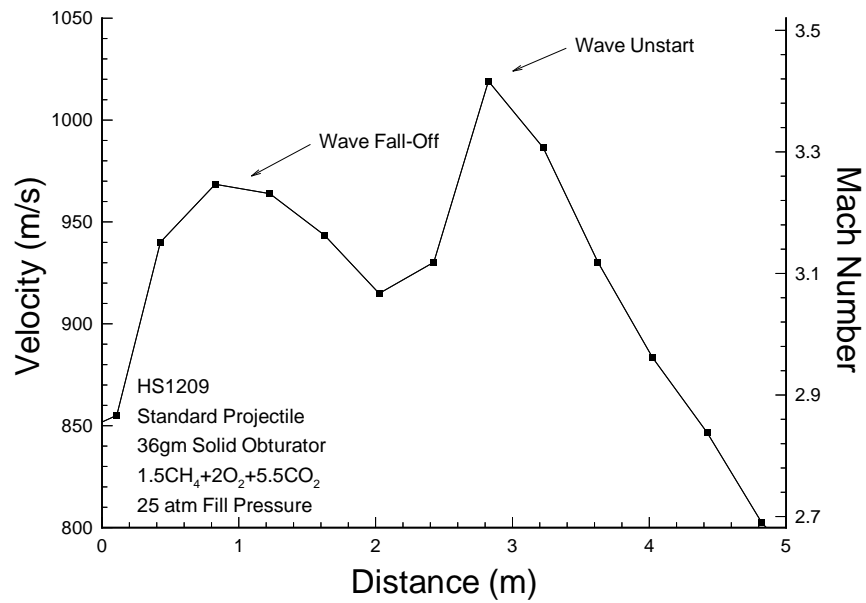
Fig. 4.12 Shock velocity versus distance data for piston initiated detonation experiments in which marginal detonations occurred.

Table 4.2 Piston experiments in 25 atm $1.5\text{CH}_4 + 2\text{O}_2 + 5.5\text{CO}_2$.

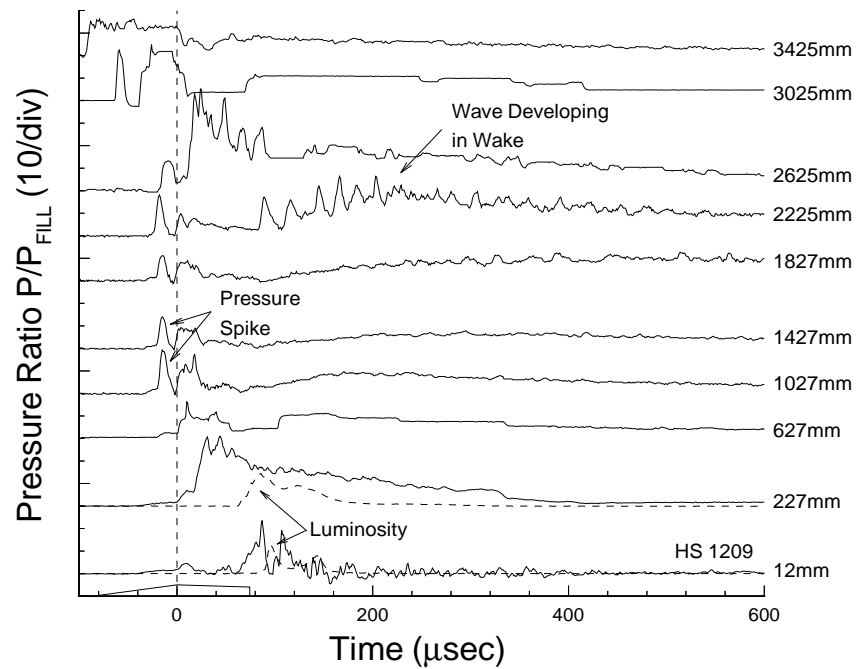
Shot	Piston	Entrance Velocity (m/s)	Entrance Mach Number	Result
DS124	35gm Solid	864	2.9	No Detonation
DS131	35gm Solid	1220	4.10	Marginal (8m)
DS132	35gm Solid	1310	4.40	Marginal (4m)
DS133	35gm Solid	1300	4.37	Marginal (9m)
DS134	26gm Solid	1333	4.48	Marginal (4m)
DS135	26gm Solid	1429	4.8	Detonation
DS136	35gm Solid	872	2.93	No Detonation
DS137	35gm Solid	1413	4.75	Marginal (3m)

4.5.2 Wave Fall-Off Followed by Wave Unstart

Projectile velocity versus distance and tube wall pressure data for an experiment in which a wave fall-off occurred followed by a wave unstart are presented in Fig. 4.13. The projectile demonstrated more than 100 m/s velocity increase, decelerated 50 m/s, and then accelerated to 1020 m/s before wave unstarting. The initial velocity increase (Fig. 4.13a)



a) Projectile velocity versus distance data.



b) Tube wall pressure data.

Fig. 4.13 Experiment in which a wave fall-off occurred, followed by a wave unstart.

is not unusual for a shot with a 36 gm solid obturator, as was discussed in Section 4.3.1 and will be supported in Section 5.1. The obturator-generated shock system surges onto the projectile body (Fig. 4.13b), causing the velocity increase, but then falls off the base by 627 mm after the entrance diaphragm. A pressure spike then appears ahead of the nose and remains there until the wave unstart occurs. At the 2225 mm instrument station, a pressure wave is observed developing in the wake of the projectile and is on the projectile body 2625 mm after entrance. A wave unstart occurs 3 m after entrance, as the shock system propagates beyond the projectile throat. Interpreting the phenomena occurring during this shot is difficult with the available data. The pressure spike ahead of the throat remains a mystery, and may be due to a timing error in the data acquisition system. As for the pressure history behind the throat, perhaps the flow on the projectile ignited, quenched, and then re-ignited again. Or maybe the shock system fell off the body without ever igniting the propellant. A combustion wave may have been generated after a suitable induction time far back in the wake of the projectile, caught up to, and then overran the projectile. This phenomenon is similar to the results of combustion stripping experiments, in which the combustion wave was stripped from a ram accelerating projectile by passing through an inert-gas-filled tube and then re-entered a combustible mixture.²⁰ A combustion wave was observed to form in the projectile wake and then to overrun the projectile. The velocity history during the combustion stripping experiment exhibited projectile acceleration while in the propellant, followed by deceleration in the inert gas, and then acceleration to a wave unstart, after propellant re-entry, once the pressure wave caught up to the projectile.

5. Analysis

Understanding of the starting process can be taken beyond just the “end results” of the start attempt results and piston detonation limits presented in Chapter 4. The following sections provide further information into several aspects of interest, including the launch tube and ram accelerator tube flowfields, an analysis of the wave unstart process involving detonations, envelopes providing the limits to successful starting, obturator dynamics, and relative time scales on which phenomena relevant to the starting process occur.

5.1 Flowfield

A great deal of pressure and luminosity data was recorded during this investigation, and some are presented here to support this and past research on the starting process.

5.1.1 Launch Tube

Launch tube wall pressure and luminosity data are shown in Fig 5.1. Negative distances indicate location of the instrument station on the launch tube side of the entrance diaphragm. The luminosity data are not scaled in a particular fashion, and therefore absolute signal amplitude is inconsequential. Note that all shocks reflecting between the diaphragm and projectile/obturator are not shown due to the scale of the plotted data. All plots illustrate the high temperature and compression of the launch tube gas prior to the projectile reaching the entrance diaphragm. This compression is shown to occur independently of the reactive nature of the propellant by Fig. 5.1a, recorded during an experiment in which the ram accelerator tube was filled with 25 atm $2\text{N}_2+8\text{CO}_2$. The pressure trace 139 mm prior to the entrance diaphragm gave no signal during this experiment. Launch tube data for a wave fall-off experiment (Fig. 5.1b) and a wave unstart experiment (Fig. 5.1c) show little difference in luminosity character and peak pressure 12 mm prior to the diaphragm. The far-field pressure in the wave unstart experiment is higher than that observed during the wave fall-off. The cause of this is not necessarily a result of the wave unstart, as the wave unstart experiment had an entrance

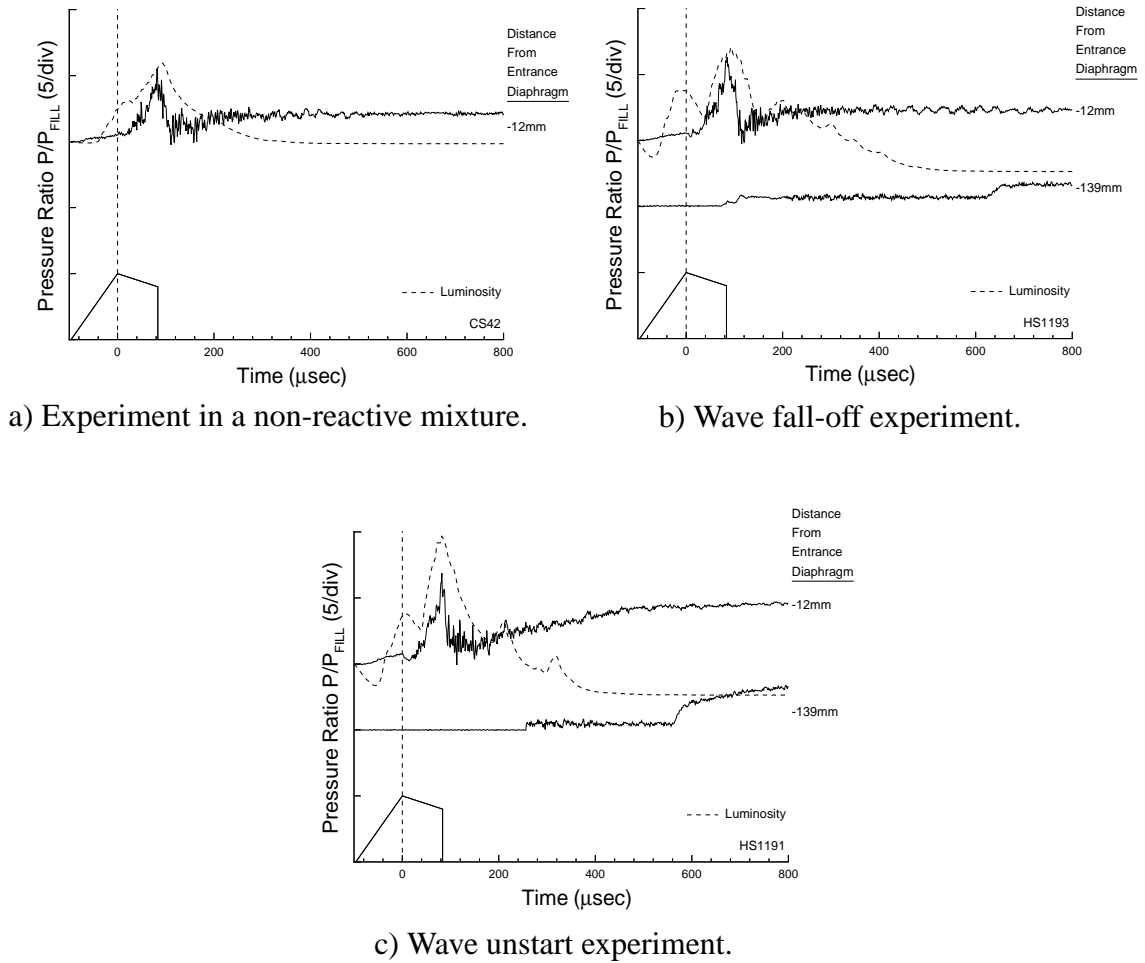
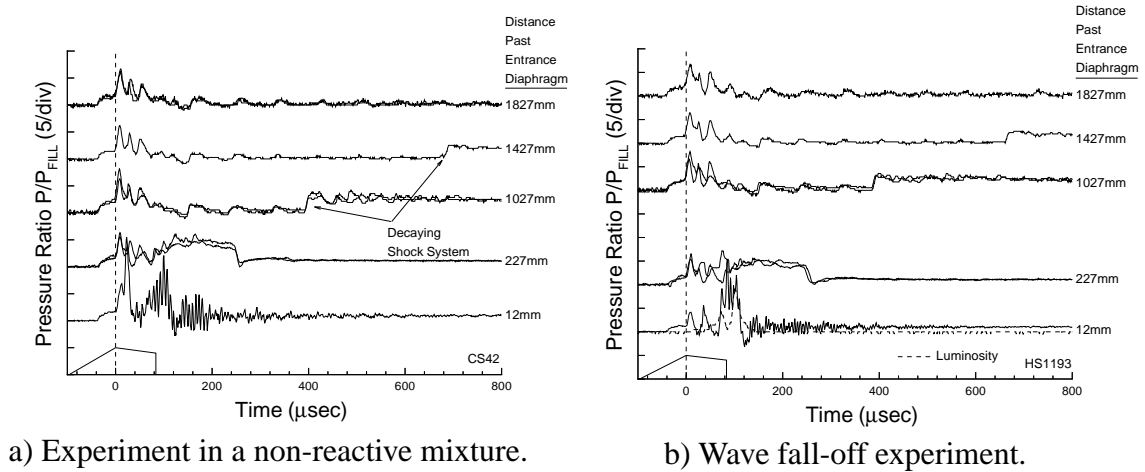


Fig. 5.1 Tube wall pressure and luminosity data from the launch tube.

velocity 200 m/s greater than the wave fall-off experiment and therefore greater initial launcher gas pressure.

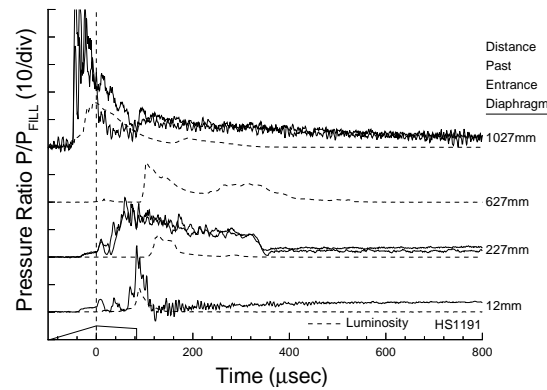
5.1.2 Ram Accelerator Tube

Tube wall pressure and luminosity data from the ram accelerator tube just after the entrance diaphragm (corresponding to the launch tube data presented above) are presented in Fig. 5.2. The pressure data from the experiment in a non-reactive mixture (Fig. 5.2a) are very similar to those of the wave fall-off experiment in a reactive mixture (Fig. 5.2b). In both experiments the obturator-driven shock system quickly recedes from the projectile



a) Experiment in a non-reactive mixture.

b) Wave fall-off experiment.



c) Wave unstart experiment.

Fig. 5.2 Tube wall pressure and luminosity data from ram accelerator tube.

body and decays into the far-field. No luminosity was observed for the non-reactive mixture experiment, while it was present 12 mm after the entrance diaphragm during the wave fall-off experiment. There is no way of discerning whether this luminosity is due to the compressed launch tube gas entering the ram accelerator tube, or propellant combustion which did not stabilize on the rear of the projectile. The wave unstart experiment (Fig. 5.2c) exhibits much greater pressure amplitudes and a prominent luminous combustion region. Note that the combustion wave follows the pressure wave as it discharges from the projectile throat 1027 mm past the entrance diaphragm.

5.1.3 Obturator Geometry

Tube wall pressure and luminosity data from the launch tube and ram accelerator tube during experiments in which the obturator geometry was varied are presented in Fig. 5.3. Essentially similar data are observed in the launch tube for the perforated obturator (Fig. 5.3a) as for the solid obturator (Fig. 5.3b). The pressure rise in the far-field 139 mm trace of the perforated obturator experiment is not present in the solid obturator experiment. This pressure rise was observed (and absent) in other solid and perforated obturator experiments, and therefore is not necessarily a consequence of the obturator geometry. The difference between the perforated (Fig. 5.3c) and solid (Fig. 5.3d)

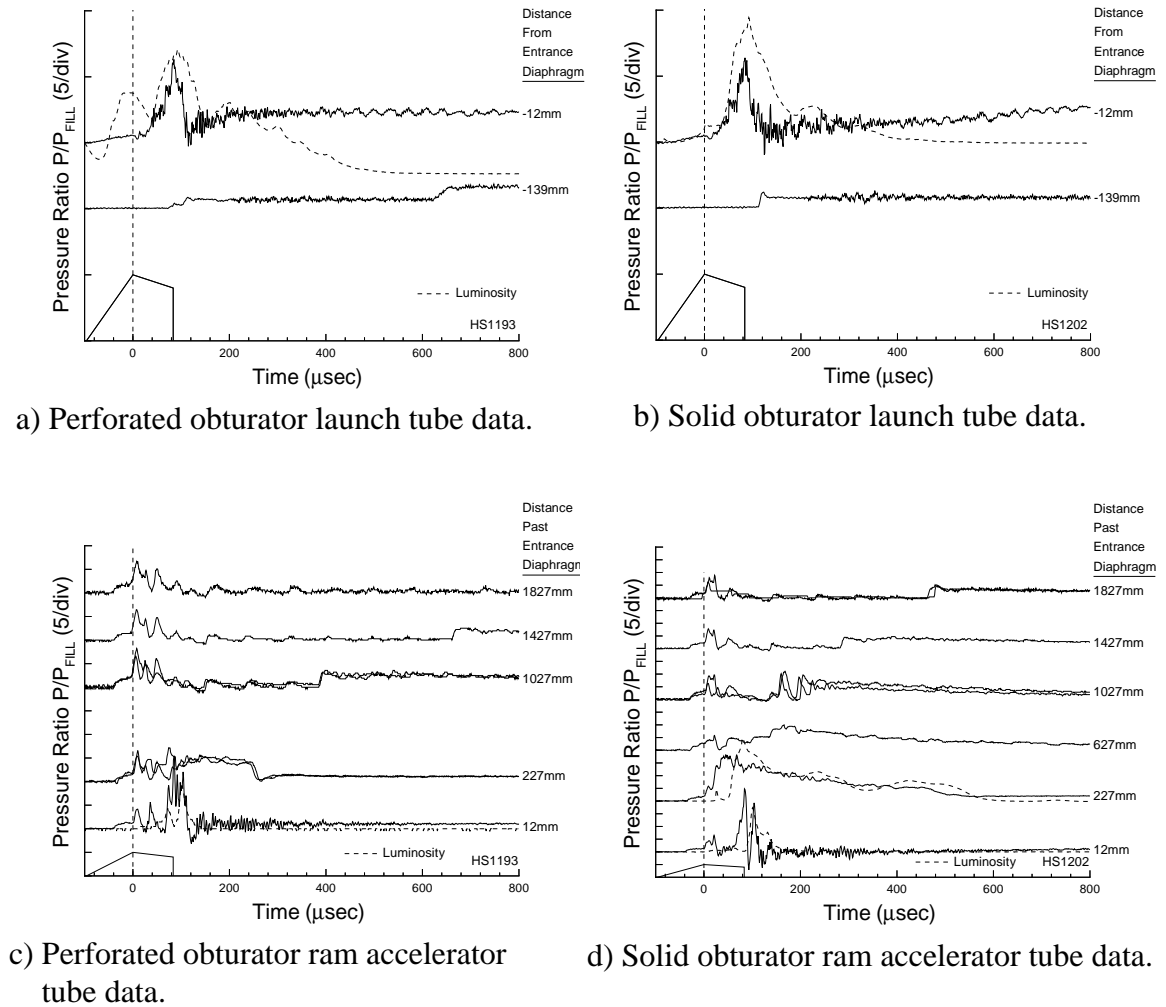


Fig. 5.3 Tube wall pressure and luminosity data from obturator geometry variation wave fall-off experiments.

obturator in the ram accelerator tube flowfield is evident. These experiments were conducted in the same propellant with the same entrance Mach number, and both resulted in a wave fall-off. The solid obturator generates a stronger shock system on the projectile body just after entrance, and supports the shock system for a greater distance after the diaphragm. Luminosity is observed on and behind the projectile body 227 mm past the entrance diaphragm in the solid obturator experiment, while no luminosity is detected after 12 mm in the perforated obturator experiment. Projectile velocity data show a greater initial velocity increase in the case of a solid obturator while the shock system is on the projectile body. The lack of pressure relief by the solid obturator helps to explain the increased magnitude and persistence of the shock system and the presence of luminosity, thus supporting the conclusions regarding piston and projectile experiments arrived at in Section 4.3.2.

5.2 Obturator Dynamics

The role that the obturator plays in the starting process is better understood by considering its motion during transition from the launch tube to the ram accelerator tube. Obturator time versus distance data from piston detonation and projectile start experiments are presented in the following sections. The effects of propellant ignition, mass, and geometry on the obturator dynamics are considered. The experimental data are supplemented by calculations from a method of characteristics (MOC) code for a non-reactive mixture impacted by a frictionless piston with no back pressure. A comparison of experimental and MOC data for conditions which resulted in no detonation are presented in Fig. 5.4. The general piston and shock trajectories are predicted by the MOC data. The piston rapidly decelerates after piercing the entrance diaphragm, comes to a stop, reverses direction, and then travels back into the launch tube. The shock is observed to decay steadily as it propagates down the ram accelerator tube, and is tracked more accurately than the piston by the MOC code. Note that the piston moves farther into the ram accelerator tube and re-enters the launch tube later for the 25 atm fill pressure case (Fig. 5.4a) than the 50 atm case (Fig. 5.4b). The pistons may have travelled farther into

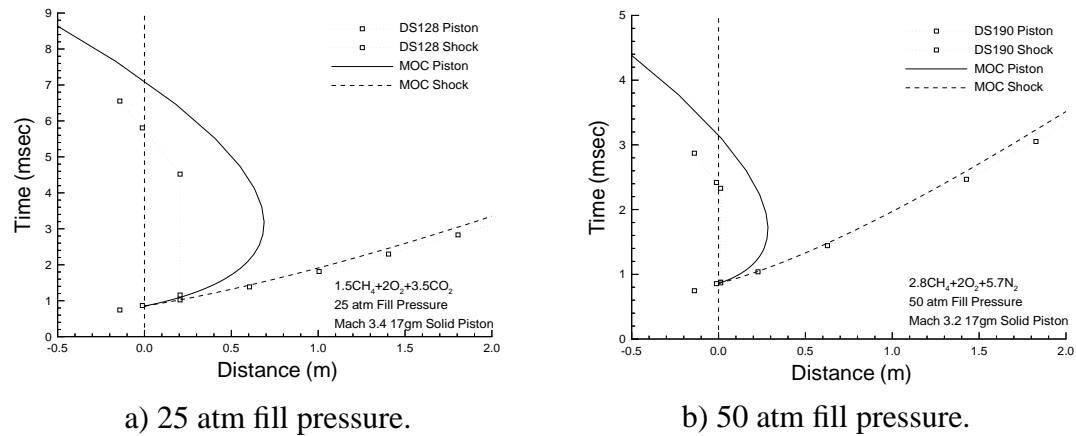


Fig. 5.4 Experimental and predicted piston and shock t - x data.

the ram accelerator tube than the experimental data indicate, because the electromagnetic sensors have difficulty detecting the magnets on relatively slow moving pistons.

5.2.1 Propellant Ignition

The effects of 25 atm fill pressure propellant ignition on the obturator dynamics are presented in Fig. 5.5. The data from piston detonation experiments (Fig. 5.5a) reveal that the piston comes to a stop and re-enters the launch tube much faster when a detonation occurs. This result is due to the higher pressure applied to the piston face by the detonation versus the no detonation experiment. The initial piston history in the ram accelerator tube is the same for the detonation and no detonation experiments. Minimal spatial measurement resolution and/or induction considerations may cause this result. During the induction process the temperature and pressure of the flow are not substantially changed by chemical reactions, thus the dynamics of the piston motion are not expected to be significantly affected by chemical reactions during the induction time. A projectile start experiment which resulted in a wave unstart with no detonation (Fig. 5.5b) exhibits an obturator history similar to that of the piston experiment which detonated. The piston/obturator in both the piston and projectile experiments re-enters the launch tube approximately 3 msec after entering the ram accelerator tube.

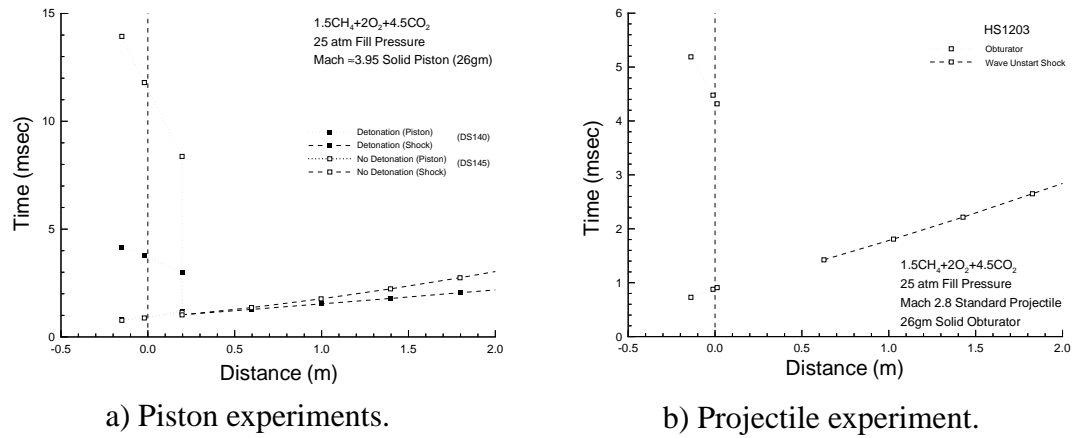


Fig. 5.5 Ignition effects on piston and shock $t-x$ data at 25 atm fill pressure.

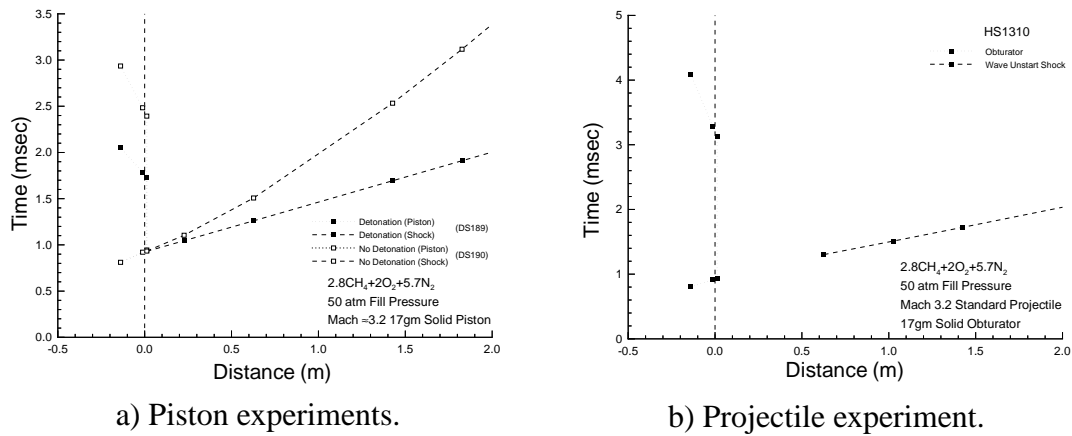


Fig. 5.6 Ignition effects on piston and shock $t-x$ data at 50 atm fill pressure.

The effects of 50 atm fill pressure propellant ignition on the obturator dynamics are presented in Fig. 5.6. The piston detonation experiments' data (Fig. 5.6a) also demonstrate the piston re-entering the launch tube faster during a detonation. Note that the non-reacting shock decays more rapidly at 50 atm fill pressure than 25 atm fill pressure, although this may be a Mach number effect. A corresponding projectile start experiment which resulted in a wave unstart followed by a detonation (Fig. 5.6b) exhibited an obturator history which re-entered the launch tube later than the detonation and

no-detonation piston experiments. The presence of a projectile causes the obturator to remain in the ram accelerator tube for a longer period of time.

While propellant ignition certainly causes the piston/obturator to decelerate and reverse direction more quickly than a no-ignition case, the piston detonation experiments do not quantitatively compare very well to the projectile start experiments. The projectile presence is probably influencing the obturator dynamics, as is the initial launcher gas behind the obturator. The piston detonation experiments utilized much lower initial launcher gas pressures for the same entrance velocity as an obturator and projectile launch package. The MOC code is not used to support any of these data because it does not model chemical reactions.

5.2.2 Obturator Mass

Mass effects on the obturator $t-x$ data are presented in Fig. 5.7. Less massive obturators decelerate and re-enter the launch tube more rapidly than obturators of greater mass, regardless of whether no detonation (Fig. 5.7a) or detonation (Fig. 5.7b) occurs. The MOC data (Fig. 5.7c) support this observation. The experiments show little effect of shock support variation by different piston masses, but the MOC data for a 100 gm piston verify that more massive pistons do support the shock for a longer period of time. Increased shock support by a more massive obturator supports the projectile start observations presented in Section 4.3.1. As noted in Section 5.2, the MOC code accurately tracks the shock but tends to overpredict the time required for the piston to re-enter the launch tube.

5.2.3 Obturator Geometry

Perforated versus solid geometry effects on the obturator $t-x$ history are presented in Fig. 5.8. The solid geometry decelerates and re-enters the launch tube more rapidly than the perforated geometry, and supports the shock over a longer period, even though it has less residence time in the ram accelerator tube. The longer shock support by the solid geometry supports the projectile start data and piston detonation limits presented in

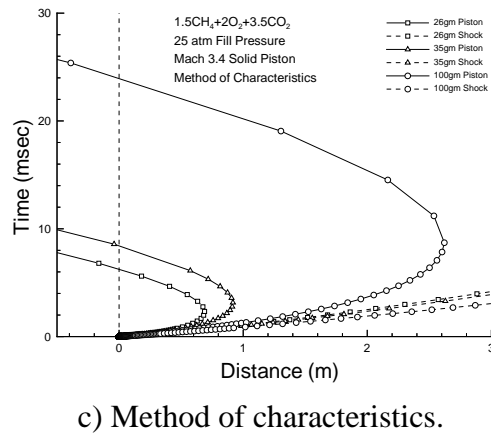
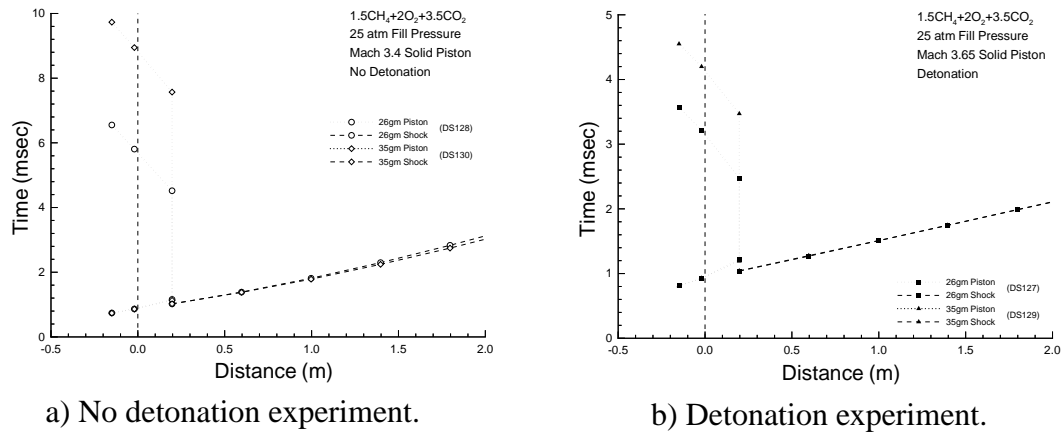


Fig. 5.7 Piston and shock $t-x$ data for mass variation.

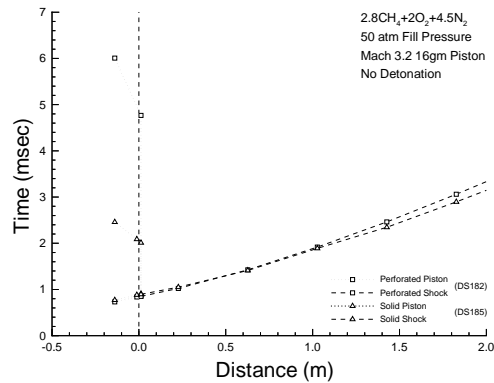


Fig. 5.8 Piston and shock $t-x$ data for geometry variation.

Section 4.3.2. MOC data are not compared with the experimental data because the code does not account for perforations in the piston.

5.3 Detonation Wave Unstart

Detonation initiation was frequently observed in conjunction with wave unstarts during this investigation, as indicated by data for three experimental series presented in Table 5.1. After a wave unstart with detonation, the shock velocity settled to approximately V_{CJ} within a few meters in all cases when the unstart wave was initially overdriven (Fig. 2.9). Detonation initiation behind the projectile throat in the subdetonative velocity regime is highly undesirable because the detonation wave will outrun the projectile.

Table 5.1 Detonation frequency in conjunction with wave unstarts.

Propellant	Pressure (atm)	Number of Wave Unstarts	% with Detonation
$1.5\text{CH}_4+2\text{O}_2+\#\text{CO}_2$	25	11	73%
$2.8\text{CH}_4+2\text{O}_2+\#\text{N}_2$	50	11	100%
$2.8\text{CH}_4+2\text{O}_2+\#\text{Ar}$	50	11	100%

Detonation initiation in tubes, either by direct initiation or deflagration to detonation transition (DDT), has been studied extensively and is widely reported in the literature.^{44,45} Piston initiated detonations have been investigated to a lesser extent experimentally and analytically.^{46,47,48} The coupling of gasdynamic and thermodynamic processes in three dimensions has created a significant challenge to quantitatively understanding how a detonation wave forms and propagates. There is no general predictive theory on detonation initiation, although initiation theories do exist for specific ideal conditions. The factors influencing detonation initiation in a tube are the ignition source, boundary conditions, and combustible mixture properties. Ignition source variables include energy, the rate at which the energy is deposited, and the source geometry. Boundary condition variables include tube diameter, surface roughness, and end-wall dynamics (fixed versus

moving). Mixture property variables include acoustic speed, activation energy, induction time, energy release, temperature, pressure, velocity, and turbulence.

Due to limited instrumentation density (approximately three projectile lengths between every instrumentation port) the location of detonation initiation relative to the projectile cannot be accurately determined. Therefore, some of the wave unstarts summarized above may be a result of detonation initiation behind the projectile throat (leading to a “detonation wave unstart”), while others may be the end result of some other phenomenon. Sufficient evidence of detonation initiation in the starting process exists to mandate further investigation, especially in those cases where detonation initiation was observed almost immediately upon entrance. Piston experiments were conducted to determine what conditions are conducive to initiating a detonation, so that these conditions can then be avoided to eliminate detonation initiation as a source of wave unstart. The piston detonation limits identified are presented in Table 4.1, and are compared to projectile start attempt data in the following paragraphs.

The short projectile geometry with 16 gm perforated obturator was fired into the 50 atm $2.8\text{CH}_4+2\text{O}_2+5.7\text{N}_2$ propellant at Mach 3.2 and 3.7 where it accelerated for almost 2 m before a wave unstart occurred. In these cases a detonation did occur, but not immediately upon entrance when the obturator was still in communication with the projectile flowfield. The projectile seems to be mitigating ignition because an immediate detonation does not occur at a Mach number above the piston detonation limit ($M_p = 3.51$). The standard projectile with a 16 gm perforated obturator successfully starts in this propellant from Mach 2.9 to 3.4. It is interesting to note that lowering the entrance Mach number of this projectile to 2.8 results in a wave unstart with a detonation, but also not immediately upon entrance. Additional experiments have shown that immediate wave unstart with detonation occurs when the standard projectile with 16 gm solid obturator enters this propellant at Mach 3.1 and 3.2. The piston detonation limit for this case is Mach 3.09.

Wave fall-off (no propellant ignition) occurs when the standard projectile ($A_{throat}/A_{tube} = 0.42$) with 16 gm perforated obturator enters the 50 atm $2.8\text{CH}_4+2\text{O}_2+11\text{Ar}$ propellant at Mach 3.0. A TAV2 projectile ($A_{throat}/A_{tube} = 0.504$) with the 16 gm perforated

obturator was successfully started in the same propellant and Mach number. These are examples of no ignition and a successful start at Mach numbers above the piston detonation limit ($M_p = 2.77$). Further increasing the flow throat area ratio to 0.588 (TAV3) with the 16 gm perforated obturator results in a wave unstart with detonation after 2 m of travel. Increasing the TAV3 Mach number from 3.0 to 3.5 with argon concentrations of 7 to 12.7 moles resulted in immediate wave unstarts with detonation. The throat area variation is clearly influencing the outcome of the start attempt, and the distance in which a detonation is initiated.

An immediate wave unstart without detonation occurs when the standard projectile with 26 gm solid obturator enters the 25 atm $1.5\text{CH}_4+2\text{O}_2+4.5\text{CO}_2$ propellant at Mach 2.83. The short projectile geometry with 16 gm perforated obturator experienced an immediate wave unstart with no detonation when it entered the $5.5\text{CH}_4+2\text{O}_2+1\text{H}_2$ propellant at Mach 3.1. These are two examples of an immediate wave unstart occurring without detonation initiation.

The comparison of piston detonation limits with start attempt data presented in the preceding paragraphs illustrates several points. First, piston detonation limits do not set an upper bound on the conditions under which the ram accelerator can successfully start. Successful starts, wave fall-offs, and wave unstarts with detonation not immediately after entrance have been observed in situations where the piston alone will initiate a detonation. This indicates that the projectile can have a mitigating effect on detonation initiation. Second, wave unstarts with detonation immediately after entrance are observed at lower Mach numbers than the piston detonation limits. These data indicate that the projectile can have an enhancing effect on detonation initiation. Data for successful starts and wave unstarts with detonation not immediately after entrance were presented to substantiate the observation that similar phenomena occur above and below the piston detonation limit. Finally, wave unstarts with no detonation immediately after entrance were observed. These data indicate that detonations are not always associated with immediate wave unstarts.

Comparison of projectile start attempt data with piston detonation limits highlights the complex nature of the wave unstart failure mode in the start process. In the process of

shedding light on wave unstart phenomena, this work has perhaps raised more questions than it has answered. Depending on the initial conditions of the start attempt, wave unstarts involving detonations have been observed to occur immediately after entrance and after several meters of travel, both at lower and higher Mach number than the piston detonation limits.

The role that detonations play in the subdetonative ram accelerator remains unclear. For the time being, whether a detonation occurring during a wave unstart is initiated behind the projectile throat or ahead of the projectile throat after shock disgorgment is left to speculation. However, a reasonable statement which can be made is that there exists a propellant composition limit under particular operating conditions in which the subdetonative ram accelerator cannot operate because the projectile and obturator have the ability to initiate a detonation.

5.4 Quasi-One-Dimensional Model

A quasi-one-dimensional model of the ram accelerator which attempts to predict an operational envelope is presented in Fig. 5.9. Global assumptions of this model include inviscid steady flow of a calorically perfect gas. Quasi-one-dimensional isentropic flow analysis is employed between stations 1-2, 2-3, and 4-5. Normal shock jump conditions are used between stations 3-4, and heat addition to thermal choking is assumed to occur at full tube area between stations 5-6. Given a projectile Mach number, this model produces three limits to ram accelerator operation: choked flow between stations 1 - 2 (sonic diffuser unstart), heat release for which the normal shock is located behind station 5 (wave fall-off), and heat release for which the normal shock is located ahead of station 2 (wave unstart). These limits represent the three start failures, and therefore it is useful to

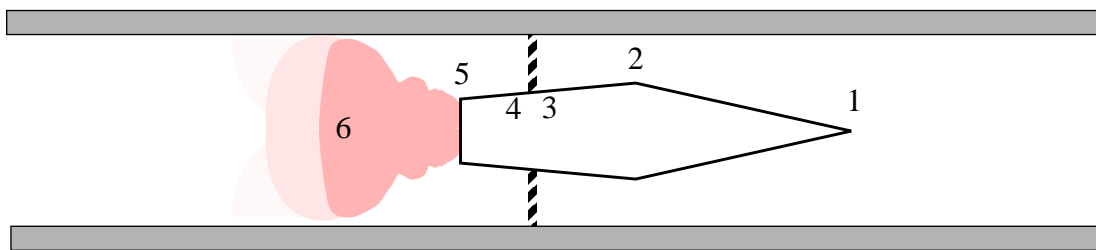


Fig. 5.9 Quasi-one-dimensional flowfield model.

compare experimental start attempt data with the envelope of operation predicted by this model. Comparison of the model operational envelope with experimental data during transition from one stage of propellant to another (several meters after the initial starting process) has shown that this model does not quantitatively predict the limits to ram accelerator operation.^{17,18,49}

The predicted envelopes for the projectiles used in this starting process investigation are presented in Fig. 5.10. Note that area input to the model is the axisymmetric projectile area, and therefore does not include the presence of fins. The model does qualitatively capture some effects of variable throat geometry presented in Section 4.2. Increasing flow throat area shifts the sonic diffuser unstart limit to a lower Mach number. Reduced flow throat area is able to contain a shock system supported by higher Q , and does this at lower M than increased flow throat areas. Increased flow throat area (with a corresponding increase in base flow area) permits operation at lower Q and higher Mach number before a wave fall-off occurs. Quantitatively the nominal starting envelope discussed in Section 4.1 ($M = 3.0-3.3$ and $Q = 4.6-4.9$) is within the limit envelope, as indicated by the shaded region in Fig. 5.10. However, many of the start failures encountered also lie within the envelope. Therefore, the quasi-one-dimensional model does not quantitatively predict under what conditions a successful start will be achieved.

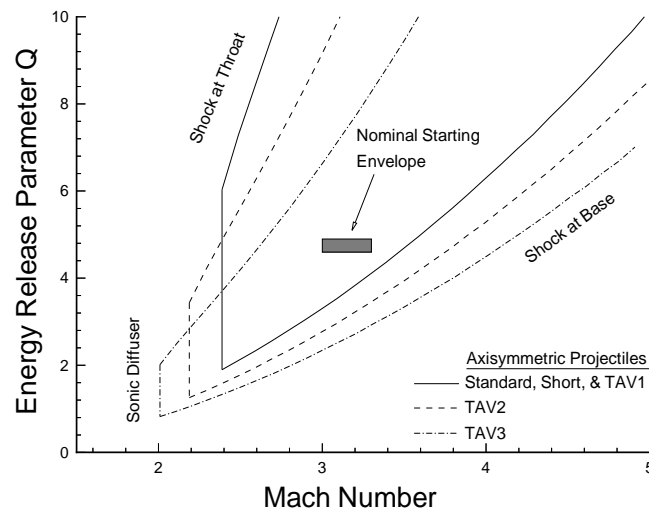


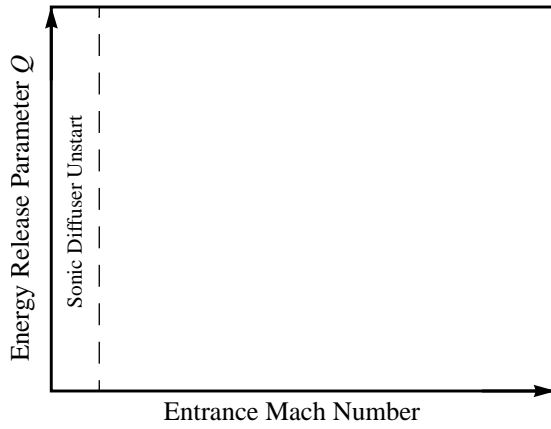
Fig. 5.10 Limits of operation predicted by quasi-one-dimensional model.

This finding is not surprising given the nature of the model. All of the assumptions made are highly inaccurate in the ram accelerator environment, although more refined models have been investigated to improve the accuracy.^{refcarlphd,ajhms} Many factors relevant to the starting process are unaccounted for including the presence of an obturator, launch tube gas, propellant reactive characteristics, and specific three-dimensional projectile geometries. The starting process is so complex in sheer number of factors involved and so rich in phenomena that CFD holds a great deal of potential for studying the starting process beyond experiments. The challenges confronting the application of CFD are many: unsteady, three-dimensional, mixed sub- and supersonic regions, turbulent and separated flow, and chemical kinetics in a variety of propellants at pressures high enough to make real gas effects important. High resolution experimental data for CFD validation could ultimately provide a complete understanding of the starting process.

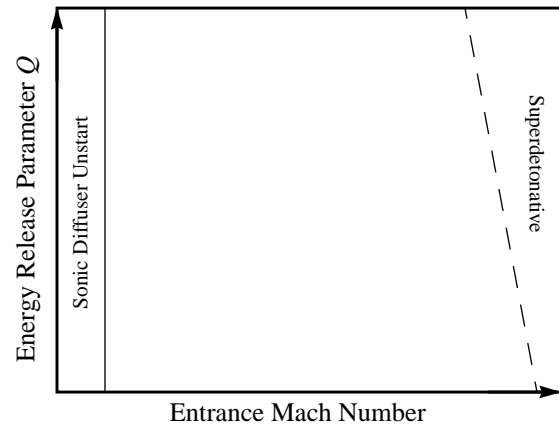
5.5 Starting Envelope

For a given projectile and obturator configuration it is desirable to obtain a starting envelope which is dependent upon the propellant chemistry and the entrance Mach number. Theoretical and computational analysis of the ram accelerator to date is inadequate for determining such a starting envelope. The lack of a comprehensive parametric experimental study to identify chemistry and Mach number regimes conducive to successful starting precludes the presentation of a quantitative starting envelope as well. However, based on this experimental investigation of the starting process, a qualitative starting envelope is suggested. This generalized starting envelope in the Q - M plane is presented in Fig. 5.11 with axes values left off to underscore its qualitative nature.

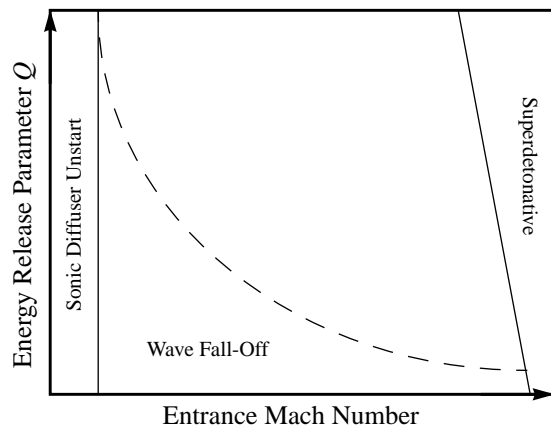
The following comments summarize the experimental and analytical observations made in this study which have been used to construct the limits drawn on the Q - M plane. A sonic diffuser unstart occurs at Mach numbers less than M_{sdu} where supersonic flow to the projectile throat cannot be maintained (Fig. 5.11a). The Chapman-Jouguet detonation Mach number, which has a modest dependence on Q (varying as \sqrt{Q}), sets an upper limit on starting in the subdetonative velocity regime (Fig. 5.11b). The wave fall-off phenomenon dominates the region of relatively low Q and Mach number where the



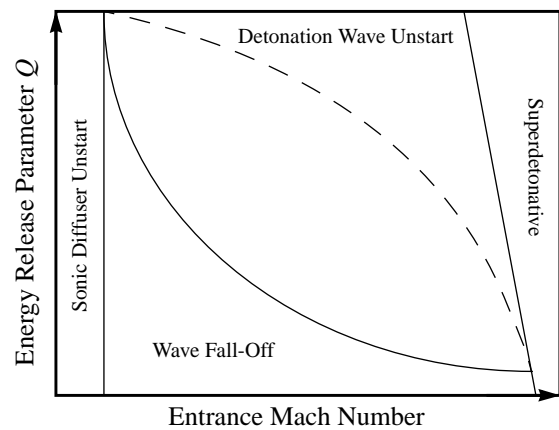
a) Sonic diffuser unstart limit.



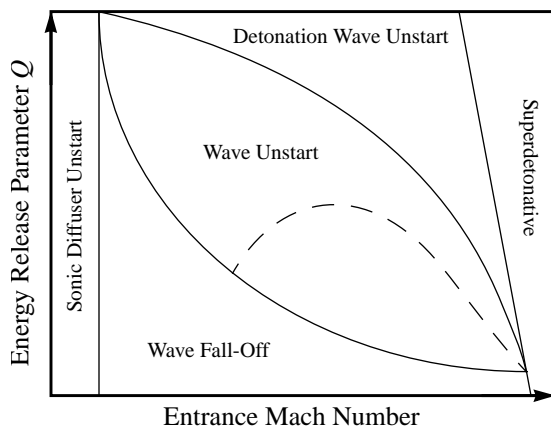
b) Subdetonative limit.



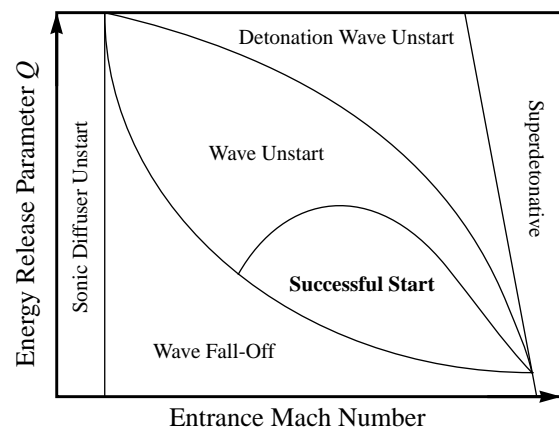
c) Wave fall-off limit.



d) Detonation wave unstart limit.



e) Wave unstart limit.



f) Successful start.

Fig. 5.11 Generalized ram accelerator starting envelope.

propellant cannot be ignited or release enough energy to keep the shock system on the projectile body (Fig. 5.11c). A “detonation wave unstart” region, in which the projectile and obturator initiate a detonation immediately upon entrance leading to a wave unstart, exists for relatively high Q and Mach number (Fig. 5.11d). Other types of wave unstarts (Fig. 5.11e), caused by yet undetermined mechanism(s), have been observed to occur at constant Q when the Mach number is: 1) increased from a wave fall-off result, 2) decreased from a detonation wave unstart result, or 3) decreased from a successful start result. Wave unstarts have also been observed to occur at constant Mach number when Q is: 1) increased from a wave fall-off result, 2) decreased from a detonation wave unstart result, or 3) increased from a successful start result. The successful start envelope is then bounded by the aforementioned failure modes (Fig. 5.11f).

Care should be exercised to realize that any quantitative Q - M plane starting envelope generated will only be applicable to a particular set of initial conditions including projectile, obturator, propellant class, etc. Furthermore, recall that Q is a parameter which cannot be used for comparison across mixture classes. Equal Q propellants from different classes have been shown to result in different start outcomes with all other conditions held the same. An improved propellant correlating parameter for the starting process other than Q would greatly simplify data presentation and understanding, but is likely very complex given the various reactive characteristics of each propellant.

5.6 Time Scales

It is important to develop an understanding of the time scales of factors involved in the starting process. Relative time scales help determine which factors are of first order effect, allowing for the implementation of improved experiments and more accurate computational modeling. In an initial step towards reaching this goal, factors briefly discussed below include the projectile, obturator, entrance diaphragm, shocks, and propellant.

5.6.1 Projectile

Since the most important frame of reference is fixed to the projectile, all time scales should be relative to this frame. Time scaling of the projectile is obviously not an issue in its own body fixed frame. However, dealing with the projectile motion one must work in the inertial laboratory frame. Typical 50 atm propellant wave fall-off experiments result in deceleration of the projectile from 1150 m/s to 1100 m/s within two meters of entrance, while a successful start experiment accelerates the projectile from 1150 m/s to 1530 m/s. The time scale on which the projectile travels 2 m past the entrance diaphragm is approximately 2.0 msec for a wave fall-off and 1.5 msec for a successful start. Average accelerations over this distance are -3000 g and 26,000 g, respectively, and accelerations just prior to a wave unstart can reach 50,000 g. The projectile acceleration will impact unsteady terms in the governing equations.

5.6.2 Obturator

The obturator dynamics data presented in Section 5.2 provide an estimation of the time scale in which the obturator resides in the ram accelerator tube. A 16 gm perforated obturator impacting a 50 atm propellant at Mach 3.2 with no detonation re-enters the launch tube approximately 4 msec later. A solid obturator under the same conditions re-enters the launch tube 1 msec after propellant impact. In general, solid and less massive obturators decelerate and re-enter the launch tube more rapidly than perforated and more massive obturators. Detonation of the propellant, taken as “worst case” conditions for obturator dynamics during a wave unstart, further decreases the obturator residence time in the ram accelerator tube. Data from projectile start experiments at 50 atm fill pressure resulting in wave unstarts shows obturator residence time to be on the order of 2 - 3 msec. Deceleration of a piston from 1150 m/s to 0 m/s within 1 msec of entrance is at an average of over 100,000 g, and therefore unsteady terms are also expected to be of importance in modeling the obturator dynamics.

5.6.3 Diaphragm

The time scale of the entrance diaphragm rupture is dependent upon the pressure differential across it. An infinitely high pressure differential results in a rupture time of zero, corresponding to an instantaneous burst. If this were the case, modeling of the diaphragm would be as simple as removing it upon projectile arrival. However, the diaphragm yield stress precludes the build-up of an overly large pressure differential. To estimate diaphragm rupture time under imminent burst conditions of a 0.35 mm thick Mylar diaphragm, assume that the uniformly distributed pressure differential is equal to the yield stress (28.6 atm). Further assuming that the entire diaphragm mass (0.56 gm) remains in one piece, the diaphragm acceleration is on the order of 10^6 g (given by $F = ma$). Such a high acceleration, albeit calculated in a very rough manner, would send the diaphragm traveling relatively instantaneously down the ram accelerator tube or launch tube, depending on which side of the diaphragm was loaded. Zero pressure differential across the diaphragm would result in rupture on the order of the time it takes for the distance from the projectile nose tip to where the fin rake meets the wall to cross through the entrance location. This event happens in 89 μ sec for a standard projectile at 1150 m/s.

5.6.4 Shocks

The movements of shock systems in the ram accelerator are very difficult to quantitatively estimate due to their dependence on the projectile and obturator dynamics, as well as the propellant energy release. The shocks attached to the projectile nose and to the fin leading edges are on the same time scale as the projectile. The Mach number of the ideal shock generated by the obturator impacting the propellant is given by⁵⁰

$$M_s = \frac{\gamma + 1}{4} M_p + \sqrt{\left(\frac{\gamma + 1}{4}\right)^2 M_p^2 + 1} \quad \text{Eqn. 5.1}$$

Given the compression process occurring in the launch tube between the obturator and diaphragm before entrance, together with the projectile presence, it is unlikely that this

ideal equation can be used for much more than a very rough estimate. Once in the ram accelerator tube, the dynamics of the obturator-generated shock system are further complicated by the propellant energy release. If an energy release time scale could be established, possibly through consideration of the turbulent flow structures on and behind the projectile body as well as propellant induction times, this may form the basis for a time scale to represent shock system fluctuations.

It is interesting to note that if the entrance diaphragm does burst in the direction of the ram accelerator tube, a relatively high strength “shock tube” could be established. Analysis of what effect this shock tube has on the starting process may hold promise for start failures observed when operating with a ventless launch tube and/or with increased launch tube residual air pressures. Complicating factors in this analysis will include the complex nature of the driver section and the diaphragm dynamics.

5.6.5 Kinetics

As alluded to above, the chemical kinetics resulting in energy release to support the shock system on the projectile body is an unknown, and for good reason. Little is known about the flowfield on and behind the projectile body; even less is known about the kinetics of very high pressure, fuel-rich, and dilute hydrocarbon based propellants; and of course the flowfield and kinetics are coupled in a non-linear fashion. The first step in identifying kinetic properties is to investigate induction times for propellants of interest. Induction times (τ_{ind}) versus incident normal shock Mach number for several propellants, all with $Q_{CJ} = 4.78$, are presented in Fig. 5.12. The induction times were computed for an ideal gas with the CHEMKIN thermochemical routines⁴¹ and the GRI-1.2 reaction mechanism for methane oxidation.⁴² The combustion induction process was determined to end when the concentration of OH radicals reached its peak. Note the variation of induction times by orders of magnitude for the shock Mach numbers presented. This is not surprising, as induction times typically vary exponentially with temperature, and the temperature behind a shock varies with the square of the Mach number. The radically different reactive characteristics of these equal- Q propellants is evident as well. The complexity of the combustion processes precludes further back-of-the-envelope analytic

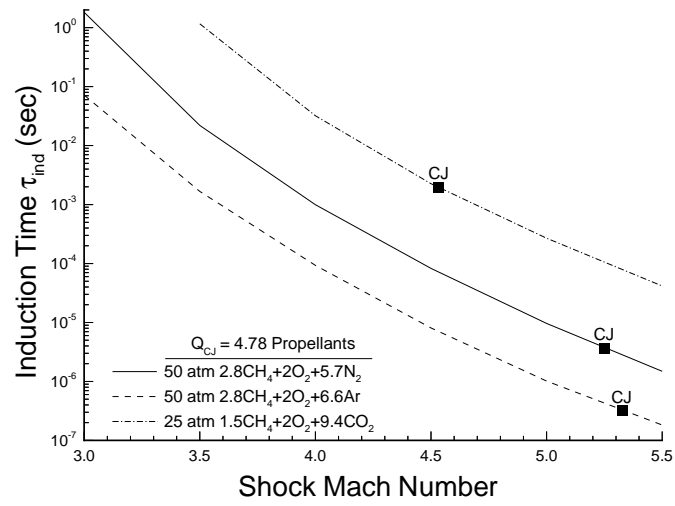


Fig. 5.12 Induction time versus Mach number for $Q_{CJ} = 4.78$ propellants.

discussion on kinetics time scales. Validated kinetics mechanisms will be instrumental in computational efforts applied to the ram accelerator.

6. Recommendations

All of the topics addressed in this effort require more in-depth study to achieve a better understanding of the starting process. With that in mind, each section of Chapter 4 and Chapter 5 represents a portion of the “things-to-do” list. No matter which issues are investigated further, care must be taken to execute experiments which answer specific questions while introducing minimal ambiguity. This is difficult at best and impossible at times, but efforts must be made to isolate factors of interest in order to understand the phenomena involved. The number of coupled factors involved makes CFD a tool ideally suited for supporting a parametric experimental investigation of the starting process. Prior to CFD application, sufficient confidence in the numerical techniques used to explore this complex environment must be gained by validating the code output against experimental data.

Understanding the mechanisms leading to wave unstart is perhaps the biggest overall challenge, but also holds the greatest promise for a very robust starting process. In the absence of improved diagnostics such as detailed flow visualization and on-board instrumentation, extensive parametric studies of projectile geometry and propellant variations will probably be required. High spatial resolution instrumented tube sections one or two meters long on each side of the entrance diaphragm would significantly help any investigation of the starting process transients. Ionization gauges are relatively simple diagnostic tools which should be added to the instrumentation system. These would replace the fiber optic luminosity probes’ function of detecting combustion regions, while eliminating the uncertainty associated with detecting visible emissions. Through knowledge of the wave unstart, the starting process conditions can be tailored to meet the goals outlined in Section 2.3: operation at high Q and low Mach number.

Much remains to be done in applying piston detonation limits to the subdetonative starting process. More extensive testing of piston mass effects could be pursued, complemented by a study of initial launcher gas pressure behind the piston. The latter is of interest because current ram accelerator facilities utilize both compressed gas and powder gun launchers, with inherently different pressure characteristics. Piston geometry

variations other than perforated and solid pistons could be investigated, and the method of characteristics code modified to account for perforations in the piston. Launch tube gas pressure ahead of the piston has been shown to play a critical role in the ignition process, mandating a more detailed survey of this parameter. The detonation limits presented here may warrant refinement to narrow the window between detonation and no detonation. Piston detonation limit studies may also be applied to starting parameters not explored in this research, such as effects of launch tube venting and entrance diaphragm thickness. Further efforts are required to understand how to use piston detonation limits for the identification of conditions to avoid in the starting process. This will involve modeling of the obturator and incorporation of projectile and launch tube gas effects to augment the piston initiated detonation limit data. The further study of kinetic induction times is expected to play a role in relating piston detonation limits to the ram accelerator as well as investigating the fundamental issue of detonation initiation by a piston.

An understanding of detonation limits may also be of use to the ram accelerator beyond the starting process. When staging is performed, the projectile transitions from one propellant to another, and so it is conceivable that a propellant transition could result in the projectile and its flowfield initiating a detonation leading to wave unstart. If a technique can be developed to model this process, with potential factors that contribute to detonation initiation including the projectile, transition diaphragm, and the propellant characteristics on either side of the diaphragm, transition conditions may be ruled out prior to expending projectiles. Finally, ram accelerator operation at superdetonative velocities is in its infancy, but it is interesting to note that in this case it may be desirable to initiate a detonation³³. Detonation limit efforts may then seek to characterize propellants and operating conditions which are conducive to detonation initiation.

7. Conclusions

A thorough review of past research as well as the current understanding of the starting process has been presented. The four possible outcomes of a start attempt are the sonic diffuser unstart, wave fall-off, wave unstart, and successful start. A sonic diffuser unstart is caused by conditions upstream of the throat resulting in subsonic flow in the diffuser. A wave fall-off occurs when insufficient energy is released from the propellant to keep the shock system on the projectile body from receding behind the base. A wave unstart is caused by conditions downstream of the throat resulting in disengagement of the shock system on the body into the diffuser. A successful start is achieved when supersonic flow is maintained throughout the diffuser, and the shock system is stabilized on the projectile body through propellant energy release.

Piston detonation experiments were conducted to define detonation limits for several propellants, study the association of detonations with the wave unstart process, gain knowledge of the obturator dynamics as it transitions from the launch tube into the ram accelerator tube, and investigate the effects of obturator mass, obturator geometry, and launch tube air pressure variations on propellant ignition. The piston detonation limits were found to not always be indicative of the upper velocity at which a ram accelerator projectile can be successfully started. In some instances a successful start or wave fall off would occur at Mach numbers above which a piston alone detonated the propellant. Thus, the goal of reducing the number of projectile firings, by narrowing the range of entrance velocity and propellant chemistry to be investigated through piston initiated detonation limits, was not realized.

Observation of the piston time-distance profiles after propellant impact, supported by a method of characteristics code, has increased the understanding of the piston dynamics in detonation experiments and ram accelerator start attempts. The piston decelerates after propellant impact and then moves backwards. Reversal of direction occurs more rapidly after propellant ignition, for less massive pistons, and for solid geometries. Piston mass had a negligible effect on the detonation limits for the conditions studied. Solid pistons were able to initiate detonation at lower Mach numbers than

perforated pistons. In addition, elevated launch tube pressure was found to increase the detonation limits.

Projectile start attempt experiments were used to explore the limits to successful starting, study the association of detonations with the wave unstart process, improve the understanding of the flowfield in the launch tube and ram accelerator tube, and investigate the effects of Mach number, propellant chemistry, obturator geometry and mass, and throat area variations on the starting process. The impossibility of performing a large number of detailed parametric experiments during this investigation precluded the presentation of quantitative starting envelopes, but a qualitative envelope was created that places the possible start outcomes relative to one another in a parameter space based on entrance Mach number and propellant composition. Increased Q is conducive to a wave unstart, while decreased Q eventually leads to a wave fall-off. Wave unstarts were found to occur at Mach numbers above and below successful starting conditions, and wave fall-offs were limited to Mach number below conditions which resulted in a successful start or wave unstart. Detonations were often observed in conjunction with wave unstarts, and for relatively high Q and Mach number these occurred immediately after entrance.

Increasing obturator mass was more conducive to igniting a propellant, as was utilizing a solid rather than a perforated geometry. Increased flow throat areas reduced the Mach number for maintaining supersonic flow throughout the diffuser, but required relatively low Q and high Mach number to contain the shock system behind the throat. Measurements of the launch tube and ram accelerator tube flowfield were in agreement with past starting research. The launch tube gas is compressed to significantly high temperature and pressure levels prior to projectile entrance. Ram accelerator tube data identified typical flowfield characteristics for all of the possible start outcomes, but are of insufficient resolution to determine how these outcomes evolve for all but the wave fall-off case. Identification of significantly different pressure data for wave unstart results under various conditions leads to the conclusion that more than one mechanism exists to cause a wave unstart.

8. References

1. Hertzberg, A., Bruckner, A.P., and Bogdanoff, D.W., "Ram Accelerator: A New Chemical Method for Accelerating Projectiles to Ultrahigh Velocities," *AIAA Journal*, Vol. 26, 1988, pp. 195-203.
2. Bruckner, A.P., Knowlen, C., Hertzberg, A., and Bogdanoff, D.W., "Operational Characteristics of the Thermally Choked Ram Accelerator," *AIAA Journal of Propulsion and Power*, Vol. 7, 1991, pp. 828-836.
3. Hertzberg, A., Bruckner, A.P., and Knowlen, C., "Experimental Investigation of Ram Accelerator Propulsion Modes," *Shock Waves*, Vol. 1, 1991, pp. 17-25.
4. Knowlen, C., Li, J.G., Hinkey, J., and Dunmire, B., "University of Washington Ram Accelerator Facility," 42nd Meeting of the Aeroballistic Range Association, Adelaide, Australia, October 22-25, 1991.
5. Bruckner, A.P., Knowlen, C., Hertzberg, A., "Applications of the Ram Accelerator to Hypervelocity Aerothermodynamic Testing," AIAA Paper 92-3949, 17th AIAA Aerospace Ground Testing Conference, Nashville, TN, July 6-8, 1992.
6. Kruczynski, D.L., "New Experiments in a 120-mm Ram Accelerator at High Pressures," AIAA Paper 93-2589, 29th AIAA/ASME/SAE/ASEE Joint Propulsion Conference, Monterey, CA, June 28-30, 1993.
7. Smeets, G., Seiler, F., Patz, G., and Srulijes, J., "First Results Obtained in a 30-mm-Caliber Scram Accelerator Using a Rail Tube for Cylindrical Projectiles," 25th International Symposium on Combustion, University of California, Irvine, Poster Number P1-56, July 31-August 5, 1994.
8. Giraud, M., Legendre, J.F., Simon, G., Henner, M., and Voisin, D., "RAMAC in 90 mm or RAMAC 90: Starting Process, Control of the Ignition Location, and Performance in Thermally Choked Propulsion Mode," Proceedings of the 2nd International Workshop on Ram Accelerators, Seattle, WA, July 17-20, 1995.
9. Sasoh, A., and Takayama, K., "RAMAC 25 at Shock Wave Research Center," Proceedings of the 2nd International Workshop on Ram Accelerators, Seattle, WA, July 17-20, 1995.
10. Chang, X., Kanemoto, H., and Taki, S., "A Ram Accelerator with Rectangular Bore is Working at Hiroshima University," AIAA Paper 95-2496, 31st AIAA/ASME/SAE/ASEE Joint Propulsion Conference, San Diego, CA, July, 1995.
11. Hinkey, J.B., Burnham, E.A., and Bruckner, A.P., "Investigation of Ram Accelerator Flow Fields Induced by Canted Projectiles," AIAA Paper 93-2186, 29th AIAA/ASME/SAE/ASEE Joint Propulsion Conference, Monterey, CA, June 28-30, 1993.

12. Hinkey, J.B., Burnham, E.A., and Bruckner, A.P., "High Spatial Resolution Measurements in a Single Stage Ram Accelerator," 29th JANNAF Combustion Subcommittee Meeting, NASA Langley Research Center, Hampton, VA, October 19-23, 1992.
13. Waltrup, P.J., and Billig, F.S., "Structure of Shock Waves in Cylindrical Ducts," *AIAA Journal*, Vol. 11, 1973, pp. 1404-1408.
14. Billig, F.S., "Research on Supersonic Combustion," *AIAA Journal of Propulsion and Power*, Vol. 9, 1993, pp. 499-514.
15. Elvander, J.E., Knowlen, C., Bruckner, A.P., "High Velocity Performance of the Ram Accelerator," AIAA Paper 96-2675, 32nd AIAA/ASME/SAE/ASEE Joint Propulsion Conference, Lake Buena Vista, FL, July 1-3, 1996.
16. Auzias de Turenne, J., "An Analysis of Ram Accelerator Projectile Materials," AIAA Paper 92-0262, 30th Aerospace Sciences Meeting, Reno, NV, January, 1992.
17. Higgins, A.J., Knowlen, C., and Bruckner, A.P., "An Investigation of Ram Accelerator Gas Dynamic Limits," AIAA Paper 93-2181, 29th AIAA/ASME/SAE/ASEE Joint Propulsion Conference, Monterey, CA, June 28-30, 1993.
18. Higgins, A.J., "Gas Dynamic Limits of the Ram Accelerator," M.S.A.A. Thesis, Department of Aeronautics and Astronautics, University of Washington, Seattle, WA, 1993.
19. Choi, J., Jeung, I., and Yoon, Y., "Numerical Study of Scram Accelerator Starting Characteristics," 35th AIAA Aerospace Sciences Meeting, Reno, NV, January 6-10, 1997.
20. Knowlen, C., Higgins, A.J., and Bruckner, A.P., "Investigation of Operational Limits to the Ram Accelerator," AIAA Paper 94-2967, 30th AIAA/ASME/SAE/ASEE Joint Propulsion Conference, Indianapolis, IN, June 27-29, 1994.
21. Knowlen, C., and Bruckner, A.P., "Investigation of Propellant Dilution on Ram Accelerator Performance," 30th JANNAF Combustion Subcommittee Meeting, Monterey, CA, November 15-18, 1993.
22. Burnham, E.A., Hinkey, J.B., and Bruckner, A.P., "Investigation of Starting Transients in the Thermally Choked Ram Accelerator," 29th JANNAF Combustion Subcommittee Meeting, NASA Langley Research Center, Hampton, VA, October 19-23, 1992.
23. Burnham, E.A., "Investigation of Starting and Ignition Transients in the Thermally Choked Ram Accelerator," Ph.D. Dissertation, Department of Aeronautics and Astronautics, University of Washington, Seattle, WA, 1993.
24. Stewart, J.F., and Bruckner, A.P., "Effects of Launch Tube Gases and Fill Pressure on Ram Acceleration," 33rd JANNAF Combustion Subcommittee Meeting, Monterey, CA, November 4-8, 1996.

25. Stewart, J.F., "Shock Dynamics in the Ram Accelerator Launch Tube," AIAA Region VI Student Conference, Seattle, WA, April 3-5, 1997.
26. Knowlen, C., and Bruckner, A.P., "A Hugoniot Analysis of the Ram Accelerator," 18th International Symposium on Shock Waves, Sendai, Japan, July 21-26, 1991.
27. McFall, K.A., Knowlen, C., Bruckner, A.P., Hertzberg, A., "Numerical Analysis of Zero Velocity Start Technique for the Ram Accelerator," AIAA Paper 96-3259, 32nd AIAA/ASME/SAE/ASEE Joint Propulsion Conference, Lake Buena Vista, FL, July 1-3, 1996.
28. Kruczynski, D.L., "Requirements, Design, Construction, and Testing of a 120 mm In-Bore Ram Accelerator," 28th JANNAF Combustion Subcommittee Meeting, San Antonio, TX, 1991.
29. Kruczynski, D.L., Liberatore, F., "Experimental Investigation of High Pressure/Performance Ram Accelerator Operation," AIAA Paper 96-2676, 32nd AIAA/ASME/SAE/ASEE Joint Propulsion Conference, Lake Buena Vista, FL, July 1-3, 1996.
30. Nusca, M.J., and Kruczynski, D.L., "Reacting Flow Simulation for a Large-Scale Ram Accelerator," *AIAA Journal of Propulsion and Power*, Vol. 12, 1996, pp. 61-69.
31. Humphrey, J.W., Brueckner, F.P., Sobota, T.H., and Pepper, D.W., "Internal Ballistics and Inlet Starting of Projectiles In Ram- and Scramaccelerator Launch Tubes with Venting," AIAA Paper 93-0746, 31st Aerospace Sciences Meeting, Reno, NV, January, 1993.
32. Humphrey, J.W., and Sobota, T.H., "A Scramaccelerator Hypervelocity Launcher," Proceedings of the 1st International Workshop on Ram Accelerators, Saint-Louis, France, September 7-10, 1993.
33. Knowlen, C., Higgins, A.J., and Bruckner, A.P., "Ram Accelerator Operation in the Superdetonative Velocity Regime," 34th AIAA Aerospace Sciences Meeting, Reno, NV, January 15-18, 1996.
34. Seiler, F., Patz, G., Smeets, G., Srulijes, J., "The Rail Tube in Ram Acceleration: Feasibility Study with ISL's RAMAC 30," Proceedings of the 2nd International Workshop on Ram Accelerators, Seattle, WA, July 17-20, 1995.
35. Patz, G., Seiler, F., Smeets, G., Srulijes, J., "Status of ISL's RAMAC 30 with Fin Guided Projectiles Accelerated in a Smooth Bore," Proceedings of the 2nd International Workshop on Ram Accelerators, Seattle, WA, July 17-20, 1995.
36. Sasoh, A., Hirakata, S., Ujigawa, Y., and Takayama, K., "Operation Tests of a 25 mm Bore Ram Accelerator," AIAA Paper 96-2677, 32nd AIAA/ASME/SAE/ASEE Joint Propulsion Conference, Lake Buena Vista, FL, July 1-3, 1996.
37. Sasoh, A., Higgins, A.J., Knowlen, C., and Bruckner, A.P., "Hollow Projectile Operation in the Ram Accelerator," *AIAA Journal of Propulsion and Power*, Vol. 12, 1996, pp. 1183-1186.

38. Chang, X., Higgins, A.J., Schultz, E., and Bruckner, A.P., "Operation of Quasi-Two-Dimensional Projectiles in a Ram Accelerator," *AIAA Journal of Propulsion and Power*, Technical Note, Vol. 13, 1997.
39. Knowlen, C., Li, J.G., Hinkey, J., and Dunmire, B., "University of Washington Ram Accelerator Facility," 42nd Meeting of the Aeroballistic Range Association, Adelaide, Australia, October 22-25, 1991.
40. Buckwalter, D.L., Knowlen, C., and Bruckner, A.P., "Ram Accelerator Performance Analysis Code Incorporating Real Gas Effects," 32nd AIAA/ASME/SAE/ASEE Joint Propulsion Conference, Lake Buena Vista, FL, July 1-3, 1996.
41. Mitchell, R.E., and Kee, R.J., "A General Purpose Computer Code for Predicting Chemical Kinetic Behavior Behind Incident and Reflected Shocks," Sandia Report, SAND82-8205, 1992.
42. Frenklach, M., Wang, H., Goldenberg, M., Smith, G.P., Golden, D.M., Bowman, C.T., Hanson, R.K., Gardiner, W.C., and Lissianski, V., "GRI-Mech-- An Optimized Detailed Chemical Reaction Mechanism for Methane Combustion," GRI Topical Report No. GRI-95/0058, 1995.
43. Oates, G.C., *Aerothermodynamics of Gas Turbine and Rocket Propulsion*, AIA Education Series, Washington D.C., 1988, pp. 206-210.
44. Strehlow, R.A., *Combustion Fundamentals*, McGraw-Hill, New York, 1984, pp. 302-307.
45. Lee, J.H.S., "Initiation of Gaseous Detonation," *Annual Review of Physical Chemistry*, Vol. 28, 1977, pp. 75-104.
46. Bauer, P., Legendre, J-F., Knowlen, C., and Higgins, A.J., "Detonation of Insensitive Dense Gaseous Mixtures in Tubes," 32nd AIAA/ASME/SAE/ASEE Joint Propulsion Conference, Lake Buena Vista, FL, July 1-3, 1996.
47. Zakharov, N.S., and Korobeinikov, V.P., "Piston in a Detonating Gas," Russian translation from Zhurnal Prikladnoi Mekhaniki i Tekhnicheskoi Fiziki, No. 2, pp. 76-79, Plenum Publishing Corp, UDC 533.601.11, 1979.
48. Levin, V.A., Markov, V.V., and Osinkin, S.F., "Detonation Initiation in a Hydrogen-Air Mixture by Means of a Piston," Doklady Akad. Nauk SSSR, Vol. 313, 1990, pp. 288-291.
49. Knowlen, C., "Theoretical and Experimental Investigation of the Thermodynamics of the Thermally Choked Ram Accelerator," Ph.D. Dissertation, Department of Aeronautics and Astronautics, University of Washington, Seattle, WA, 1991.
50. Anderson, J.D., *Modern Compressible Flow*, McGraw-Hill, New York, 1990, pp. 206-240.

Appendix A: Projectile Experiment Data

Notes: 1) Fin thickness, number of fins, and projectile material data are available, but were left out due to space constraints.
 2) Failure modes: ERR=Human Error, WU=Wave Unstart, SDU = Sonic Diffuser Unstart, WFO = Wave Fall Off

HS #	Projectile				Sabot		Propellant				V (m/s)	M	Start?	Failure	
	Nose	Throat	Body	Base	M (g)	Type	Composition	P (atm)	Fill	Qcj				Mode	Comments
	A (deg)	D (mm)	L (mm)	D (mm)	M (g)	Type	Composition	P (atm)	Qcj	Mode				Comments	
1320	10	29	71	18	77	16	Perf	2.8CH4+2O2+5.7N2	50	4.6		3.2	yes		Plt 3.0psi
1319	10	29	71	18	77	16	Perf	2.8CH4+2O2+5.7N2	50	4.6		3.1	no	SDU	Plt 3.4psi
1318	10	29	71	18	77	16	Perf	2.8CH4+2O2+5.7N2	50	4.6		3.1	yes		Plt 3.1psi
1317	10	29	71	18	76	16	Perf	2.8CH4+2O2+5.7N2	50	4.6		3.2	no	ERR	Plt 2.9psi
1316	15	29	46	18	55	16	Perf	5CH4+2O2+2He	50	4.8		3.	yes		
1315	10	29	71	18	77	16	Perf	2.8CH4+2O2+5.7N2	50	4.6		3.1	no	SDU	Plt 4psi
1314	10	29	71	18	77	16	Perf	2.8CH4+2O2+5.7N2	50	4.6		3.2	yes		Plt 2psi
1313	10	29	71	18	77	16	Perf	2.8CH4+2O2+5.7N2	50	4.6		3.1	yes		Plt 2psi
1312	10	29	71	18	77	16	Perf	2.8CH4+2O2+5.7N2	50	4.6		3.2	yes		Plt 1psi
1311	10	29	71	18	76	16	Solid	2.8CH4+2O2+5.7N2	50	4.6		3.1	no	WU	
1310	10	29	71	18	76	16	Solid	2.8CH4+2O2+5.7N2	50	4.6		3.2	no	WU	
1309	15	29	46	18	51	16	Perf	2.8CH4+2O2+5.7N2	50	4.6		3.7	no	WU	
1308	15	29	46	18	51	16	Perf	2.8CH4+2O2+5.7N2	50	4.6		3.2	no	WU	
1307	10	29	71	18	76	16	Perf	2.8CH4+2O2+5.7N2	25	4.6		3.2	yes		
1306	10	29	71	18	76	16	Perf	2.8CH4+2O2+5.7N2	35	4.6		3.2	yes		
1305	15	29	46	18	50	16	Perf	5CH4+2O2+2He	50	4.8		2.9	yes		

HS #	Projectile					Sabot		Propellant					Start?	Mode	Comments
	Nose A (deg)	Throat D (mm)	Body L (mm)	Base D (mm)	M (g)	M (g)	Type	Composition	P (atm)	Qc _j	V (m/s)	M			
1304	15	29	46	18	50	16	Perf	5CH4+2O2+2He	50	4.8	1330	3.	yes		
1303	15	29	46	18	50	16	Perf	5CH4+2O2+2He	50	4.8	1307	2.9	yes		
1302	15	29	46	18	50	16	Perf	5CH4+2O2+2He	50	4.8	1305	2.9	yes		
1301	15	29	46	18	50	16	Perf	5CH4+2O2+2He	50	4.8	1309	2.9	yes		
1300	15	29	46	18	50	16	Perf	5CH4+2O2+2He	50	4.8	1312	2.9	yes		
1299	15	29	46	18	50	16	Perf	5CH4+2O2+2He	50	4.8	1309	2.9	yes		
1298	15	29	46	18	50	16	Perf	5CH4+2O2+2He	50	4.8	1312	2.9	yes		
1297	15	29	46	18	50	16	Perf	5CH4+2O2+2He	50	4.8	1317	2.9	no	WU	
1296	15	29	46	18	50	16	Perf	5CH4+2O2+2He	50	4.8	1319	2.9	no	WU	
1295	15	29	46	18	50	16	Perf	5CH4+2O2+2He	50	4.8	1319	2.9	yes		
1294	15	29	46	18	50	16	Perf	5CH4+2O2+2He	50	4.8	1322	2.9	yes		
1293	15	29	46	18	50	16	Perf	5CH4+2O2+2He	50	4.8	1327	3.	yes		
1292	15	29	46	18	50	16	Perf	5CH4+2O2+2He	50	4.8	1312	2.9	yes		
1291	15	29	46	18	50	16	Perf	5CH4+2O2+2He	50	4.8	1307	2.9	yes		
1290	15	29	46	18	50	16	Perf	5CH4+2O2+2He	50	4.8	1317	2.9	yes		
1289	15	29	46	18	50	16	Perf	5CH4+2O2+2He	50	4.8	1309	2.9	yes		
1288	15	29	46	18	50	16	Perf	5CH4+2O2+2He	50	4.8	1322	2.9	yes		
1287	15	29	46	18	50	16	Perf	5CH4+2O2+2He	50	4.8	1314	2.9	yes		
1286	15	29	46	18	50	16	Perf	5CH4+2O2+2He	50	4.8	1314	2.9	yes		
1285	15	29	46	18	50	16	Perf	5CH4+2O2+2He	50	4.8	1309	2.9	yes		

HS #	Projectile					Sabot		Propellant					Failure Mode	Comments
	Nose A (deg)	Throat D (mm)	Body L (mm)	Base D (mm)	M (g)	M (g)	Type	Composition	P (atm)	Qc _j	V (m/s)	M		
1284	15	29	46	18	50	16	Perf	5CH ₄ +2O ₂ +2He	50	4.8			yes	
1283	10	29	71	18	69	16	Perf	2.8CH ₄ +2O ₂ +10Ar	50	4.	973	3.	no	WU
1282	10	29	71	18	70	16	Perf	2.8CH ₄ +2O ₂ +9.7Ar	50	4.	966	2.9	no	WU
1281	10	29	71	18	70	16	Perf	2.8CH ₄ +2O ₂ +9.2Ar	50	4.1	981	3.	no	WU
1280	10	25	71	13	69	16	Perf	2.8CH ₄ +2O ₂ +11.3Ar	50	3.7	992	3.	no	WU
1279	10	25	71	13	62	16	Perf	2.8CH ₄ +2O ₂ +11.3Ar	50	3.7	951	2.9	no	WFO
1278	10	25	71	13	62	16	Perf	2.8CH ₄ +2O ₂ +12Ar	50	3.6	943	2.9	no	WFO
1277	10	25	71	13	62	16	Perf	2.8CH ₄ +2O ₂ +13Ar	50	3.4	969	3.	no	WFO
1276	10	27	71	16	62	16	Perf	2.8CH ₄ +2O ₂ +11.3Ar	50	3.7	1004	3.1	no	WU
1275	10	29	71	18	72	16	Perf	2.8CH ₄ +2O ₂ +10.2Ar	50	3.9	977	3.	no	WFO
1274	10	29	71	18	70	16	Perf	2.8CH ₄ +2O ₂ +11Ar	50	3.8	977	3.	no	WFO
1273	10	27	71	16	70	16	Perf	2.8CH ₄ +2O ₂ +11Ar	50	3.8	984	3.	yes	
1272	10	27	71	16	72	16	Perf	2.8CH ₄ +2O ₂ +12Ar	50	3.6	988	3.	no	WFO
1271	10	27	71	16	72	16	Perf	2.8CH ₄ +2O ₂ +12.5Ar	50	3.5	996	3.	no	WFO
1270	10	27	71	16	72	16	Perf	2.8CH ₄ +2O ₂ +13Ar	50	3.4	984	3.	no	WFO
1269	10	27	71	16	72	16	Perf	2.8CH ₄ +2O ₂ +13.5Ar	50	3.4	988	3.	no	WFO
1268	10	27	71	16	72	16	Perf	2.8CH ₄ +2O ₂ +14.5Ar	50	3.2	992	3.	no	WFO
1267	10	27	71	16	72	16	Perf	2.8CH ₄ +2O ₂ +14.5Ar	50	3.2			no	ERR
1266	10	27	71	16	72	16	Perf	2.8CH ₄ +2O ₂ +12.7Ar	50	3.5	1020	3.1	no	WU
1265	10	25	71	13	62	16	Perf	2.8CH ₄ +2O ₂ +12.7Ar	50	3.5	992	3.	no	WU

HS #	Projectile				Sabot		Propellant				M	Start?	Failure Mode	Comments	
	Nose A (deg)	Throat D (mm)	Body L (mm)	Base D (mm)	M (g)	Type	Composition	P (atm)	Fill	Qcj					V (m/s)
1264	10	25	71	13	62	16	Perf	2.8CH4+2O2+12.7Ar	50	3.5	1176	3.6	no	WU	
1263	10	25	71	13	62	16	Perf	2.8CH4+2O2+10.1Ar	50	3.9	1165	3.5	no	WU	
1262	10	25	71	13	62	16	Perf	2.8CH4+2O2+8.5Ar	50	4.3	1165	3.5	no	WU	
1261	10	25	71	13	62	16	Perf	2.8CH4+2O2+7Ar	50	4.7	1171	3.5	no	WU	
1260	10	25	71	13	62	16	Perf	2.8CH4+2O2+8N2	50	4.	1245	3.4	yes		
1259	10	25	71	13	62	16	Perf	2.8CH4+2O2+7.2N2	50	4.2	1250	3.5	no	WU	
1258	10	25	71	13	62	16	Perf	2.8CH4+2O2+6.7N2	50	4.3	1210	3.3	no	WU	
1257	10	27	71	16	72	16	Perf	2.8CH4+2O2+6.7N2	50	4.3	1187	3.3	yes		
1256	10	27	71	16	72	16	Perf	2.8CH4+2O2+5.7N2	50	4.6	1187	3.3	no	WU	
1255	10	27	71	16	72	16	Perf	2.8CH4+2O2+5.7N2	50	4.6	1134	3.1	no	WU	
1254	10	29	71	18	69	16	Perf	2.8CH4+2O2+7.5N2	50	4.1	1016	2.8	no	WFO	
1253	10	29	71	18	69	16	Perf	2.8CH4+2O2+6.7N2	50	4.3	1012	2.8	no	WU	
1252	10	29	71	18	69	16	Perf	2.8CH4+2O2+6.2N2	50	4.5	1017	2.8	no	WU	
1251	10	29	71	18	69	16	Perf	2.8CH4+2O2+5.7N2	50	4.6	1020	2.8	no	WU	
1250	10	29	71	18	69	16	Perf	2.8CH4+2O2+5.7N2	50	4.6	1067	2.9	yes		
1249	10	29	71	18	69	16	Perf	2.8CH4+2O2+5.7N2	50	4.6	1149	3.2	yes		
1248	15	29	46	18	51	16	Perf	5CH4+2O2+2He	50	4.8			no		
1247	15	29	46	18	50	16	Perf	5CH4+2O2+2He	50	4.8	1327	3.	yes		
1246	15	29	46	18	45	16	Perf	5CH4+2O2+2He	50	4.8	1337	3.	yes		
1245	15	29	46	18	50	16	Perf	4.8CH4+2O2+2He	50	4.9	1322	3.	no	WU	

HS #	Projectile				Sabot		Propellant				M	Start?	Failure Mode	Comments		
	Nose A (deg)	Throat D (mm)	Body L (mm)	Base D (mm)	M (g)	Type	Composition	P (atm)	Qcj	V (m/s)						
1244	15	29	46	18	50	16	Perf	4.7CH4+2O2+3He	50	4.6	1317	2.8	no	WU		
1243	15	29	46	18	50	16	Perf	4.7CH4+2O2+2He	50	5.	1327	3.	no	WU		
1242	15	29	46	18	50	16	Perf	4.4CH4+2O2+2He	50	5.1	1324	3.	no	WU		
1241	15	29	46	18	50	16	Perf	5CH4+2O2+2He	50	4.8	1319	2.9	yes			
1240	15	29	46	18	50	16	Perf	5.5CH4+2O2+1H2	50	5.1	1314	3.1	no	WU		
1239	15	29	46	18	50	16	Perf	5.7CH4+2O2	50	5.4	1314	3.3	yes			
1238	15	29	46	18	50	16	Perf	6CH4+2O2	50	5.2	1327	3.3	yes			
1237	15	29	46	18	50	16	Perf	6.5CH4+2O2	50	5.1	1327	3.3	yes			
1236	15	29	46	18	49	16	Perf	5.5CH4+2O2	50	5.4	1327	3.3	no	WU		
1235	10	29	71	18	76	16	Perf	2.8CH4+2O2+5.7N2	25	4.6	1139	3.1	yes			
1234	10	29	71	18	76	16	Perf	2.8CH4+2O2+5.7N2	25	4.6	1160	3.2	yes			
1233	10	29	71	18	75	16	Perf	2.8CH4+2O2+5.7N2	25	4.6	1175	3.2	no	Unst		
1232	10	29	71	18	77	16	Perf	2.8CH4+2O2+5.7N2	25	4.6	1139	3.1	no	Unst	ventless	
1231	10	29	71	18	76	16	Perf	2.8CH4+2O2+5.7N2	25	4.6	1144	3.1	no	Unst	ventless	
1230	10	29	71	18	76	16	Perf	2.8CH4+2O2+5.7N2	50	4.6	1124	3.1	yes		ventless	
1229	10	29	71	18	76	16	Perf	2.8CH4+2O2+5.7N2	30	4.6	1155	3.2	yes		ventless	
1228	10	29	71	18	76	16	Perf	2.8CH4+2O2+5.7N2	25	4.6	1150	3.2	no	Unst	ventless	
1227	10	29	71	18	76	16	Perf	2.8CH4+2O2+5.7N2	25	4.6	1139	3.1	no	Unst	ventless	
1226	10	29	71	18	76	16	Perf	2.8CH4+2O2+5.7N2	35	4.6	1154	3.2	yes		ventless	
1213-1225 Quasi-2D Proj																

HS #	Projectile					Sabot		Propellant				V (m/s)	M	Start?	Failure Mode	Comments
	Nose A (deg)	Throat D (mm)	Body L (mm)	Base D (mm)	M (g)	M (g)	Type	Composition	P (atm)	Qc _j						
1212	10	29	71	18	78	16	Perf	2.8CH4+2O2+5.7N2	49	4.6	3.2	yes				
1211	15	29	46	18	44	16	Perf	2.8CH4+2O2+5.7N2	30	4.6	3.3	yes				
1210	10	29	71	18	75	36	Solid	1.5CH4+2O2+5.4CO2	25	7.	2.8	no	WFO			
1209	10	29	71	18	73	36	Solid	1.5CH4+2O2+5.5CO2	25	6.9	2.8	no	WFO			
1208	10	29	71	18	73	36	Solid	1.5CH4+2O2+5.3CO2	25	7.1	2.9	no	WU			
1207	10	29	71	18	73	35	Solid	1.5CH4+2O2+5CO2	25	7.3	2.8	no	WU			
1206	10	29	71	18	73	36	Solid	1.5CH4+2O2+5CO2	25	7.3	2.8	no	WU			
1205	10	29	71	18	73	26	Solid	1.5CH4+2O2+4.9CO2	25	7.4	2.9	no	WFO			
1204	10	29	71	18	73	26	Solid	1.5CH4+2O2+4.8CO2	25	7.6	2.9	no	WU			
1203	10	29	71	18	73	26	Solid	1.5CH4+2O2+4.5CO2	25	7.8	2.8	no	WU			
1202	10	29	71	18	73	26	Solid	1.5CH4+2O2+5CO2	25	7.3	2.9	no	WFO			
1201	10	29	71	18	73	16	Perf	1.5CH4+2O2+3.9CO2	25	8.5	2.6	no	WFO			
1200	10	29	71	18	73	16	Perf	1.5CH4+2O2+3.9CO2	25	8.5	1.8	no	SDU			
1199	10	29	71	18	74	16	Perf	1.5CH4+2O2+3.8CO2	25	8.7	2.5	no	WU			
1198	10	29	71	18	74	16	Perf	1.5CH4+2O2+3.5CO2	25	9.	2.5	no	WU			
1197	10	29	71	18	73	16	Perf	1.5CH4+2O2+4CO2	25	8.4	2.6	no	WFO			
1196	10	29	71	18	73	16	Perf	1.5CH4+2O2+4.4CO2	25	8.	2.8	no	WU			
1195	10	29	71	18	73	16	Perf	1.5CH4+2O2+4.2CO2	25	8.1	2.8	no	WU			
1194	10	29	71	18	73	16	Perf	1.5CH4+2O2+4.5CO2	25	7.8	2.8	no	WFO			
1193	10	29	71	18	74	16	Perf	1.5CH4+2O2+5CO2	25	7.3	2.8	no	WFO			

HS #	Projectile					Sabot		Propellant				M	Start?	Failure		
	Nose A (deg)	Throat D (mm)	Body L (mm)	Base D (mm)	M (g)	M (g)	Type	Composition	P (atm)	Fill	Qc _j			V (m/s)	Mode	Comments
1192	10	29	71	18	73	16	Perf	1.5CH4+2O2+6CO2	25		6.5	850	2.9	no	WFO	
1191	10	29	71	18	72	16	Perf	1.5CH4+2O2+4CO2	25		8.4	890	2.9	no	WU	
1190	15	29	46	18	50	16	Perf	2.8CH4+2O2+5.7N2	30		4.6	1176	3.2	yes		
1189	15	29	71	18	66	16	Perf	2.8CH4+2O2+5.7N2	40		4.6	1155	3.2	yes		
1188	10	29	46	18	56	16	Perf	2.8CH4+2O2+5.7N2	35		4.6	1176	3.2	yes		
1187	15	29	46	18	50	16	Perf	2.8CH4+2O2+5.7N2	30		4.6	1180	3.2	yes		
1186	15	29	46	18	50	16	Perf	2.8CH4+2O2+5.7N2	30		4.6	1168	3.2	yes		
1185	15	29	46	18	50	16	Perf	2.8CH4+2O2+5.7N2	30		4.6	1180	3.2	yes		
1184	15	29	46	18	49	16	Perf	2.8CH4+2O2+5.7N2	30		4.6	1186	3.3	yes		
1183	15	29	46	18	50	15	Perf	2.8CH4+2O2+5.7N2	25		4.6	1182	3.2	yes		
1182	15	29	46	18	49	14	Perf	2.8CH4+2O2+5.7N2	25		4.6	1161	3.2	no	WU	
1181	10	29	71	18	99	15	Perf	2.8CH4+2O2+5.7N2	50		4.6	1161	3.2	yes		
1180	10	29	71	18	98	16	Perf	2.8CH4+2O2+5.7N2	50		4.6	1161	3.2	yes		
1179	10	29	71	18	74	14	Perf	2.8CH4+2O2+5.7N2	50		4.6	1153	3.2	yes		
1178	10	29	71	18	109	14	Perf	2.8CH4+2O2+5.7N2	50		4.6	1105	3.	no	Unst	
1177	10	29	71	18	77	14	Perf	2.8CH4+2O2+5.7N2	25		4.6	1190	3.3	yes		
1176	10	29	71	18	98	16	Perf	2.8CH4+2O2+5.7N2	50		4.6	1168	3.2	yes		
1175	10	29	71	18	77	16	Perf	2.8CH4+2O2+5.7N2	40		4.6	1161	3.2	yes		
1174	10	29	71	18	77	16	Perf	2.8CH4+2O2+5.7N2	50		4.6	1157	3.2	yes		
1173	10	29	71	18	77	16	Perf	2.8CH4+2O2+5.7N2	40		4.6	1170	3.2	yes		

HS #	Projectile					Sabot		Propellant					Start?	Failure Mode	Comments
	Nose A (deg)	Throat D (mm)	Body L (mm)	Base D (mm)	M (g)	M (g)	Type	Composition	P (atm)	Qcj	V (m/s)	M			
1172	10	29	71	18	77	15	Perf	2.8CH4+2O2+5.7N2	40	4.6	1150	3.2	yes		
1171	10	29	71	18	77	16	Perf	2.8CH4+2O2+5.7N2	40	4.6	1157	3.2	yes		
1165-1170 Hollow Proj															
1164	10	29	71	18	77	15	Perf	2.8CH4+2O2+5.7N2	50	4.6	1137	3.1	yes		
1163	10	29	71	18	77	16	Perf	2.8CH4+2O2+5.7N2	49	4.6	1132	3.1	yes		
1162	10	29	71	18	77	15	Perf	2.8CH4+2O2+5.7N2	49	4.6	1150	3.2	yes		
1161	10	29	71	18	77	15	Perf	2.8CH4+2O2+5.7N2	50	4.6	1143	3.1	yes		
1160	10	29	71	18	77	16	Perf	2.8CH4+2O2+5.7N2	50	4.6	1132	3.1	yes		
1159	10	29	71	18	77	15	Perf	2.8CH4+2O2+5.7N2	50	4.6	1136	3.1	yes		
1158	10	29	71	18	68	15	Perf	2.8CH4+2O2+5.7N2	38	4.6	1150	3.2	yes		
1157	10	29	71	18	66	15	Perf	2.8CH4+2O2+5.7N2	38	4.6	1156	3.2	yes		
1156	10	29	71	18	59	15	Perf	2.8CH4+2O2+5.7N2	38	4.6	1164	3.2	yes		
1155	10	29	71	18	64	15	Perf	2.8CH4+2O2+5.7N2	38	4.6	1141	3.1	yes		
1154	10	29	97	18	85	15	Perf	2.8CH4+2O2+5.7N2	25	4.6	1088	3.	yes		
1153	10	29	36	18	40	15	Perf	2.8CH4+2O2+5.7N2	26	4.6			yes		
1152	10	29	46	18	47	15	Perf	2.8CH4+2O2+5.7N2	26	4.6	1159	3.2	yes		
1151	10	29	55	18	52	15	Perf	2.8CH4+2O2+5.7N2	26	4.6	1157	3.2	yes		
1150	10	29	64	18	59	15	Perf	2.8CH4+2O2+5.7N2	26	4.6	1180	3.2	yes		
1149	10	29	71	18	79	15	Perf	2.8CH4+2O2+5.7N2	38	4.6	1157	3.2	yes		
1148	10	29	71	18	63	15	Perf	2.8CH4+2O2+5.7N2	37	4.6	1145	3.1	yes		

HS #	Projectile					Sabot		Propellant					Start?	Failure Mode	Comments
	Nose A (deg)	Throat D (mm)	Body L (mm)	Base D (mm)	M (g)	M (g)	Type	Composition	P (atm)	Qcj	V (m/s)	M			
1147	10	29	72	18	64	15	Perf	2.8CH4+2O2+5.7N2	26	4.6	1149	3.2	no	WU	
1146	15	29	36	18	35	15	Perf	2.8CH4+2O2+5.7N2	26	4.6	1116	3.1			
1145	15	29	46	18	41	15	Perf	2.8CH4+2O2+5.7N2	26	4.6	1161	3.2	yes		
1144	15	29	54	18	46	15	Perf	2.8CH4+2O2+5.7N2	26	4.6	1176	3.2	yes		
1143	15	29	54	18	46	15	Perf	2.8CH4+2O2+5.7N2	25	4.6			no	ERR	
1142	15	29	63	18	53	15	Perf	2.8CH4+2O2+5.7N2	25	4.6	1145	3.1	yes		
1141	15	29	72	18	57	15	Perf	2.8CH4+2O2+5.7N2	26	4.6	1145	3.1	yes		
1140-1113 Hollow Proj															
1112	13	29	71	18	59	15	Perf	2.8CH4+2O2+5.7N2	26	4.6	1157	3.2	yes		
1111	7	29	71	18	74	15	Perf	2.8CH4+2O2+5.7N2	26	4.6	1061	2.9	yes		
1110	18	29	71	18	54	15	Perf	2.8CH4+2O2+5.7N2	26	4.6	1145	3.1	yes		
1109	15	29	71	18	56	15	Perf	2.8CH4+2O2+5.7N2	26	4.6	1138	3.1	yes		
1108	13	29	71	18	59	16	Perf	2.8CH4+2O2+5.7N2	26	4.6	1157	3.2	yes		
1107	20	29	71	18	53	15	Perf	2.8CH4+2O2+5.7N2	26	4.6	1152	3.2	no	WU	
1106	10	29	71	18	62	15	Perf	2.8CH4+2O2+5.7N2	26	4.6	1180	3.2	yes		
1104	10	29	71	18	77	15	Perf	2.8CH4+2O2+5.7N2	40	4.6	1164	3.2	yes		
1103	10	29	71	18	77	16	Perf	2.8CH4+2O2+5.7N2	40	4.6	1164	3.2	yes		
1102	10	29	71	18	77	16	Perf	2.8CH4+2O2+5.7N2	40	4.6	1123	3.1	yes		
1101	10	29	71	18	77	16	Perf	2.8CH4+2O2+5.7N2	39	4.6	1116	3.1	yes		
1100	10	29	71	18	78	15	Perf	2.8CH4+2O2+5.7N2	30	4.6	1138	3.1	yes		

HS #	Projectile					Sabot		Propellant					Start?	Failure Mode	Comments
	Nose A (deg)	Throat D (mm)	Body L (mm)	Base D (mm)	M (g)	M (g)	Type	Composition	P (atm)	Qcj	V (m/s)	M			
1099	10	29	71	18	63	15	Perf	2.8CH4+2O2+5.7N2	30	4.6	1134	3.1	yes		
1098	10	29	71	18	72	15	Perf	2.8CH4+2O2+5.7N2	30	4.6	1121	3.1	yes		
1097	10	29	71	18	66	15	Perf	2.8CH4+2O2+5.7N2	30	4.6	1130	3.1	yes		
1096	10	29	71	18	63	15	Perf	2.8CH4+2O2+5.7N2	30	4.6	1136	3.1	yes		
1095	10	29	71	18	65	15	Perf	2.8CH4+2O2+5.7N2	30	4.6	1134	3.1	yes		
1094	10	29	71	18	63	15	Perf	2.8CH4+2O2+5.7N2	30	4.6	1140	3.1	yes		
1093	10	29	71	18	84	15	Perf	2.8CH4+2O2+5.7N2	50	4.6	1161	3.2	yes		
1092	10	29	71	18	77	15	Perf	2.8CH4+2O2+5.7N2	50	4.6	1157	3.2	yes		
1091	10	29	71	18	77	15	Perf	2.8CH4+2O2+5.7N2	49	4.6	1188	3.3	yes		
1090	10	29	71	18	77	15	Perf	2.8CH4+2O2+5.7N2	50	4.6	1172	3.2	yes		
1089	10	29	71	18	77	15	Perf	2.8CH4+2O2+5.7N2	50	4.6	1164	3.2	yes		
1088	10	29	71	18	77	15	Perf	2.8CH4+2O2+5.7N2	50	4.6	1164	3.2	yes		
1087	10	29	71	18	77	15	Perf	2.8CH4+2O2+5.7N2	50	4.6	1149	3.2	yes		
1086	10	29	71	18	77	15	Perf	2.8CH4+2O2+5.7N2	50	4.6	1166	3.2	yes		
1085	10	29	71	18	77	15	Perf	2.8CH4+2O2+5.7N2	50	4.6	1174	3.2	yes		
1084	10	29	71	18	77	15	Perf	2.8CH4+2O2+5.7N2	50	4.6	1156	3.2	yes		
1083	10	29	71	18	77	15	Perf	2.8CH4+2O2+5.7N2	50	4.6	1162	3.2	yes		
1082	10	29	71	18	76	15	Perf	2.8CH4+2O2+5.7N2	50	4.6	1166	3.2	yes		
1081	10	29	71	18	76	15	Perf	2.8CH4+2O2+5.7N2	50	4.6	1160	3.2	yes		
1080	10	29	71	18	77	15	Perf	2.8CH4+2O2+5.7N2	50	4.6	1166	3.2	yes		

HS #	Projectile					Sabot		Propellant				Start?	Failure Mode	Comments	
	Nose A (deg)	Throat D (mm)	Body L (mm)	Base D (mm)	M (g)	M (g)	Type	Composition	P (atm)	Qcj	V (m/s)				M
1079	10	29	71	18	77	15	Perf	2.8CH4+2O2+5.7N2	49	4.6	1157	3.2	yes		
1078	10	29	71	18	77	15	Perf	2.8CH4+2O2+5.7N2	50	4.6	1153	3.2	yes		
1077	10	29	71	18	77	15	Perf	2.8CH4+2O2+5.7N2	49	4.6	1161	3.2	yes		
1076	10	29	71	18	77	15	Perf	2.8CH4+2O2+5.7N2	50	4.6	1164	3.2	yes		
1075	10	29	71	18	77	15	Perf	2.8CH4+2O2+5.7N2	50	4.6	1155	3.2	yes		
1074	10	33		18	85	16	Perf	2.8CH4+2O2+5.7N2	25	4.6	1180	3.2	yes		
1073	10	32		18	77	16	Perf	2.8CH4+2O2+5.7N2	25	4.6	1180	3.2	yes		
1072	10	33		18	86	15	Perf	2.8CH4+2O2+5.7N2	25	4.6	1134	3.1	no	SDU	
1071	10	32		18	78	16	Perf	2.8CH4+2O2+5.7N2	25	4.6	241	.7	no	SDU	
1070	10	31		18	73	16	Perf	2.8CH4+2O2+5.7N2	25	4.6	1130	3.1	yes		
1069	10	30		18	65	15	Perf	2.8CH4+2O2+5.7N2	25	4.6	1098	3.	yes		
1068	10	29	71	18	63	15	Perf	2.8CH4+2O2+5.7N2	25	4.6	1138	3.1	yes		
1067	10	29	71	18	63	15	Perf	2.8CH4+2O2+5.7N2	25	4.6	1105	3.	yes		
1066	10	29	71	18	109	15	Perf	3CH4+2O2+5.7N2	51	4.4	1119	3.1	yes		
1065	10	29	71	18	107	15	Perf	3CH4+2O2+5.7N2	51	4.4	1116	3.1	yes		
1064	10	29	71	18	101	14	Perf	3CH4+2O2+5.7N2	51	4.4	1155	3.2	yes		
1063	10	29	71	18	87	13	Perf	3CH4+2O2+5.7N2	50	4.4	1155	3.2	yes		
1062	10	29	71	18	77	14	Perf	3CH4+2O2+5.7N2	49	4.4	1168	3.2	yes		
1061	10	29	71	18	77	14	Perf	2.8CH4+2O2+5.7N2	36	4.6	1141	3.1	no	WU	
1060	10	29	71	18	70	14	Perf	2.8CH4+2O2+5.7N2	35	4.6	1118	3.1	yes		

HS #	Projectile				Sabot		Propellant				M	Start?	Failure		
	Nose A (deg)	Throat D (mm)	Body L (mm)	Base D (mm)	M (g)	Type	Composition	P (atm)	Qcj	V (m/s)			Mode	Comments	
1059	10	29	71	18	61	14	Perf	2.8CH4+2O2+5.7N2	28	4.6	1161	3.2	yes		
1058	10	29	71	18	68	14	Perf	2.8CH4+2O2+5.7N2	35	4.6				ERR	
1057	10	29	71	18	64	14	Perf	2.8CH4+2O2+5.7N2	35	4.6	1136	3.1	no	WU	
1056	10	29	71	18	68	15	Perf	2.8CH4+2O2+5.7N2	37	4.6	1110	3	yes		
1055	10	29	71	18	79	14	Perf	2.8CH4+2O2+5.7N2	37	4.6	1130	3.1	yes		
1054	10	29	71	18	73	14	Perf	2.8CH4+2O2+5.7N2	37	4.6	1132	3.1	yes		
1053	10	29	71	18	74	14	Perf	2.8CH4+2O2+5.7N2	28	4.6	1145	3.1	yes		
1052	10	29	71	18	62	14	Perf	2.8CH4+2O2+5.7N2	25	4.6	1170	3.2	yes		
1051	10	29	71	18	62	15	Perf	2.8CH4+2O2+5.5N2	21	4.7	1136	3.1	yes		
1050	10	29	71	18	61	16	Perf	2.8CH4+2O2+5.5N2	21	4.7	1138	3.1	yes		
1049	10	29	71	18	62	15	Perf	2.8CH4+2O2+5.5N2	25	4.7	1158	3.2	yes		
1048	10	29	71	18	61	13	Perf	2.8CH4+2O2+5N2	14	4.9	1160	3.2	yes		
1047	10	29	71	18	62	13	Perf	2.8CH4+2O2+5N2	14	4.9	1158	3.2	yes		
1046	10	29	71	18	63	13	Perf	2.8CH4+2O2+5N2	14	4.9	1172	3.2	yes		
1045	10	29	71	18	62	15	Perf	2.8CH4+2O2+5N2	14	4.9	1165	3.2	no	WU	
1044	10	29	71	18	61	15	Perf	2.8CH4+2O2+5N2	14	4.9				ERR	
1043	10	29	71	18	63	13	Perf	2.8CH4+2O2+5N2	13	4.9	1178	3.2	no	WFO	
1042	10	29	71	18	63	13	Perf	2.8CH4+2O2+5N2	13	4.9	1204	3.3	yes		
1041	10	29	71	18	62	16	Perf	2.8CH4+2O2+5.5N2	26	4.7	1151	3.2	yes		
1040	10	29	71	18	63	15	Perf	2.8CH4+2O2+5N2	13	4.9	1140	3.1	yes		

HS #	Projectile					Sabot		Propellant					Failure Mode	Comments		
	Nose A (deg)	Throat D (mm)	Body L (mm)	Base D (mm)	M (g)	M (g)	Type	Composition	P (atm)	Fill	Qc _j	V (m/s)			M	Start?
1039	10	29	71	18	63	15	Perf	2.8CH4+2O2+4.5N2	13		5.1	1138	3.1	no	WU	
1038	10	29	71	18	62	15	Perf	2.8CH4+2O2+5.5N2	25		4.7	1128	3.1	yes		
1037	10	29	71	18	63	16	Perf	2.8CH4+2O2+5.5N2	25		4.7	1136	3.1	yes		
1036	10	29	71	18	63	15	Perf	2.8CH4+2O2+5.5N2	25		4.7	1117	3.1	yes		
1035	10	29	71	18	63	15	Perf	2.8CH4+2O2+5.5N2	23		4.7	1143	3.1	no	WFO	
1034	10	29	71	18	63	15	Perf	2.8CH4+2O2+5.5N2	21		4.7	1159	3.2	no	WFO	
1033	10	29	71	18	64	15	Perf	2.8CH4+2O2+5.6N2	25		4.7	1136	3.1	yes		
1032	10	29	71	18	66	15	Perf	2.8CH4+2O2+5N2	12		4.9	1076	2.9	no	WFO	
1031	10	29	71	18	67	15	Perf	2.8CH4+2O2+5.6N2	12		4.7	1158	3.2	no	WFO	
1030	10	29	71	18	75	15	Perf	2.8CH4+2O2+5.5N2	12		4.7	1150	3.2	no	WU	
1029	10	29	71	18	82	15	Perf	2.8CH4+2O2+5.6N2	12		4.7	1200	3.3	no	WFO	
1028	10	29	71	18	62	15	Perf	2.8CH4+2O2+5.7N2	27		4.6	1213	3.3	yes		
1027	10	29	71	18	63	16	Perf	2.8CH4+2O2+5.7N2	25		4.6	1319	3.6	yes		
1026	10	29	71	18	63	16	Perf	2.8CH4+2O2+5.7N2	25		4.6	1134	3.1	yes		
1025	10	29	71	18	63	16	Perf	2.8CH4+2O2+5.7N2	25		4.6	1157	3.2	yes		
1024	10	29	71	18	63	16	Perf	2.8CH4+2O2+5.7N2	25		4.6	1116	3.1	yes		
1023	10	29	71	18	63	16	Perf	2.8CH4+2O2+5.7N2	25		4.6	1119	3.1	yes		
1022	10	29	71	18	63	16	Perf	2.8CH4+2O2+5.7N2	25		4.6	1130	3.1	yes		
1021	10	29	71	18	63	16	Perf	2.8CH4+2O2+5.7N2	25		4.6	1125	3.1	yes		
1020	10	29	71	18	63	16	Perf	2.8CH4+2O2+5.7N2	25		4.6	1105	3.	yes		

HS #	Projectile					Sabot		Propellant					Start?	Failure Mode	Comments
	Nose A (deg)	Throat D (mm)	Body L (mm)	Base D (mm)	M (g)	M (g)	Type	Composition	P (atm)	Qcj	V (m/s)	M			
1019	10	29	71	18	52	16	Perf	2.8CH4+2O2+5.7N2	25	4.6	1127	3.1	yes		
1018	10	29	71	18	63	16	Perf	2.8CH4+2O2+5.7N2	25	4.6	1121	3.1	yes		
1017	10	29	71	18	65	16	Perf	2.8CH4+2O2+5.7N2	25	4.6	1112	3.1	yes		
1016	10	29	71	18	64	16	Perf	2.8CH4+2O2+5.7N2	25	4.6	1130	3.1	yes		
1015	10	29	71	18	62	16	Perf	2.8CH4+2O2+5.7N2	25	4.6	1153	3.2	yes		
1014	10	29	71	18	64	16	Perf	2.8CH4+2O2+5.7N2	25	4.6	1126	3.1	yes		
1013	10	29	71	18	65	16	Perf	2.8CH4+2O2+5.7N2	25	4.6	1132	3.1	yes		
1012	10	29	71	18	65	16	Perf	2.8CH4+2O2+5.7N2	25	4.6	1125	3.1	yes		
1011	10	29	71	18	64	15	Perf	2.8CH4+2O2+5.7N2	25	4.6	1119	3.1	no	WU	
1010	10	29	71	18	64	16	Perf	2.8CH4+2O2+5.7N2	25	4.6	1136	3.1	no	WU	
1009	10	29	71	18	65	16	Perf	2.8CH4+2O2+5.7N2	25	4.6	1136	3.1	yes		
1008	10	29	71	18	64	16	Perf	2.8CH4+2O2+5.7N2	25	4.6	1153	3.2	yes		
1007	10	29	71	18	64	16	Perf	2.8CH4+2O2+5.7N2	25	4.6	1096	3.	no	WFO	
1006	10	29	71	18	64	16	Perf	2.8CH4+2O2+5.7N2	25	4.6	1127	3.1	yes		
1005	10	29	71	18	64	16	Perf	2.8CH4+2O2+5.7N2	25	4.6	1130	3.1	yes		
1004	10	29	71	18	64	16	Perf	2.8CH4+2O2+5.7N2	25	4.6	1116	3.1	yes		
1003	10	29	71	18	65	16	Perf	2.8CH4+2O2+5.7N2	25	4.6	1116	3.1	yes		
1002	10	29	71	18	64	16	Perf	2.8CH4+2O2+5.7N2	25	4.6	1130	3.1	yes		
1001	10	29	71	18	63	16	Perf	2.8CH4+2O2+5.7N2	25	4.6	1125	3.1	yes		
1000	10	29	71	18	65	15	Perf	2.8CH4+2O2+5.7N2	25	4.6	1145	3.1	yes		

HS #	Projectile				Sabot		Propellant				M	V (m/s)	Start?	Failure	
	Nose A (deg)	Throat D (mm)	Body L (mm)	Base D (mm)	M (g)	Type	Composition	P (atm)	Qcj	Mode				Comments	
999	10	29	71	18	64	16	Perf	2.8CH4+2O2+5.7N2	25	4.6	3.1	1141	yes		
998	10	29	71	18	64	16	Perf	2.8CH4+2O2+5.7N2	25	4.6	3.	1108	yes		
997	10	29	71	18	63	16	Perf	2.8CH4+2O2+5.7N2	25	4.6	3.1	1123	yes		
996	10	29	71	18	64	16	Perf	2.8CH4+2O2+5.8N2	25	4.6	3.1	1112	no	WFO	
995	10	29	71	18	64	16	Perf	2.8CH4+2O2+5.8N2	25	4.6	3.1	1123	yes		
994	10	29	71	18	64	16	Perf	2.8CH4+2O2+5.8N2	25	4.6	3.1	1143	yes		
993	10	29	71	18	63	16	Perf	2.6CH4+2O2+5.8N2	25	4.9	3.1	1141	yes		
992	10	29	71	18	76	12	solid	2.7CH4+2O2+5.8N2	25	4.7					
991	10	29	71	18	69	13	solid	2.7CH4+2O2+5.8N2	24	4.7					
990	10	29	71	18	74	16	Perf	2.7CH4+2O2+5.8N2	29	4.7					
989	10	29	71	18	74	16	Perf	2.7CH4+2O2+5.8N2	29	4.7					
988	10	29	71	18	73	16	Perf	2.7CH4+2O2+5.8N2	35	4.7					
987	10	29	71	18	74	15	Perf	2.7CH4+2O2+5.8N2	32	4.7					
986	10	29	71	18	74	15	Perf	2.7CH4+2O2+5.8N2	29	4.7			yes		
985	10	29	71	18	74	15	Perf	2.7CH4+2O2+5.8N2	34	4.7					
984	10	29	71	18	74	15	Perf	2.7CH4+2O2+5.8N2	33	4.7					
983	10	29	71	18	72	15	Perf	2.7CH4+2O2+5.8N2	29	4.7					
982	10	29	71	18	65	16	Perf	2.7CH4+2O2+5.8N2	25	4.7					
981	10	29	71	18	64	16	Perf	2.7CH4+2O2+5.8N2	25	4.7					
980	10	29	71	18	62	16	Perf	2.7CH4+2O2+5.8N2	25	4.7					

HS #	Projectile					Sabot		Propellant					Start?	Failure Mode	Comments
	Nose A (deg)	Throat D (mm)	Body L (mm)	Base D (mm)	M (g)	M (g)	Type	Composition	P (atm)	Qc _j	V (m/s)	M			
979	10	29	71	18	67		Perf	2.7CH4+2O2+5.7N2	27	4.8	1109	3.1	yes		
978	10	29	71	18	67	15	Perf	2.7CH4+2O2+5.7N2	26	4.8	1141	3.1	yes		
977	10	29	71	18	66	15	Perf	2.7CH4+2O2+5.7N2	26	4.8	1134	3.1	yes		
976	10	29	71	18	88	15	Perf	2.7CH4+2O2+5.8N2	22	4.7	1115	3.1	yes		
975	10	29	71	18	89	15	Perf	2.7CH4+2O2+5.8N2	22	4.7	1109	3.1			
974	10	29	71	18	71	15	Perf	2.7CH4+2O2+5.8N2	22	4.7			no	WFO	
973	10	29	71	18	73	15	Perf	2.7CH4+2O2+5.8N2	22	4.7	1102	3.	yes		
972	10	29	71	18	72	15	Perf	2.7CH4+2O2+5.8N2	22	4.7	1095	3.	yes		
971	10	29	71	18	66	15	Perf	2.7CH4+2O2+5.8N2	21	4.7	1197	3.3	yes		
970	10	29	71	18	65	15	Perf	2.7CH4+2O2+5.7N2	21	4.8	1200	3.3	no	WU	
969	10	29	71	18	65	15	Perf	2.7CH4+2O2+5.7N2	22	4.8			yes		
968	10	29	71	18	74	15	Perf	2.7CH4+2O2+5.7N2	30	4.8	1110	3.1	yes		
967	10	29	71	18	74	15	Perf	2.7CH4+2O2+5.7N2	30	4.8			yes		
966	10	29	71	18	66	15	Perf	2.7CH4+2O2+5.7N2	30	4.8			yes		
965	10	29	71	18	64	15	Perf	2.7CH4+2O2+5.7N2	21	4.8			yes		
964	10	29	71	18	63	15	Perf	2.7CH4+2O2+5.7N2	20	4.8			yes		
963	10	29	71	18	67	15	Perf	2.7CH4+2O2+5.7N2	30	4.8			yes		
962	10	29	71	18	65	15	Perf	2.7CH4+2O2+5.7N2	30	4.8	1257	3.5	yes		
961	10	29	71	18	66	15	Perf	2.7CH4+2O2+5.7N2	30	4.8	1196	3.3	yes		
960	10	29	71	18	64	16	Perf	2.7CH4+2O2+5.7N2	21	4.8			yes		

HS #	Projectile				Sabot		Propellant				M	Start?	Failure		
	Nose A (deg)	Throat D (mm)	Body L (mm)	Base D (mm)	M (g)	Type	Composition	P (atm)	Qcj	V (m/s)			Mode	Comments	
959	10	29	71	18	67	15	Perf	2.7CH4+2O2+5.7N2	20	4.8	1158	3.2	yes		
958	10	29	71	18	74	15	Perf	2.7CH4+2O2+5.7N2	21	4.8	1202	3.3	yes		
957	10	29	71	18	70	15	Perf	2.7CH4+2O2+5.7N2	20	4.8	1134	3.1	yes		
956	10	29	71	18	69	15	Perf	2.7CH4+2O2+5.7N2	20	4.8					
955	10	29	71	18	71	15	Perf	2.7CH4+2O2+5.8N2	20	4.7	1127	3.1	no	WFO	
954	10	29	71	18	73	15	Perf	2.7CH4+2O2+5.8N2	21	4.7			yes		
953	10	29	71	18	83	15	Perf	2.7CH4+2O2+5.8N2	30	4.7					
953	10	29	71	18	75	15	Perf	2.7CH4+2O2+5.8N2	32	4.7	1157	3.2			
951	10	29	71	18	74	15	Perf	2.7CH4+2O2+5.8N2	30	4.7	1169	3.2			
950	10	29	71	18	65	9	solid	2.7CH4+2O2+5.8N2	24	4.7					
949	10	29	71	18	71	10	solid	2.7CH4+2O2+5.8N2	24	4.7					
948	10	29	71	18	71	15	Perf	2.7CH4+2O2+5.8N2	24	4.7	1162	3.2	yes		Plt 1psi
947	10	29	71	18	73	15	Perf	2.7CH4+2O2+5.8N2	24	4.7	1102	3.	no	Unst	Plt 1psi
946	10	29	71	18	62	16	Perf	2.5CH4+2O2+5.6N2	20	5.3					
945	10	29	71	18	69	15	Perf	2.7CH4+2O2+5.8N2	21	4.7	1160	3.2	yes		
944	10	29	71	18	66	15	Perf	2.7CH4+2O2+5.8N2	30	4.7	1176	3.2	yes		
943	10	29	71	18	70	15	Perf	2.7CH4+2O2+5.8N2	27	4.7					
942	10	29	71	18	68	15	Perf	2.7CH4+2O2+5.8N2	27	4.7	1105	3.	yes		Plt .5psi
941	10	29	71	18	80	15	Perf	2.7CH4+2O2+5.8N2	27	4.7	1071	3.	no	WU	Plt .5psi
940	10		97		89	15	Perf	2.7CH4+2O2+5.6N2	28	4.8	1128	3.1	no	WU	Plt 1psi

HS #	Projectile					Sabot		Propellant				V (m/s)	M	Start?	Failure Mode	Comments
	Nose A (deg)	Throat D (mm)	Body L (mm)	Base D (mm)	M (g)	M (g)	Type	Composition	P (atm)	Qcj	Fill					
939	10		97		89	15	Perf	2.7CH4+2O2+5.6N2	28	4.8						Plt Ipsi
938	10		97		89	15	Perf	2.7CH4+2O2+5.6N2	38	4.8	3.1	1127	no	WU		Plt Ipsi
937	10				73	15	Perf	2.5CH4+2O2+5.6N2	21	5.3	3.1	1127	yes			Plt Ipsi
936	10				70	15	Perf	2.4CH4+2O2+5N2	12	5.8	3.3	1197	no	WU		
935	10		71		72	15	Perf	2.6CH4+2O2+5.6N2	12	5.			no	WFO		
934	10				70	15	Perf	2.7CH4+2O2+5.8N2	12	4.7	3.1	1123	no	WFO		
933	10				90	15	Perf	2.7CH4+2O2+5.8N2	38	4.7	3.1	1140	no	WU		Plt Ipsi
932	10	29	71	18	72	15	Perf	2.7CH4+2O2+5.8N2	38	4.7	3.1	1110	yes			1 psi lt
931	10	29	71	18	90	16	Perf	2.7CH4+2O2+5.8N2	38	4.7	3.1	1123	yes			1 psi lt
930	10	29	97	18	87	15	Perf	2.7CH4+2O2+5.6N2	38	4.7	3.1	1112	no	WU		
929	10	29	71	18	88	15	Perf	2.7CH4+2O2+5.8N2	38	4.7	3.1	1130	no	WFO		
928	10	29	71	18	73	15	Perf	2.7CH4+2O2+5.8N2	29	4.7						
927	10	29	71	18	83	15	Perf	2.7CH4+2O2+5.8N2	29	4.7						
926	10	29	71	18	72	15	Perf	2.7CH4+2O2+5.8N2	24	4.7						
925	10	29	51		48	16	Perf	2.7CH4+2O2+5.8N2	21	4.7	3.5	1261	yes			.7 psi lt
924	10	29	71	18	70	15	Perf	2.7CH4+2O2+5.8N2	28	4.7						
923	10	29	71	18	82	15	Perf	2.7CH4+2O2+5.8N2	28	4.7						
922	10	29	71	18	73	15	Perf	2.7CH4+2O2+5.8N2	18	4.7						
921	10	29	71	18	74	15	Perf	2.7CH4+2O2+5.8N2	28	4.7						
920					74	15	Perf	2.7CH4+2O2+5.8N2	28	4.7						

HS #	Projectile				Sabot		Propellant				M	Start?	Failure Mode	Comments
	Nose A (deg)	Throat D (mm)	Body L (mm)	Base D (mm)	M (g)	Type	Composition	P (atm)	Qc _j	V (m/s)				
919					74	15	Perf	2.7CH4+2O2+5.8N2	28	4.7				
918					74	15	Perf	2.7CH4+2O2+5.8N2	28	4.7				
917					74	15	Perf	2.7CH4+2O2+5.8N2	28	4.7				
916					74	15	Perf	2.7CH4+2O2+5.8N2	24	4.7				
915					78	15	Perf	2.8CH4+2O2+5.8N2	34	4.6		yes		
914					74	15	Perf	2.8CH4+2O2+5.8N2	47	4.6				
913					74	15	Perf	2.8CH4+2O2+5.8N2	47	4.6	3.2	yes		
912					77	15	Perf	2.8CH4+2O2+5.8N2	49	4.6				
911 ULTEM														
910					74	15	Perf	2.8CH4+2O2+5.8N2	47	4.6	3.2	yes		
909					71	15	Perf	2.8CH4+2O2+5.8N2	46	4.6	3.2	yes		
908					74	15	Perf	2.8CH4+2O2+5.8N2	47	4.6	3.2	yes		
907					70	15	Perf	2.8CH4+2O2+5.8N2	47	4.6	3.2	yes		
906					70	15	Perf	2.8CH4+2O2+5.8N2	27	4.6	3.2	yes		
905					79	15	Perf	2.8CH4+2O2+5.8N2	47	4.6	3.2	yes		
904					80	15	Perf	2.8CH4+2O2+5.8N2	47	4.6	3.2	yes		
903					80	15	Perf	2.8CH4+2O2+5.8N2	47	4.6	3.2	yes		
902					73	15	Perf	2.8CH4+2O2+5.8N2	44	4.6	3.3	yes		
901	10		71		71	15	Perf	2.8CH4+2O2+5.8N2	46	4.6	3.3	yes		
900					71	15	Perf	2.8CH4+2O2+5.8N2	45	4.6	3.3	yes		

HS #	Projectile				Sabot		Propellant				V (m/s)	M	Start?	Failure	
	Nose A (deg)	Throat D (mm)	Body L (mm)	Base D (mm)	M (g)	Type	Composition	P (atm)	Fill	Qcj				Mode	Comments
899	10		71		71	15	Perf	2.8CH4+2O2+5.8N2	42		4.6	3.3	yes		
898					80	15	Perf	2.8CH4+2O2+5.8N2	47		4.6	3.3	yes		
897					78	15	Perf	2.8CH4+2O2+5.8N2	46		4.6	3.2	yes		
896					76	15	Perf	2.8CH4+2O2+5.8N2	47		4.6	3.2	yes		
895					78	15	Perf	2.8CH4+2O2+5.8N2	46		4.6	3.2	yes		
894					61	15	Perf	2.8CH4+2O2+5.8N2	36		4.6	3.2	yes		
893					80	15	Perf	2.8CH4+2O2+5.8N2	47		4.6	3.2	yes		
892					80	15	Perf	2.8CH4+2O2+5.8N2	46		4.6	3.2	yes		
891					70	15	Perf	2.7CH4+2O2+5.8N2	24		4.7				
890					69	15	Perf	2.7CH4+2O2+5.8N2	24		4.7				
889					62	15	Perf	2.7CH4+2O2+5.8N2	24		4.7				
888					61	15	Perf	2.7CH4+2O2+5.8N2	24		4.7				
887	10	29	71	18	79	15	Perf	2.8CH4+2O2+5.8N2	46		4.6	3.1	yes		
886	10	29	71	18	80	15	Perf	2.8CH4+2O2+5.8N2	47		4.6	3.2	yes		
885	13	29	58	18	58	15	Perf	2.8CH4+2O2+5.9N2	34		4.6	3.2	yes		
884	10	29	71	18	80	15	Perf	2.8CH4+2O2+5.8N2	47		4.6	3.2	yes		
883	10	29	71	18	80	15	Perf	2.8CH4+2O2+5.8N2	44		4.6	3.2	yes		
882	10	29	71	18	80	15	Perf	2.8CH4+2O2+5.8N2	38		4.6	3.2	yes		
881	10	29	71	18	80	15	Perf	2.8CH4+2O2+5.8N2	38		4.6	3.2	yes		
880	10	29	71	18	83	15	Perf	2.8CH4+2O2+5.8N2	39		4.6	3.2	yes		

HS #	Projectile					Sabot		Propellant				M	Start?	Failure	
	Nose A (deg)	Throat D (mm)	Body L (mm)	Base D (mm)	M (g)	M (g)	Type	Composition	P (atm)	Qcj	V (m/s)			Mode	Comments
879	10	29	71	18	80	15	Perf	2.8CH4+2O2+5.8N2	38	4.6	1160	3.2	yes		
878	10	29	71	18	80	15	Perf	2.8CH4+2O2+5.8N2	38	4.6	1155	3.2	yes		
877	10	29	71	18	82	15	Perf	2.8CH4+2O2+5.8N2	39	4.6	1153	3.2	yes		
876	10	29	71	18	75	15	Perf	2.8CH4+2O2+5.8N2	36	4.6	1164	3.2	yes		
875	10	29	71	18	80	15	Perf	2.8CH4+2O2+5.8N2	38	4.6	1157	3.2	yes		
874	10	29	71	18	80	15	Perf	2.8CH4+2O2+5.8N2	38	4.6	1145	3.1	yes		
873	10	29	71	18	80	15	Perf	2.8CH4+2O2+5.8N2	38	4.6	1151	3.2	yes		
872	10	29	71	18	80	15	Perf	2.8CH4+2O2+5.8N2	38	4.6	1155	3.2	yes		
871	10	29	71	18	79	15	Perf	2.8CH4+2O2+5.8N2	37	4.6	1159	3.2	yes		
870	10	29	71	18	79	15	Perf	2.8CH4+2O2+5.8N2	37	4.6	1163	3.2	yes		
869	10	29	71	18	64	15	Perf	2.8CH4+2O2+5.8N2	19	4.6	1161	3.2	yes		
868	10	29	71	18	67	15	Perf	2.8CH4+2O2+5.8N2	29	4.6	1147	3.2	yes		
867	10	29	84	18	68	15	Perf	2.8CH4+2O2+5.8N2	29	4.6	1151	3.2	yes		
866	10	29	71	18	72	15	Perf	2.8CH4+2O2+5.8N2	34	4.6	1155	3.2	yes		
865	10	29	71	18	70	15	Perf	2.8CH4+2O2+5.8N2	21	4.6	1153	3.2	yes		
864	10	29	84	18	68	15	Perf	2.8CH4+2O2+5.8N2	29	4.6	1160	3.2	yes		
863	10	29	71	18	71	15	Perf	2.8CH4+2O2+5.8N2	34	4.6	1157	3.2	yes		
862	10	29	84	18	74	15	Perf	2.8CH4+2O2+5.8N2	32	4.6	1153	3.2	yes		
861	10	29	71	18	71	15	Perf	2.8CH4+2O2+5.8N2	21	4.6	1157	3.2	yes		
860	10	29	71	18	63	15	Perf	2.8CH4+2O2+5.8N2	19	4.6	1164	3.2	yes		

HS #	Projectile					Sabot		Propellant				M	Start?	Failure		Comments
	Nose A (deg)	Throat D (mm)	Body L (mm)	Base D (mm)	M (g)	M (g)	Type	Composition	P (atm)	Qcj	V (m/s)			Mode		
859	10	29	71	18	73	15	Perf	2.8CH4+2O2+5.8N2	34	4.6	1161	3.2	yes			
858	10	29	71	18	63	15	Perf	2.8CH4+2O2+5.8N2	19	4.6	1164	3.2	yes			
857	10	29	71	18	74	15	Perf	2.8CH4+2O2+5.8N2	22	4.6	1153	3.2	yes			
856	10	29	71	18	75	15	Perf	2.8CH4+2O2+5.8N2	32	4.6	1161	3.2	yes			
855	10	29	71	18	74	15	Perf	2.8CH4+2O2+5.8N2	32	4.6	1160	3.2	yes			
854	10	29	71	18	70	15	Perf	2.8CH4+2O2+5.8N2	33	4.6	1161	3.2	yes			
853	14	29	51	18	45	15	Perf	2.8CH4+2O2+5.8N2	20	4.6	1164	3.2	yes			
852	10	29	71	18	62	15	Perf	2.8CH4+2O2+5.8N2	27	4.6	1161	3.2	yes			
851	13	29	51	18	49	15	Perf	2.8CH4+2O2+5.8N2	32	4.6	1170	3.2	yes			
850	10	29	71	18	62	15	Perf	2.8CH4+2O2+5.8N2	27	4.6	1190	3.3	yes			
849	13	29	58	18	56	15	Perf	2.8CH4+2O2+5.8N2	24	4.6	1160	3.2	yes			
848	13	29	51	18	50	15	Perf	2.8CH4+2O2+5.8N2	21	4.6	1160	3.2	yes			
847	10	29	71	18	70	15	Perf	2.9CH4+2O2+5.9N2	33	4.4	1172	3.2	yes			
846	10	29	71	18	72	15	Perf	2.7CH4+2O2+5.8N2	31	4.7	1160	3.2	no	Unst		
845	10	29	71	18	69	15	Perf	2.8CH4+2O2+5.8N2	31	4.6	1157	3.2	no	WU		
844	10	29	71	18	72	15	Perf	2.8CH4+2O2+5.8N2	31	4.6	1168	3.2	yes			
843	10	29	71	18	64	15	Perf	2.8CH4+2O2+5.8N2	28	4.6	1153	3.2	yes			
842	10	29	71	18	64	15	Perf	2.8CH4+2O2+5.8N2	27	4.6	1149	3.2	yes			
841	10	29	71	18	72	15	Perf	2.8CH4+2O2+5.8N2	31	4.6	1182	3.2	yes			
840	10	29	71	18	67	15	Perf		26		1172		yes			

HS #	Projectile				Sabot		Propellant				V (m/s)	M	Start?	Failure Mode	Comments
	Nose A (deg)	Throat D (mm)	Body L (mm)	Base D (mm)	M (g)	Type	Composition	P (atm)	Fill	Qcj					
839	10	29	71	18	83	15	Perf	2.7CH4+2O2+5.6N2	36	4.8	4.8	3.1	yes		
838	14	29	71	18	65	15	Perf	2.7CH4+2O2+5.5N2	18	4.9	4.9	3.2	no		
837	13	29	71	18	70	15	Perf	2.7CH4+2O2+5.6N2	20	4.8	4.8	3.1	no	WFO	
836	12	29	64	18	58	15	Perf	2.7CH4+2O2+5.6N2	16	4.8	4.8	3.1	yes		
835	8	29	84	18	88	15	Perf	2.7CH4+2O2+5.6N2	24	4.8	4.8	3.1	yes		
834 Hollow Proj															
833	10	29	71	18	69	15	Perf	2.7CH4+2O2+5.6N2	13	4.8	4.8	3.	yes		
832	10	29	71	18	73	15	Perf	1CH4+2O2+5.5CO2	20	8.6	8.6	3.2	no	WU	
831	10	29	71	18	71	15	Perf	1CH4+2O2+5CO2	18	9.1	9.1	3.2	no	Unst	
830	10	29	71	18	72	15	Perf	1CH4+2O2+6CO2	20	8.1	8.1	3.3	no	Unst	
829	10	29	71	18	70	14	Perf	2.7CH4+2O2+5.6N2	20	4.8	4.8	3.2	yes		
828	10	29	71	18	72	15	Perf	2.7CH4+2O2+5.6N2	20	4.8	4.8	3.2	yes		
827	10	29	71	18	71	15	Perf	2.7CH4+2O2+5.6N2	32	4.8	4.8	3.2	yes		
826	10	29	71	18	72	15	Perf	2.7CH4+2O2+5.6N2	32	4.8	4.8	3.3	yes		
825	10	29	71	18	73	15	Perf	2.7CH4+2O2+5.6N2	31	4.8	4.8	3.2	yes		
824	10	29	71	18	82	15	Perf	2.7CH4+2O2+5.6N2	40	4.8	4.8	3.1	yes		
823	10	29	71	18	74	15	Perf	2.7CH4+2O2+5.6N2	36	4.8	4.8	3.2	yes		
822	10	29	71	18	74	15	Perf	2.7CH4+2O2+5.6N2	22	4.8	4.8	3.1	yes		
821	10	29	71	18	73	15	Perf	2.7CH4+2O2+5.6N2	35	4.8	4.8	3.2	yes		
820	10	29	71	18	70	15	Perf	2.7CH4+2O2+5.6N2	34	4.8	4.8	3.1	yes		

HS #	Projectile				Sabot		Propellant				V (m/s)	M	Start?	Failure	
	Nose A (deg)	Throat D (mm)	Body L (mm)	Base D (mm)	M (g)	Type	Composition	P (atm)	Qcj	Mode				Comments	
819	10	29	71	18	83	15	Perf	2.7CH4+2O2+5.6N2	40	4.8	3.1	yes			
818	10	29	71	18	83	15	Perf	2.7CH4+2O2+5.6N2	39	4.8	3.1	yes			
817	10	29	71	18	83	15	Perf	2.7CH4+2O2+5.6N2	39	4.8	3.1	yes			
816	10	29	71	18	83	15	Perf	2.7CH4+2O2+5.6N2	38	4.8	3.1	yes			
815	10	29	71	18	74	16	Perf	2.7CH4+2O2+5.6N2	35	4.8	3.2	yes			
814	10	29	71	18	83	15	Perf	2.7CH4+2O2+5.6N2	38	4.8	3.1	yes			
813	10	29	71	18	83	15	Perf	2.7CH4+2O2+5.6N2	37	4.8	3.1	yes			
812	10	29	71	18	74	15	Perf	2.7CH4+2O2+5.6N2	35	4.8	3.2	yes			
811	10	29	71	18	68	15	Perf	2.7CH4+2O2+5.8N2	22	4.7	3.2	yes			
810	10	29	71	18	74	15	Perf	2.7CH4+2O2+5.6N2	36	4.8	3.2	yes			
809	10	29	58	18	54	15	Perf	2.7CH4+2O2+5.6N2	26	4.8	3.2	yes			
808	10	29	71	18	74	15	Perf	2.7CH4+2O2+5.6N2	36	4.8	3.2	yes			
807	10	29	71	18	73	15	Perf	2.7CH4+2O2+5.6N2	35	4.8	3.2	yes			
806	10	29	71	18	74	15	Perf	2.7CH4+2O2+5.6N2	36	4.8					
805	10	29	71	18	73	15	Perf	2.7CH4+2O2+5.6N2	35	4.8	3.2	yes			
804	10	29	84	18	69	15	Perf	2.7CH4+2O2+5.8N2	23	4.7		no	WFO		
803	10	29	71	18	63	15	Perf	2.7CH4+2O2+5.8N2	21	4.7		no	WFO		
802	10	29	71	18	70	15	Perf	2.7CH4+2O2+5.6N2	42	4.8					
801	10	29	71	18	72	15	Perf	2.7CH4+2O2+5.8N2	42	4.7		yes			
800					82	15	Perf	2.7CH4+2O2+5.8N2	36	4.7	3.	yes			

HS #	Projectile					Sabot		Propellant				M	V (m/s)	Start?	Failure	
	Nose A (deg)	Throat D (mm)	Body L (mm)	Base D (mm)	M (g)	M (g)	Type	Composition	P (atm)	Qcj	Mode				Comments	
799		29	84	18	80	15	Perf	2.7CH4+2O2+5.8N2	22	4.7						
798					77	15	Perf	2.7CH4+2O2+5.6N2	40	4.8			yes			
797					73	16	Perf	2.7CH4+2O2+5.6N2	38	4.8	3.2	1157	yes			
796					75	16	Perf	2.7CH4+2O2+5.6N2	39	4.8	3.2	1164	yes			
795					57	16	Perf	2.7CH4+2O2+5.6N2	41	4.8	3.3	1197	yes			
794	13	29	58	18	55	16	Perf	2.7CH4+2O2+5.6N2	40	4.8			yes			
793	10	29	71	18	70	15	Perf	2.7CH4+2O2+5.6N2	42	4.8			yes			
792	13	29	58	18	59	16	Perf	2.7CH4+2O2+5.6N2	36	4.8	3.2	1180	yes			
791	10	29	71	18	71	16	Perf	2.7CH4+2O2+5.6N2	42	4.8	3.2	1180	yes			
790	10	29	71	18	67	15	Perf	2.7CH4+2O2+5.6N2	41	4.8	3.4	1250	no	WU		
789	10	29	71	18	68	15	Perf	2.7CH4+2O2+5.6N2	41	4.8	3.3	1197	yes			
788	10	29	71	18	62	15	Perf	2.7CH4+2O2+5.6N2	37	4.8	3.2	1180	yes			
787	13	29	71	18	68	16	Perf	2.7CH4+2O2+5.6N2	41	4.8	3.2	1180	yes			
786	10	29	65	18	65	15	Perf	2.7CH4+2O2+5.6N2	39	4.8	3.3	1190	yes			
785	13	29	64	18	60	15	Perf	2.7CH4+2O2+5.6N2	35	4.8	3.2	1180	yes			
784	13	29	58	18	56	15	Perf	2.7CH4+2O2+5.6N2	34	4.8	3.3	1188	yes			
783	13	29	58	18	57	15	Perf	2.7CH4+2O2+5.6N2	34	4.8	3.3	1188	yes			
782	10	29	71	18	70	15	Perf	2.7CH4+2O2+5.6N2	42	4.8	3.2	1164	yes			
781	10	29	71	18	70	14	Perf	2.7CH4+2O2+5.6N2	42	4.8	3.2	1168	yes			
780	10	29	71	18	69	15	Perf	2.7CH4+2O2+5.6N2	42	4.8	3.2	1157	yes			

HS #	Projectile					Sabot		Propellant				V (m/s)	M	Start?	Failure	
	Nose A (deg)	Throat D (mm)	Body L (mm)	Base D (mm)	M (g)	M (g)	Type	Composition	P (atm)	Qcj	Mode				Comments	
779	10	29	71	18	69	15	Perf	2.7CH4+2O2+5.6N2	42	4.8	3.3	yes				
778	10	29	71	18	74	15	Perf	2.7CH4+2O2+5.6N2	35	4.8	3.3	yes				
777	10	29	71	18	65	15	Perf	2.7CH4+2O2+5.6N2	30	4.8	3.2	yes				
776	10	29	71	18	69	15	Perf	2.7CH4+2O2+5.6N2	33	4.8	3.2	yes				
775	10	29	71	18	68	15	Perf	2.7CH4+2O2+5.6N2	33	4.8	3.2	yes				
774	10	29	71	18	63	15	Perf	2.7CH4+2O2+5.6N2	31	4.8	3.3	yes				
773	10	29	71	18	67	15	Perf	2.7CH4+2O2+5.6N2	32	4.8	3.3	yes				
772	10	29	71	18	66	15	Perf	2.7CH4+2O2+5.6N2	32	4.8	3.3	yes				
771	10	29	71	18	72	15	Perf	2.7CH4+2O2+5.6N2	35	4.8	3.3	yes				
770	10	29	71	18	65	15	Perf	2.7CH4+2O2+5.6N2	35	4.8	3.4	yes				
769					72	15	Perf	2.7CH4+2O2+5.6N2	35	4.8	3.2	yes				
768	10	29	71	18	69	15	Perf	2.7CH4+2O2+5.6N2	35	4.8	3.3	yes				
767	10	29	71	18	68	15	Perf	2.7CH4+2O2+5.6N2	35	4.8	3.3	yes				
766	10	29	71	18	67	15	Perf	2.7CH4+2O2+5.6N2	34	4.8	3.3	yes				
765	10	29	71	18	54	15	Perf	2.7CH4+2O2+5.6N2	36	4.8	3.3	yes				
764	10	29	71	18	74	15	Perf	2.7CH4+2O2+5.6N2	31	4.8	3.2	yes				
763	10	29	71	18	75	15	Perf	2.7CH4+2O2+5.6N2	29	4.8	3.1	yes				
762	10	29	71	18	74	15	Perf	2.7CH4+2O2+5.6N2	34	4.8	3.2	yes				
761	10	29	71	18	74	15	Perf	2.5CH4+2O2+5.6N2	35	5.3	3.2	yes				
760	10	29	84	18	79	15	Perf	2.5CH4+2O2+5.6N2	28	5.3	3.1	yes				

HS #	Projectile				Sabot		Propellant				M	Start?	Failure		
	Nose A (deg)	Throat D (mm)	Body L (mm)	Base D (mm)	M (g)	Type	Composition	P (atm)	QcJ	V (m/s)			Mode	Comments	
759	10	29	84	18	78	15	Perf	2.5CH4+2O2+5.6N2	27	5.3	1134	3.1	yes		
758	10	29	84	18	79	15	Perf	2.5CH4+2O2+5.6N2	25	5.3	1130	3.1	yes		
757	10	29	84	18	79	15	Perf	2.5CH4+2O2+5.6N2	27	5.3	1120	3.1	yes		
756	10	29	84	18	78	15	Perf	2.8CH4+2O2+5.6N2	27	4.7	1110	3.	yes		
755	10	29	84	18	77	16	Perf	2.8CH4+2O2+5.6N2	34	4.7	1140	3.1	yes		
754	10	29	84	18	78	15	Perf	2.8CH4+2O2+5.6N2	25	4.7	1147	3.2	yes		
Poor mixture control prior to 754															
753	10	29	84	18	67	16	Perf	2.7CH4+2O2+5.8N2	22	4.7	1157	3.2	yes		
752	10	29	84	18	77	15	Perf	2.7CH4+2O2+5.8N2	23	4.7	1149	3.2	yes		
751	10	29	84	18	71	15	Perf	2.7CH4+2O2+5.8N2	22	4.7	1153	3.2	yes		
750	10	29	84	18	66	15	Perf	2.7CH4+2O2+5.8N2	21	4.7	1145	3.2	yes		
749	10	29	84	18	67	16	Perf	2.7CH4+2O2+5.8N2	24	4.7	1145	3.2	no	WU	
748	10	29	84	18	71	16	Perf	2.7CH4+2O2+5.8N2	25	4.7	1149	3.2	yes		
747	10	29	84	18	84	16	Perf	2.7CH4+2O2+5.8N2	35	4.7	1130	3.1	yes		
746	10	29	84	18	69	16	Perf	2.7CH4+2O2+5.8N2	28	4.7	1186	3.3	yes		
745	10	29	84	18	83	16	Perf	2.7CH4+2O2+5.8N2	35	4.7	1138	3.1	yes		
744	10	29	84	18	83	16	Perf	2.7CH4+2O2+5.8N2	35	4.7	1141	3.1	yes		
743	10	29	84	18	69	16	Perf	2.7CH4+2O2+5.8N2	35	4.7	1197	3.3	yes		
742	10	29	84	18	84	16	Perf	2.7CH4+2O2+5.8N2	43	4.7	1138	3.1	yes		
741	10	29	84	18	83	16	Perf	2.7CH4+2O2+5.8N2	35	4.7	1130	3.1	yes		

HS #	Projectile					Sabot		Propellant				M	Start?	Failure	
	Nose A (deg)	Throat D (mm)	Body L (mm)	Base D (mm)	M (g)	M (g)	Type	Composition	P (atm)	Qc _j	V (m/s)			Mode	Comments
740	10	29	84	18	84	16	Perf	2.7CH4+2O2+5.8N2	31	4.7	1151		yes		
739					70	16	Perf	2.7CH4+2O2+5.8N2	26	4.7	1183		yes		
738	10	29	84	18	90	16	Perf	2.7CH4+2O2+5.8N2	33	4.7	1127		yes		
737	10	29	84	18	72	16	Perf	2.7CH4+2O2+5.8N2	35	4.7	1164		yes		
736	10	29	84	18	70	16	Perf	2.7CH4+2O2+5.8N2	25	4.7	1141		yes		
735		28			80	16	Perf	2.7CH4+2O2+5.8N2	24	4.7	1157		yes		
734		28			94	16	Perf	2.7CH4+2O2+5.8N2	34	4.7	1105		no	WU	
733					76	16	Perf	2.7CH4+2O2+5.8N2	30	4.7	1141		no	WU	
732					88	16	Perf	2.7CH4+2O2+5.8N2	34	4.7	1153		yes		
731					85	16	Perf	2.7CH4+2O2+5.8N2	38	4.7	1123		yes		
730					86	16	Perf	2.7CH4+2O2+5.8N2	30	4.7	1138		yes		
729	10	29	84	18	86	16	Perf	2.7CH4+2O2+5.8N2	30	4.7	1145		yes		
728	10				93	15	Perf	2.7CH4+2O2+5.8N2	30	4.7	1102		yes		
727	13	28	84	18	80	16	Perf	2.7CH4+2O2+5.8N2	22	4.7	1149		yes		
726					69	16	Perf	2.7CH4+2O2+5.8N2	21	4.7	1145		yes		
725					69	16	Perf	2.7CH4+2O2+5.8N2	22	4.7	1161		yes		
724					71	16	Perf	2.7CH4+2O2+5.8N2	22	4.7	1157		yes		
723	13				82	16	Perf	2.6CH4+2O2+5.8N2	22	4.9	1153		no	WU	
722		28			83	15	Perf	2.5CH4+2O2+5.8N2	22	5.2	1138		no	WU	
721		28			82	15	Perf	2.3CH4+2O2+5.8N2	21	5.7	1149		no	WU	

HS #	Projectile					Sabot		Propellant				Start?	Failure Mode	Comments	
	Nose	Throat	Body	Base	M (g)	M (g)	Type	Composition	P (atm)	Qc _j	V (m/s)				M
	A (deg)	D (mm)	L (mm)	D (mm)			Perf								
720					64	15	Perf	2.7CH4+2O2+5.8N2	16	4.7			no		
719	10	29	84	18	83	15	Perf	2.7CH4+2O2+5.8N2	22	4.7	1134	3.1	yes		
718	10	28	84	18	84	15	Perf	2.7CH4+2O2+5.8N2	21	4.7	1130	3.1	no	WFO	
717	10	28	84	18	85		Perf	2.7CH4+2O2+5.8N2	21	4.7	1138	3.1	no	WFO	
716	10	28	84	18	85	15	Perf	2.7CH4+2O2+5.8N2	22	4.7			no	WU	
715	10	28	84	18	83	15	Perf	2.7CH4+2O2+5.8N2	22	4.7					
714	10	28	84	18	68	15	Perf	2.7CH4+2O2+5.8N2	31	4.7					
713					69	15	Perf	2.7CH4+2O2+5.8N2	23	4.7					
712					68	15	Perf	2.7CH4+2O2+5.8N2	23	4.7	1160	3.2	yes		
711					70	15		2.7CH4+2O2+5.8N2	22	4.7	1149	3.2	yes		
710					70	15		2.7CH4+2O2+5.8N2	22	4.7	1151	3.2	yes		
709					67	15		2.7CH4+2O2+5.8N2	22	4.7					
708					71	15		2.7CH4+2O2+5.8N2	23	4.7			yes		
707					70	15		2.7CH4+2O2+5.8N2	23	4.7	1153	3.2	yes		
706					65			2.9CH4+2O2+5.6N2	23	4.5	1172	3.2	yes		
705					65	15		2.9CH4+2O2+5.6N2	22	4.5					
704					69	15		2.9CH4+2O2+5.6N2	21	4.5			yes		
703								2.9CH4+2O2+5.6N2	21	4.5			yes		
702	10	29	84	18	79	15		2.9CH4+2O2+5.6N2	22	4.5			yes		
701					68	15		2.9CH4+2O2+5.6N2	22	4.5	1168	3.2	yes		

HS #	Projectile					Sabot		Propellant					Start?	Failure Mode	Comments
	Nose A (deg)	Throat D (mm)	Body L (mm)	Base D (mm)	M (g)	M (g)	Type	Composition	P (atm)	Qc _j	V (m/s)	M			
700					68	16		2.9CH ₄ +2O ₂ +5.6N ₂	22	4.5	1157	3.2	yes		
699	10	29	84	18	69	16		2.9CH ₄ +2O ₂ +5.6N ₂	21	4.5	1153	3.2	yes		
698	10	29	84	18	68	18		2.9CH ₄ +2O ₂ +5.6N ₂	26	4.5	1172	3.2	yes		
697	10	29	84	18	69	18		2.9CH ₄ +2O ₂ +5.6N ₂	25	4.5					
696	10	29	110	18	94	16		2.9CH ₄ +2O ₂ +5.6N ₂	28	4.5	1112	3.	yes		
695	13	29	84	18	68	15		2.9CH ₄ +2O ₂ +5.6N ₂	22	4.5					
694	13	29	110	18	89	15		2.9CH ₄ +2O ₂ +5.6N ₂	27	4.5	880	2.4	no		
693					71	16		2.9CH ₄ +2O ₂ +5.6N ₂	22	4.5	1176	3.2	yes		
692	10	29	84	18	67	16		2.7CH ₄ +2O ₂ +5.8N ₂	22	4.7	1156	3.2	yes		
691	10	29	84	18	69	16		2.7CH ₄ +2O ₂ +5.8N ₂	22	4.7					
690					70	16		2.7CH ₄ +2O ₂ +5.8N ₂	22	4.7	1213	3.3	yes		
689					66	16		2.7CH ₄ +2O ₂ +5.8N ₂	23	4.7			yes		
688					68	16		2.7CH ₄ +2O ₂ +5.8N ₂	22	4.7			yes		
687					66	16		2.7CH ₄ +2O ₂ +5.8N ₂	21	4.7	1100	3.	yes		
686	10	29	84	18	69	16		2.7CH ₄ +2O ₂ +5.8N ₂	21	4.7			no	ERR	
685	10	29	84	18	70	15		2.7CH ₄ +2O ₂ +5.8N ₂	21	4.7			no	ERR	
684	10	29	84	18	68	15		2.7CH ₄ +2O ₂ +5.8N ₂	27	4.7	1100	3.	yes		
683	10	29	84	18	84	15		2.7CH ₄ +2O ₂ +5.8N ₂	27	4.7			yes		
682					84	15		2.7CH ₄ +2O ₂ +5.8N ₂	28	4.7			yes		
681					83	15		2.7CH ₄ +2O ₂ +5.8N ₂	32	4.7			yes		

HS #	Projectile				Sabot		Propellant				V (m/s)	M	Start?	Failure	
	Nose A (deg)	Throat D (mm)	Body L (mm)	Base D (mm)	M (g)	Type	Composition	P (atm)	Fill	QcJ				Mode	Comments
680					79	15			26	4.7					
679	10	29	84	18	79	15			35	4.7		yes			
678	10	29	84	18	77	15			33	4.7		yes			
677-676 Quasi-2D Proj															
675		29			84	15			26	4.7	1140	3.1	yes		
674	10	29	84	18	76	14			25	4.7					
673-669 Quasi-2D Proj															
668					76	15			23	4.7			yes		
667					75	15			23	4.7				ERR	
666	10	29	84	18	76	14			23	4.7	1134	3.1	no	WFO	
665	10	29	84	18	78	14			23	4.7			no	Unst	
664	10	29	84	18	78				27	4.7	1159	3.2	yes		
663					89	14			25	4.7					
662					83	14			25	4.7					
661					82	14			25	4.7			no		
660					87	14			26	4.7					
659	10	30	84	18	84	14			23	4.7	1134	3.1	yes		
658	10	30	84	18	87	14			26	4.7					
657	10	30	84	18	85	14			26	4.7					
656	10	30	84	18	88	14			26	4.7					

HS #	Projectile				Sabot		Propellant			M	Start?	Failure		
	Nose A (deg)	Throat D (mm)	Body L (mm)	Base D (mm)	M (g)	Type	Composition	P (atm)	Qcj			V (m/s)	Mode	Comments
655	10	30	84	18	90	14		2.7CH4+2O2+5.8N2	26	4.7				
654	10	30	109	18	101	13		2.7CH4+2O2+5.8N2	26	4.7				
653	10	30	109	15	91	13		2.7CH4+2O2+5.8N2	25	4.7	820	2.3		
652	10	30	84	18	89	14		2.7CH4+2O2+5.8N2	22	4.7				
651	10	30	84	18	90	14		2.7CH4+2O2+5.8N2	24	4.7		yes		
650	13	29	84	18				2.7CH4+2O2+6N2	23	4.7				
649	13	29	84	18	81	13		2.7CH4+2O2+6N2	21	4.7				
648	13	29	84	18	78	10		2.7CH4+2O2+6N2	21	4.7	1130	3.1	Unst	
647	10	30	84	18	89	13		2.7CH4+2O2+6N2	24	4.7	857	2.4	SDU	
End of 16 m facility config, Pre-647														

Appendix B: Piston Experiment Data

DS	Geometry	Mass (gm)	Launch Tube Pressure (torr)	Fuel	Ox	Dil	Fill Pressure (atm)	Piston Velocity (m/s)	Piston Mach	Result	Comment
124	Solid	35	4.5	1.5CH ₄	2O ₂	5.5CO ₂	25	864	2.90	No Det	
125	Solid	35	4.5	1.5CH ₄	2O ₂	3.5CO ₂	25	864	2.81	No Det	
126	Solid	26	4.5	1.5CH ₄	2O ₂	3.5CO ₂	25	970	3.16	No Det	
127	Solid	26	4.5	1.5CH ₄	2O ₂	3.5CO ₂	25	1130	3.68	Det	
128	Solid	26	4.5	1.5CH ₄	2O ₂	3.5CO ₂	25	1048	3.41	No Det	
129	Solid	35	4.5	1.5CH ₄	2O ₂	3.5CO ₂	25	1111	3.62	Det	
130	Solid	35	4.5	1.5CH ₄	2O ₂	3.5CO ₂	25	1032	3.36	No Det	
131	Solid	35	4.5	1.5CH ₄	2O ₂	5.5CO ₂	25	1220	4.10	Marginal	8 m Det
132	Solid	35	4.5	1.5CH ₄	2O ₂	5.5CO ₂	25	1310	4.40	Marginal	4 m Det
133	Solid	35	4.5	1.5CH ₄	2O ₂	5.5CO ₂	25	1300	4.37	Marginal	9 m Det
134	Solid	26	4.5	1.5CH ₄	2O ₂	5.5CO ₂	25	1333	4.48	Marginal	4 m Det
135	Solid	26	4.5	1.5CH ₄	2O ₂	5.5CO ₂	25	1429	4.8	Det	
136	Solid	35	4.5	1.5CH ₄	2O ₂	5.5CO ₂	25	872	2.93	No Det	
137	Solid	35	4.5	1.5CH ₄	2O ₂	5.5CO ₂	25	1413	4.75	Marginal	3 m Det
138	Solid	26	4.5	1.5CH ₄	2O ₂	4.5CO ₂	25	1121	3.72	No Det	

DS	Geometry	Mass (gm)	Launch Tube Pressure (torr)	Fuel	Ox	Dil	Fill Pressure (atm)	Piston Velocity (m/s)	Piston Mach	Result	Comment
139	Solid	26	4.5	1.5CH ₄	2O ₂	4.5CO ₂	25	1313	4.35	Det	
140	Solid	26	4.5	1.5CH ₄	2O ₂	4.5CO ₂	25	1209	4.01	Det	
141	Solid	35	4.5	1.5CH ₄	2O ₂	4.5CO ₂	25	1204	3.99	Det	
142	Solid	35	4.5	1.5CH ₄	2O ₂	4.5CO ₂	25	1111	3.68	No Det	
143	Solid	35	4.5	1.5CH ₄	2O ₂	4.5CO ₂	25	133	0.44	No Det	
144	Solid	35	4.5	1.5CH ₄	2O ₂	4.5CO ₂	25	1130	3.75	No Det	
145	Solid	26	4.5	1.5CH ₄	2O ₂	4.5CO ₂	25	1182	3.92	No Det	
146	Solid	35	4.5	1.5CH ₄	2O ₂	3.5CO ₂	25	1057	3.44	No Det	
177	Solid	17	4.5	2.8CH ₄	2O ₂	4.5N ₂	50	1494	4.08	Det	
178	Solid	17	4.5	2.8CH ₄	2O ₂	4.5N ₂	50	1085	2.97	No Det	
179	Solid	18	4.5	2.8CH ₄	2O ₂	4.5N ₂	50	1330	3.64	Det	
180	Solid	17	4.5	2.8CH ₄	2O ₂	4.5N ₂	50	1270	3.47	Det	
181	Solid	16	4.5	2.8CH ₄	2O ₂	4.5N ₂	50	1198	3.28	Det	
182	Perforated	16	4.5	2.8CH ₄	2O ₂	4.5N ₂	50	1192	3.26	No Det	
183	Perforated	16	4.5	2.8CH ₄	2O ₂	4.5N ₂	50	1283	3.51	Det	
184	Perforated	16	4.5	2.8CH ₄	2O ₂	4.5N ₂	50	1233	3.37	Det	

DS	Geometry	Mass (gm)	Launch Tube Pressure (torr)	Fuel	Ox	Dil	Fill Pressure (atm)	Piston Velocity (m/s)	Piston Mach	Result	Comment
185	Solid	17	4.5	2.8CH ₄	2O ₂	4.5N ₂	50	1144	3.13	No Det	
186	Perforated	16	4.5	2.8CH ₄	2O ₂	5.7N ₂	50	1530	4.2	Det	
187	Perforated	16	4.5	2.8CH ₄	2O ₂	5.7N ₂	50	1309	3.6	Det	
188	Solid	17	4.5	2.8CH ₄	2O ₂	5.7N ₂	50	1257	3.45	Det	
189	Solid	17	4.5	2.8CH ₄	2O ₂	5.7N ₂	50	1187	3.26	Det	
190	Solid	17	4.5	2.8CH ₄	2O ₂	5.7N ₂	50	1160	3.19	No Det	
191	Perforated	16	4.5	2.8CH ₄	2O ₂	5.7N ₂	50	1257	3.45	No Det	
192	Perforated	16	4.5	2.3CH ₄	2O ₂	5.7N ₂	50	1155	3.2	No Det	
193	Perforated	16	4.5	2.3CH ₄	2O ₂	5.7N ₂	50	1245	3.45	No Det	
194	Perforated	16	4.5	2.3CH ₄	2O ₂	5.7N ₂	50	1309	3.62	Det	
195	Solid	17	4.5	2.3CH ₄	2O ₂	5.7N ₂	50	1221	3.38	Det	
196	Solid	17	4.5	2.3CH ₄	2O ₂	5.7N ₂	50	1176	3.26	Det	
197	Solid	17	4.5	2.3CH ₄	2O ₂	5.7N ₂	50	1085	3.0	No Det	
198	Solid	17	4.5	2.3CH ₄	2O ₂	5.7N ₂	50	1155	3.2	Det	
199	Perforated	16	4.5	5CH ₄	2O ₂	2He	50	1316	2.93	No Det	
200	Perforated	16	4.5	5CH ₄	2O ₂	2He	50	1503	3.35	No Det	

DS	Geometry	Mass (gm)	Launch Tube Pressure (torr)	Fuel	Ox	Dil	Fill Pressure (atm)	Piston Velocity (m/s)	Piston Mach	Result	Comment
201	Perforated	16	4.5	5CH ₄	2O ₂	2He	50	1628	3.63	No Det	
202	Perforated	16	4.5	5CH ₄	2O ₂	2He	50	1728	3.85	No Det	
203	Perforated	16	4.5	5CH ₄	2O ₂	2He	50	1841	4.10	No Det	
204	Perforated	16	4.5	5.5CH ₄	2O ₂	1H ₂	50	1512	3.53	No Det	
205	Perforated	16	4.5	5.5CH ₄	2O ₂	1H ₂	50	1716	4.01	No Det	
206	Perforated	16	4.5	5.5CH ₄	2O ₂	1H ₂	50	1841	4.3	No Det	
207	Perforated	16	29.8	2.8CH ₄	2O ₂	5.7N ₂	50	1233	3.38	No Det	
208	Perforated	16	29.8	2.8CH ₄	2O ₂	5.7N ₂	50	1309	3.58	No Det	
209	Perforated	16	29.8	2.8CH ₄	2O ₂	5.7N ₂	50	1309	3.58	No Det	
210	Perforated	16	29.8	2.8CH ₄	2O ₂	5.7N ₂	50	1477	4.04	No Det	
211	Perforated	16	29.8	2.8CH ₄	2O ₂	5.7N ₂	50	1588	4.35	Det	
253	Perforated	16	1.2	2.8CH ₄	2O ₂	5.7N ₂	50	1245	3.42	No Det	
254	Perforated	16	1.2	2.8CH ₄	2O ₂	5.7N ₂	50	1323	3.63	Det	
255	Perforated	16	4.5	2.8CH ₄	2O ₂	8.5Ar	50	1204	3.64	Det	
256	Perforated	16	4.5	2.8CH ₄	2O ₂	8.5Ar	50	1076	3.25	Det	
257	Perforated	16	4.5	2.8CH ₄	2O ₂	8.5Ar	50	917	2.77	Det	

DS	Geometry	Mass (gm)	Launch Tube Pressure (torr)	Fuel	Ox	Dil	Fill Pressure (atm)	Piston Velocity (m/s)	Piston Mach	Result	Comment
258	Perforated	16	4.5	2.8CH ₄	2O ₂	8.5Ar	50	885	2.67	No Det	
259	Perforated	16	4.5	2.8CH ₄	2O ₂	11Ar	50	1072	3.26	Det	
260	Perforated	16	4.5	2.8CH ₄	2O ₂	11Ar	50	940	2.86	Det	
261	Perforated	16	4.5	2.8CH ₄	2O ₂	11Ar	50	882	2.68	No Det	